2018-01-01

Facies Changes Associated With Formation Of An Extensive Salt Shoulder By The Coastal And Eolian Carmel And Entrada Formations, Gypsum Valley, Colorado

Ryan Burtron Ronson
University of Texas at El Paso, rbronson@miners.utep.edu

FACIES CHANGES ASSOCIATED WITH FORMATION OF AN EXTENSIVE SALT SHOULDER BY THE COASTAL AND EOLIAN CARMEL AND ENTRADA FORMATIONS, GYPSUM VALLEY, COLORADO

RYAN BURTRON RONSON

Master's Program in Geological Sciences

APPROVED:

Richard P. Langford, Ph.D., Chair

Katherine A. Giles, Ph.D.

Elizabeth Walsh, Ph.D.

Charles Ambler, Ph.D.
Dean of the Graduate School

Dedication

To my grandmother, Janice Tustian McBride, who was always a true example of perseverance, and inspired me to pursue my greatest ambitions.

FACIES CHANGES ASSOCIATED WITH FORMATION OF AN EXTENSIVE SALT SHOULDER BY THE COASTAL AND EOLIAN CARMEL AND ENTRADA FORMATIONS, GYPSUM VALLEY, COLORADO

by

RYAN BURTRON RONSON, B.S.

THESIS

Presented to the Faculty of the Graduate School of

The University of Texas at El Paso

in Partial Fulfillment

of the Requirements

for the Degree of

MASTER OF SCIENCE

Department of Geological Sciences

THE UNIVERSITY OF TEXAS AT EL PASO

August 2018

Acknowledgments

I would like to thank my professors, field assistants, the Institute of Tectonic Studies, family, friends, and all others who have supported me in any way. I could not have completed this research without you and this accomplishment has been motivated by your generosity.

Abstract

A salt shoulder forms a zone at the margin of a salt diapir where that margin steps relatively abruptly inward. These shoulders form when the salt rise rate near the diapir margin substantially decreases or stops relative to the salt rise rate at the inboard central part of the diaper. Based on current models of interactions between these salt shoulders and overlying sediment, it was anticipated that the thickness changes of the Entrada and Carmel formations would be only gradual and that any notable thinning would take place proximal to the neck portion of the diapir that would still have been moving upward during the time of deposition. Facies distributions of the Entrada and Carmel were expected to be consistent with the typical drying upward sequence observed in other parts of the region across which the erg extends. In this study, one stratigraphic section was measured at Slick Rock Canyon, away from the influence of the diapir, that exemplifies these characteristic facies and was compared to those on the shoulder. Sections measured across the shoulder at Little Gypsum Valley revealed occurrences of relatively drastic thickness variations (up to 50 percent) observed across short distances (less than 1km) on the salt shoulder. Careful documentation of the facies distributions also showed that the salt-sediment interaction between the shoulder and the Entrada/Carmel formations resulted in aqueous facies being present at a stratigraphically higher position than what was previously predicted and the unique presence of a paleosol in one of the sections. In addition, petrographic analysis exposed the presence of carbonate material within some petrofacies associations that is interpreted as originating from the diapir.

Table of Contents

List of Figures

Chapter 1: Introduction

Few studies have described outcrop analysis of sediments in areas with local variation in accommodation space (Giles and Lawton 2002; Matthews 2007). The unique conditions that are produced by salt tectonics allow for the observation of notable changes to facies distributions across hundreds of meters to kilometers. Understanding how unique geologic settings, such as one influenced by salt diapirism, affected paleoenvironments and potential hydrocarbon reservoirs such as the Entrada Sandstone and Carmel Formations is important to understand for analogous environments that are likely to transport petroleum accumulations (Giles and Lawton 2002). Because salt-sediment interactions are poorly understood, outcomes of studies like this one are of particular interest; not only because of how they affect potential reservoirs, but also because the impermeable nature of salt structures, which is ideal for the generation of hydrocarbon traps (Carter 1970; Pollastro 2003). An important motivation for the research that follows is to provide a valuable contribution to this limited knowledge of how these hydrocarbon reservoirs are influenced by salt tectonics.

The Gypsum Valley Salt Wall (GVSW) is a collapsed salt structure in the Paradox Basin of Southwest Colorado. It provides exceptional 3-D exposures of salt-sediment interactions with the Jurassic Carmel Formation and Entrada Sandstone (Fig. 1.5). The salt wall is in direct contact with these formations in several important locations. In the study area, the Entrada is exposed overlying salt and other older strata and exhibits changes in thickness and depositional facies can be observed over an area of approximately 2 X 3 km (Fig. 1.1). When compared to Carmel and Entrdada Sandstone Formations in Slick Rock Canyon, 13 km southwest of the diapir margin, evidence suggests that these variations can be accredited to an indirect influence of the

(GVSW). Previous studies on salt-related interactions with the Entrada and Carmel Formations are of a more structural nature and discuss the effects of faulting on stratigraphic units. Most were conducted proximal to Moab, Utah northwest of Gypsum Valley and are distal from diapir margins (Doelling 1987; Cruikshank and Ayden 1993; Foxford, et al. 1996). This study provides the most detailed and proximal analysis of salt-related depositional changes to the Carmel and Entrada Sandstone Formations heretofore completed.

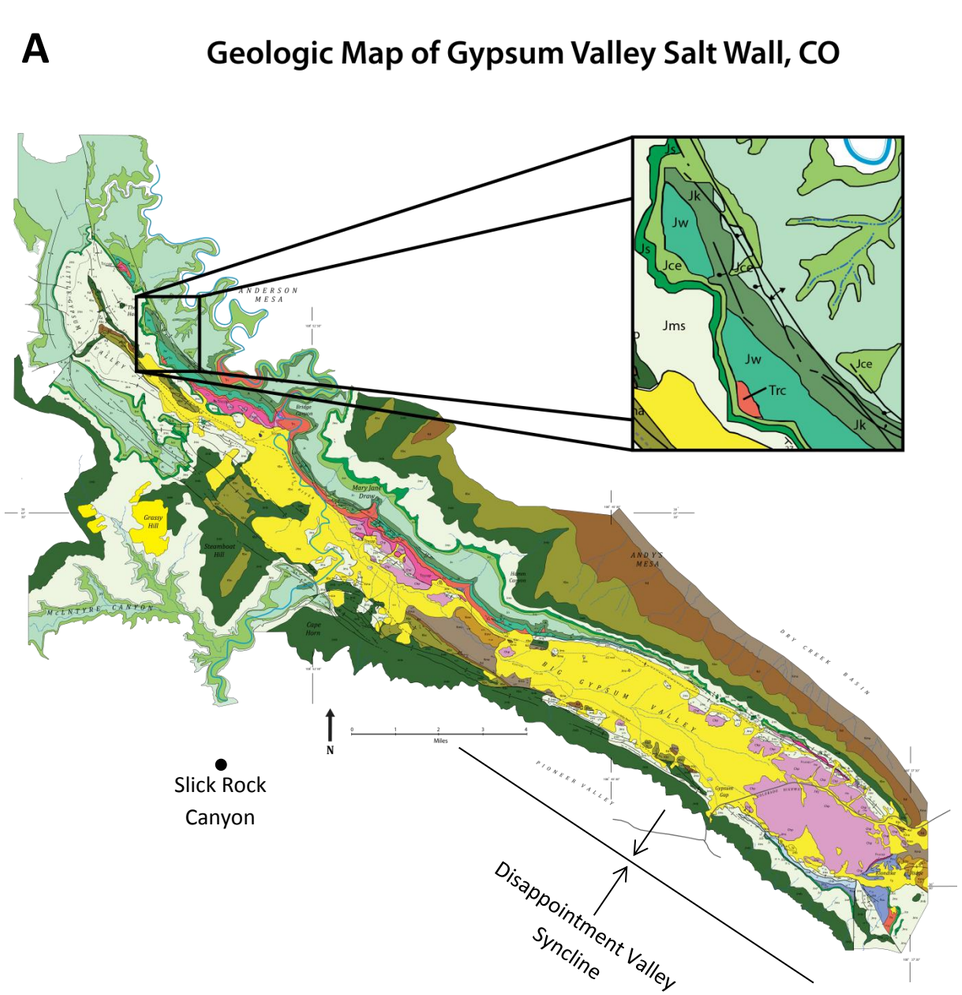

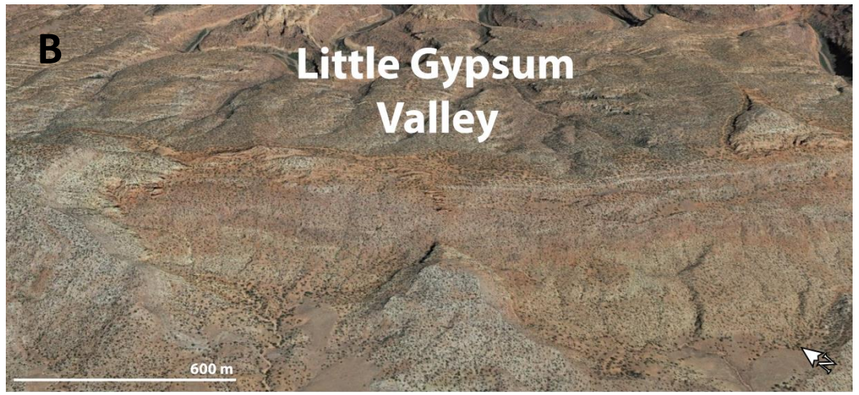

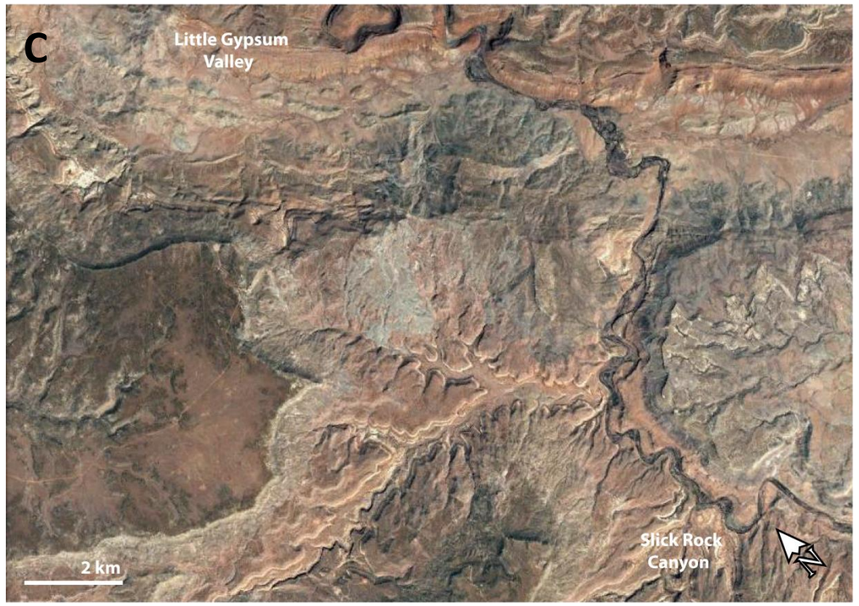

Figure 1.1: A) Geologic Map of Gypsum Valley. A black box outlines the study area and is enlarged to show the stratigraphic formations with respect to the Entrada (light green-yellow). The location of the Slick Rock Canyon section relative to the map is marked with a black point. B) Google Earth aerial map view showing the extent of the Little Gypsum Valley study study area C) Google Earth aerial map view showing the Little Gypsum Valley and Slick Rock Canyon locations to give a visual reference for the distance between them.

1.1 Background and Geological Setting

1.1.1 Paradox Basin

The Paradox Basin extends across southwestern Colorado and southeastern Utah and includes parts of Arizona and New Mexico (Fig. 1.2). The basin formed in the Late Pennsylvanian to the Early Permian and is associated with the Ancestral Rocky Mountain orogeny (White and Jacobson 1983; Barbeau 2003). The Ancestral Rockies orogeny was characterized by intracratonic block uplifts that formed in Colorado and the surrounding region (Barbeau 2003). Their development was related to the collision of North America with South America-Africa (Kluth 1981). The Paradox Basin is considered an asymmetric intraforeland flexural basin and formed as a result of thick skinned, basement cored uplifts (Handschy and Dyer 1987; Blakey and Knepp 1989; Barbeau 2003; Trudgill 2011). These types of basins form adjacent to a mountain belts as the weight of the belt creates accommodation space by causing a flexure in the lithosphere (Allen &Allen 2013). They are proximal to strongly eroding source areas and are typically filled with large thicknesses of syn-orogenic sediment (Allen & Allen 2013). Heat flows in regions with lithospheric flexure are generally normal, or can be somewhat reduced due to thickening from convergence (Allen & Allen 2013).

To the northeast, the Paradox Basin is bounded by thrust faults that separate it from the southwestern flank of the Uncompahgre Uplift (Elston, et al. 1962; Mack and Rasmussen 1984; Trudgill & Paz 2009) (Fig. 1.2). This uplift is believed to be the main source of clastic Jurassic debris to the basin (Peterson 1989; Trudgill & Paz 2009). Active subsidence took place from the Early Desmoinesian until the Middle Permian diminishing when the region became part of the Mesozoic Rocky Mountain Shelf (Peterson 1989). The rapid subsidence combined with restricted marine circulation between the distal northwest part of the trough and the open marine

to the southeast resulted in deposition of thick evaporites during the Desmoinesian (Baars and Stevenson 1981; Peterson 1989). This highland-basin boundary is where the deepest parts of the basin are located (Baars and Stevenson 1981). Compressional tectonics related to growth of the Ancestral Rocky Mountains caused rapid subsidence in the Paradox Basin along rejuvenated basement structures (Barbeau 2003; Peterson 1989). Accelerated subsidence during the Pennsylvanian resulted in flexing and faulting along the fold and fault belt and mid-basin arching along the Uncompahgre uplift (Nuccio & Condon 1996; Peterson 1989). This resulted in the separation of the Paradox and Eagle basins in to two distinct half-basins (Baars & Stevenson1981; Peterson 1989) (Fig. 1.2). The subsidence resulted in a concurrent filling of the basin with approximately 2500 meters of cyclically deposited dolostone, evaporite and shale of the Paradox Formation in the foredeep of the basin (Trudgill 2011). At the basin's forebulge, or western distal margin biohermal carbonates formed synchronously (Peterson and Hite 1969; Baars and Stevenson 1981; Trudgill 2010). In the center of the basin as many as 35-40 complete, or partially complete depositional cycles of shale, dolomite, and evaporite occured (Peterson and Hite 1969; Peterson 1989). These cycles were driven by various factors including eustatic sea level change from glaciation and seafloor spreading, local changes in clastic influx, climatic effect, and basin subsidence rates (Nuccio & Condon 1996; Peterson 1989).

Depositional extent of the Paradox Formation is what defines the geographic boundaries of the Paradox Basin (Condon 1997) (Fig. 1.2). Diapirism began as a consequence of differential loading of the evaporites resulting from localized sediment overburden when an alluvial wedge at the southwest margin of the Uncompahgre uplift prograded southwest during the Late Pennsylvanian to Early Permian (Mack and Rasmussen 1984; Barbeau 2003, Trudgill and Paz 2009) formed in the north portion of the basin (Doelling 1988, Trudgill, et al. 2004) (Fig. 1.2).

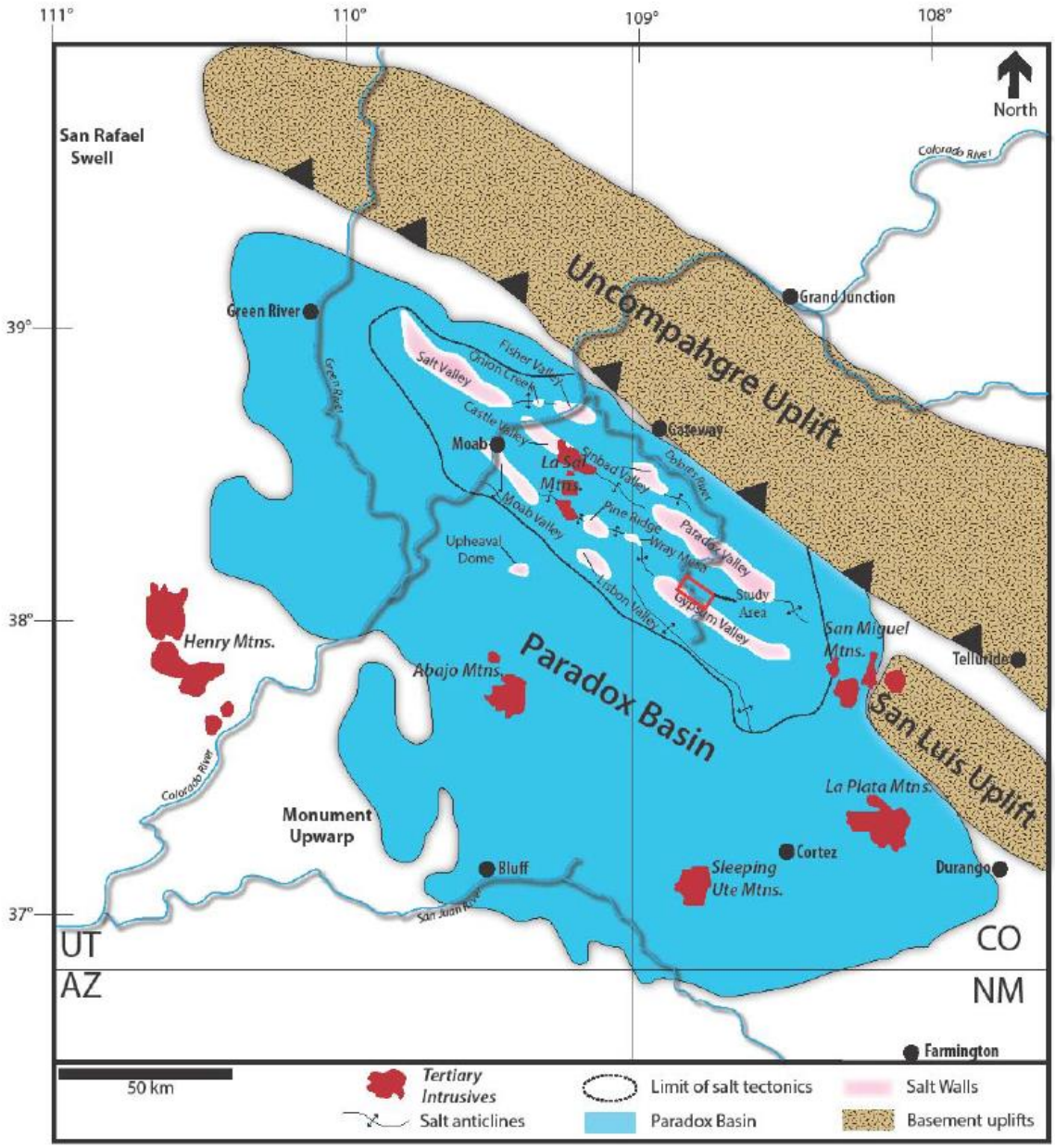

Figure 2.2: Map view of Paradox Basin extent and tectonic features. The location of the study area with respect to the Gypsum Valley Salt Wall (GSVW) is outlined by the red box. Extent of the paradox evaprorite is from Condon, 1997. Distribution of the salt walls is from Shoemaker, et al. 1958.

Units of Jurassic and Triassic age have been observed to thin on the flanks of salt anticlines and thicken in synclines (Cater 1970). Sediment thickness and facies depositions was influenced by salt withdrawal mini-basins developed adjacent to the flanks of steep sided salt walls (Doelling 1988, Trudgill, et al. 2004) (Fig. 1.2). The primary mechanism for salt structure growth is understood to be passive diapirism, which was followed by possible shortening during the development of the Sevier Foreland Basins during the Laramide orogenic event (Grout and Verbeek 1997; Trudgill, et al. 2004). These salt anticlines and accompanying synclines trend northwest roughly parallel to the orientation of the Uncompahgre Plateau and likely parallel with post salt deposition basement faults being confined to the Paradox fold and fault belt (Shawe, et al. 1968; Trudgill, et al. 2004, Trudgill and Paz 2009) (Fig 1.2). Regional west-east shortening may have folded the salt diapirs during the Laramide Orogeny (Rasmussen 2015). Salt dissolution is attributed to normal faults that typically strike parallel to the salt wall structures (Trudgill 2011). Paradox Basin salt structures were buried with an overburden thickness of over 1.6km during the Late Jurassic to Early Cretaceous and continued through the Paleogene 5 million years after the end of the Laramide Orogeny (Rasmussen 2015). During the Neogene, extensive incision within the Rocky Mountains and Colorado Plateau exhumed diapir evaporites, and the relatively wet climate during the Pleistocene increased erosion and dissolution that led to the collapse of salt anticlines (Rasmussen 2015). During this time, approximately 3km of overburden were also eroded (Nuccio and Condon 1996). In the Neogene, extension may have significantly modified the diapirs through formation of large normal faults (Ge and Jackson 1994)

1.1.2 Gypsum Valley Salt Wall

Gypsum Valley is an exhumed elongate salt diapir that trends NW-SE. Its length is approximately 50 km and has a relatively uniform width at approximately 3.2 km (Cater 1970). The Cretaceous and Upper Jurassic units that make up the hogback ridges surrounding the valley are inclined more steeply, and reveal the interactions between the salt core and overlying stata better than those of the Paradox and Sinbad valleys (Cater 1970).

Gypsum Valley can be divided into two domains or sections. In the southeast, exposed diapiric caprock of the Paradox salts are exposed, with a few blocks of Latest Jurassic Morrison Formation and Cretaceous strata exposed, within the salt near the rim of the diapir (Fig. 1.1). In contrast, Little Gypsum Valley to the northwest is largely covered under Jurassic and younger strata, with Carmel and Entrada Formations as well as Morrison formation forming the basal units, in contact with the salt (Stokes and Pheonix 1948; Cater 1970) (Fig. 1.1).

On the northeast side of Little Gypsum Valley unconformable relations are well exposed including the Entrada Sandstone and Carmel Formation.

At Little Gypsum Valley, the Gypsum Valley anticline curves northward and collapse blocks are interpreted as a consequence of downfolding, rather than faulting (Cater 1970). This area provides a well exposed basin, within the salt at the top of the diapir, which is lined by Entrada and Carmel formations that form a shoulder on the diapir (Fig. 5). Stratal geometries that flank and overly the salt shoulder are associated with an antiformal trap that is bounded by post-depositional faults (McFarland 2016) (Fig. 1.3).

A salt shoulder forms a zone at the margin of a salt diapir where the margin steps relatively abruptly inward. Salt shoulder strata display parallel to onlapping geometries and often overlie regional subaerial or submarine unconformities that truncated the crest of the diapir. The

shoulder may be progressively rotated and upturned by drape folding as the inboard part of the diapir continues to rise. As this happens, topography on the rising part of the diapir may confine sand prone channel facies to the shoulder area resulting in stacked sand-prone reservoir facies in the onlapping shoulder strata. Shoulders form when the salt rise rate near the margin of the diapir substantially decreases or stops relative to the salt rise rate in the inboard central part of the diapir (McFarland, et al. 2018) (Fig. 1.3).

During the Morrison time, the Entrada and older formations were folded into the syncline, subsiding to form a basin in Little Gypsum Valley (Fig. 1.5). Basin formation began after the initial deposition of the Morrison Formation (Bailey, 2016). The Entrada now sits unconformably on Kayenta and the salt within the study area. Today, the Entrada forms an anticline, with the southwestern limb dipping SW into the diapir, and the crest runs through the NE part of the study area. Subsequent faulting and folding that postdates the Entrada occurred as a result of flexure in the basin.

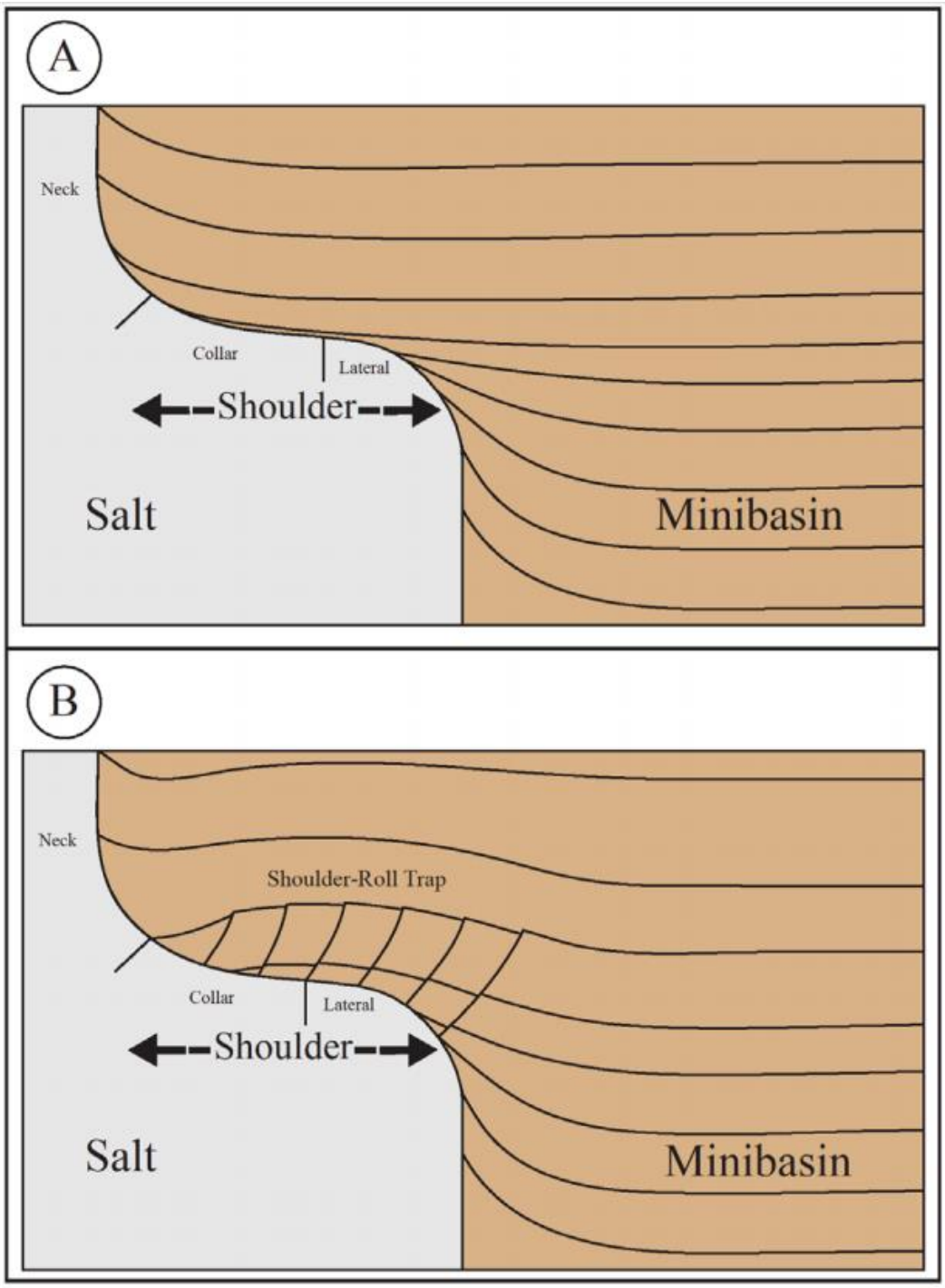

Figure 1.3: Conceptual models that illustrate A) stratal geometries of flanking and overlying a salt shoulder structure without a rollover anticline trap associated with it, and B) stratal geometries flanking and overlying a salt shoulder with associated antiformal trap bounded by post-depositional faults (McFarland 2016)

1.2 Previous Research

1.2.1 Carmel Formation

The Late Jurassic Carmel Formation is interpreted as being deposited during two major transgressive cycles in both offshore and shoreline environments of the southern margin of the Western Interior Seaway (Cater 1953; Blakey, et al. 1983) (Fig. 1.4). Prevailing evidence for a hot, arid climate is found in the abundance of evaporated present throughout the Carmel (Kocurek, 1981). It consists largely of red to buff, non-resistant, horizontally bedded siltstone, mudstone, sandstone, and carbonates (Carter 1953; Blakey, et al. 1983). This diverse set of lithologies suggests marine, sabkha, shoreline, eolian, and fluvial environments (Blakey, et al. 1983). At the base of the formation abundant pebbles with angular fragments of white to grey chert, as much as an inch across, are scattered and locally form bands of conglomerate (Cater 1953). Carter also observed barite nodules towards the top of the formation. The Carmel has also been described as a calcareous silty red unit that displays spheroidal weathering and extensive bands of white spots reaching thickness of a foot are present along some bedding planes. (Harshbarger, et al. 1957; O'Sullivan 2003). In some places, impersistent sand lenses of various sizes pass laterally into siltstones (Foxford et al. 1996).

In other studies regionally proximal to Gypsum Valley, the Carmel ranges from 6 to 11 m thick (Simmons and Archbold 1956; Shawe, et al. 1968). It has been described as a reddish-brown siltstone to very-fine sandstone with spheroidal weathering (Simmons and Archbold 1956; Shawe 1968; O'Sullivan 1981). Grain size experiences a grading upward sequence to the Entrada in most places (Carter 1953). Grain size is predominantly fine grained sands and silt and is moderately sorted (Foxford et al. 1996). It displays massive textures, horizontal bedding and Entradaberries, or coarse white chert grains (Shawe 1968 et al.; O'Sullivan 1981). Formation

thickness is relatively uniform and displays only slight erosional irregularities (Carter 1953; Shawe 1968). It is interpreted as being a nearshore marine environment (Shawe, et al. 1968; O'Sullivan 1981).

1.2.2 Entrada Sandstone

The Late Jurassic Entrada Sandstone is a complex and extensive eolian system that stretches across portions of Utah, Colorado, Wyoming, Arizona, New Mexico, and Texas (O'Sullivan 1981; O'Sullivan 2003; Lucas 2014) (Fig. 1.4 and Fig. 1.1). It was deposited on the eastern flank of the Cordilleran geosyncline (Kocurek 1981). In addition to sediment from the Uncompahgre uplift, the J2 unconformity eastward of the depositional termination is characterized by curving channel deposits of pebbly sandstone providing a significant sediment source to the Entrada (Kocurek 1981) (Fig. 1.2). Stratigraphic reconstruction indicates the Entrada erg occupied a cratonic basin bounded on the north, west, and parts of the south by continental, shallow marine, and sabkha deposits (Kocurek 1981; Crabaugh & Kocurek 1993). Northwestern progradation of the Entrada erg accompanied the regional retreat of the Carmel sea during Early to Middle Callovian (Kockurek 1981). Stratigraphically, after initial progradation of the Entrada these marine-sabkha and eolian units stack vertically and subsequently the marine-sabkha units onlap onto the eolian sand units of the Entrada (Pipiringos & O'Sullivan 1978; O'Sullivan 1981; Lucas 2014; Crabaugh & Kocurek 1993). Paleowind directions (NW-SE) suggest that the overall circulation pattern of the Entrada formed by trade winds, sea breeze effects, and frictional drag of the wind over land. Previous measurements have revealed the mean paleowind direction is roughly south at the northeast extent of the Entrada erg, becomes progressively NE-SW towards the southeastern extent, and is relatively variable towards the western extent (McKee 1956, Otto & Picard 1975, Kocureck 1981). Evidence for storm events

is found in interdune deposits where sedimentary structures of more paleocoastal areas indicate frequent flooding and deposition by flowing water (Kockurek 1981). Development of the Entrada was terminated by widespread by widespread transgression from the north in Middle Callovian time (Kocurek 1981).

The Entrada is composed of a coarse sandy unit above the Carmel that weathers into rounded cliffs. According to O'Sullivan 2003, these facies occur in three distinct members; two clean sandy facies separated by a red silty facies that range in color from moderate reddish orange to grayish orange pink. Doelling (1987) described it as a massive sandstone cliff former with well-developed large scale cross-stratification of eolian origin. In some instances the lower part of the Entrada has been described as discontinuous eolian dune sandstones interbedded with muddy to sandy sabkha and interdune siltstones indicating interdune flooding (Crabaugh and Krokurek, 1993, Foxford, et al. 1996). Additionally, the upper part of the entrada is comprised of interbedded eolian interdune and dune deposits that become large scale eolian dune sets up section (Foxford et al. 1996). Cross strata of the Entrada proximal to the paleocoastline are notably smaller than other places on the scale of a few meters in width as opposed to upwards of 80 meters (Kocurek 1981). Inland margins of the erg are characterized by eolian reworked wadi deposits, small dunes and wind ripples (Kocurek 1981). Sand sheet deposits are local, but persistent throughout the Entrada, which is uncommon in other eolian formations suggesting that these sandy facies may have been deposited in water. Alternating layers of cross stratified and plane bedded sandstone is also common (Fryberger 1979; Kocurek 1981; O'Sullivan 2003). Some coarse well-rounded white and amber colored quartz grains are concentrated along the bedding planes in many places (Foxford et al. 1996). Formation thickness is typically very

uniform in the Entrada thinning and abruptly terminating at the first pronounced break in slope, which is consistent of most modern ergs (Kocurek 1981).

In previous studies regionally proximal to Gypsum Valley the Entrada Sandstone ranges in thickness from 30-40 meters (Simmons and Archbold 1956; Shawe 1968). It is described as a reddish orange to grayish pink unit that weathers into smooth cliffs (Simmons and Archbold 1956; Shawe 1968). Three units are recognized based on primary sedimentary features that include massive, cross-bedded, and horizontally bedded sandstones. (Shawe 1968, O'sullivan 2003). The sandstone is composed of fine-medium grains that coarsen slightly and mature upwards. Grains are subrounded to subangular sand and are moderately well- sorted (O'Sullivan 2003).

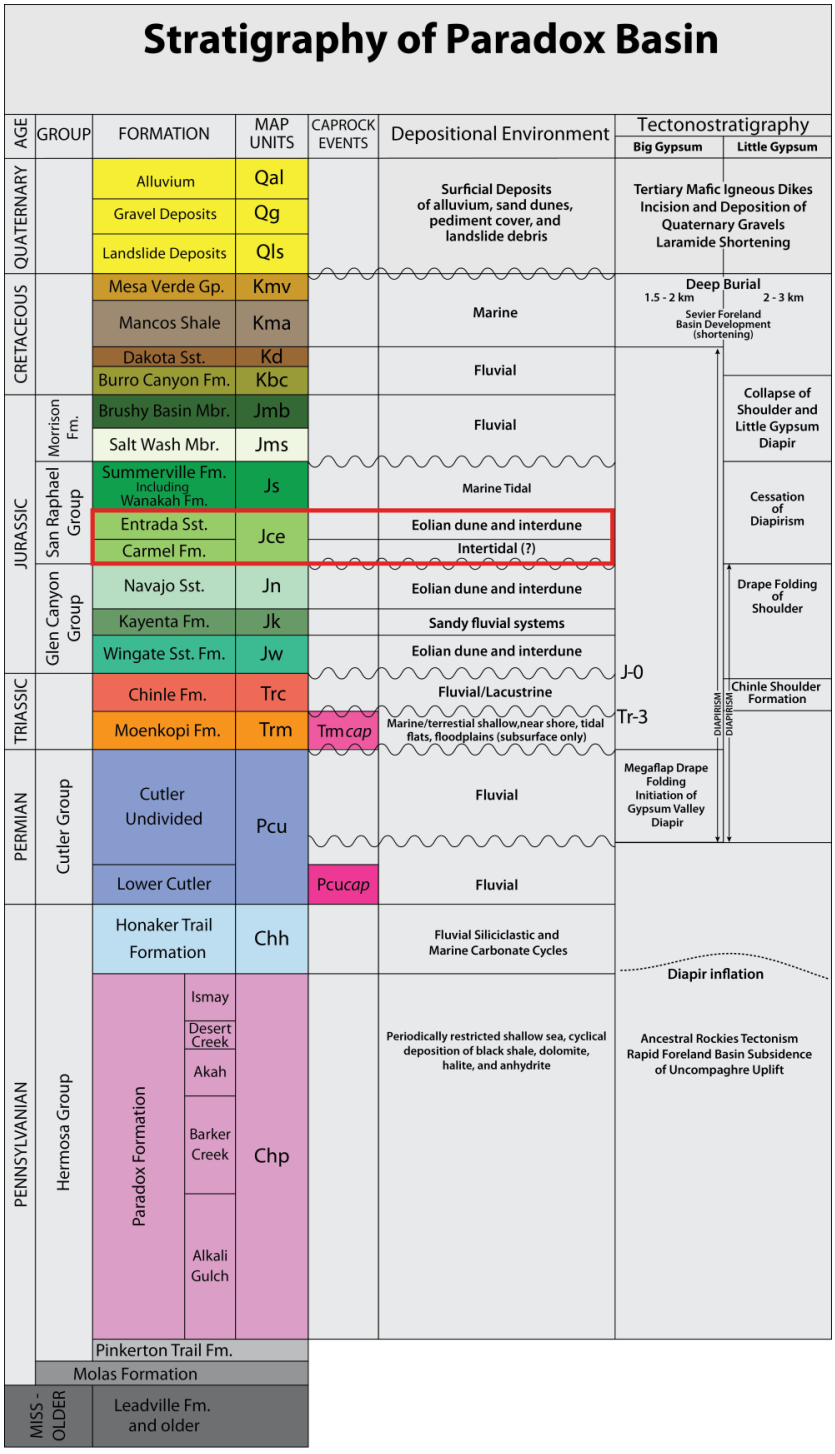

Figure 1.4: Stratigraphic column of units in the Northern Paradox Basin of the Gypsum Valley area. Colors match those on the geologic map (Fig. 1.1). Depositional environment, events and controls are after Stokes and Phoenix (1948); Doelling (1998); and Trudgill (2011). Formations of interest are outlined by a red box.

1.3 Study Area

The area of interest for this study is located at the northeastern portion of the (GVSW) in Little Gypsum Valley (Fig. 1.1). A cross-sectional view of units can be seen on top of the crest of the salt shoulder and continue down the flanks as they dip into the diapir eventually continuing into the subsurface beneath the Summerville and Morrison Formations. Exposed units of the Entrada Sandstone and Carmel Formation at Little Gypsum Valley allow for an in depth study of the study of facies variations both along strike and perpendicular to it. An additional stratigraphic section was collected at Slick Rock Canyon (13km to the southwest of the GVSW) to compare equivalent formations that are distal from GVSW and, therefore have remained affected by salt tectonics (Fig. 1.1). Fracturing related to salt tectonism has caused varying degrees of alteration from fluid flow in nearly all exposures giving a yellowed appearance to affected units.

The study area is located in the best exposed part of the Entrada Shoulder (Fig. 1.5). The outcrops resemble an amphitheater in their geometry shaped by a small amount of subsidence at the NE part of the study area and local folding towards the SW (Fig. 1.1 and 1.5). The study area extends to just outside of the shoulder moving up and over the shoulder crest and continues approximately 400 meters as their units dip to the southwest of study area into the valley below. The southwest edge of the outcrops marks their burial under younger strata of the Morrison and Summerville Formations (Fig. 1.5). The salt shoulder extends to the margin of the diapir at the northeast marked by the crest of the anticline and progresses down into a syncline formed during Morrison time (Fig. 1.5). The salt shoulder extends approximately 5 kilometers to the southwest, to where no Entrada outcrops are found and it inferred that the diapir continued to rise until Morrison deposition (Fig. 1.5)

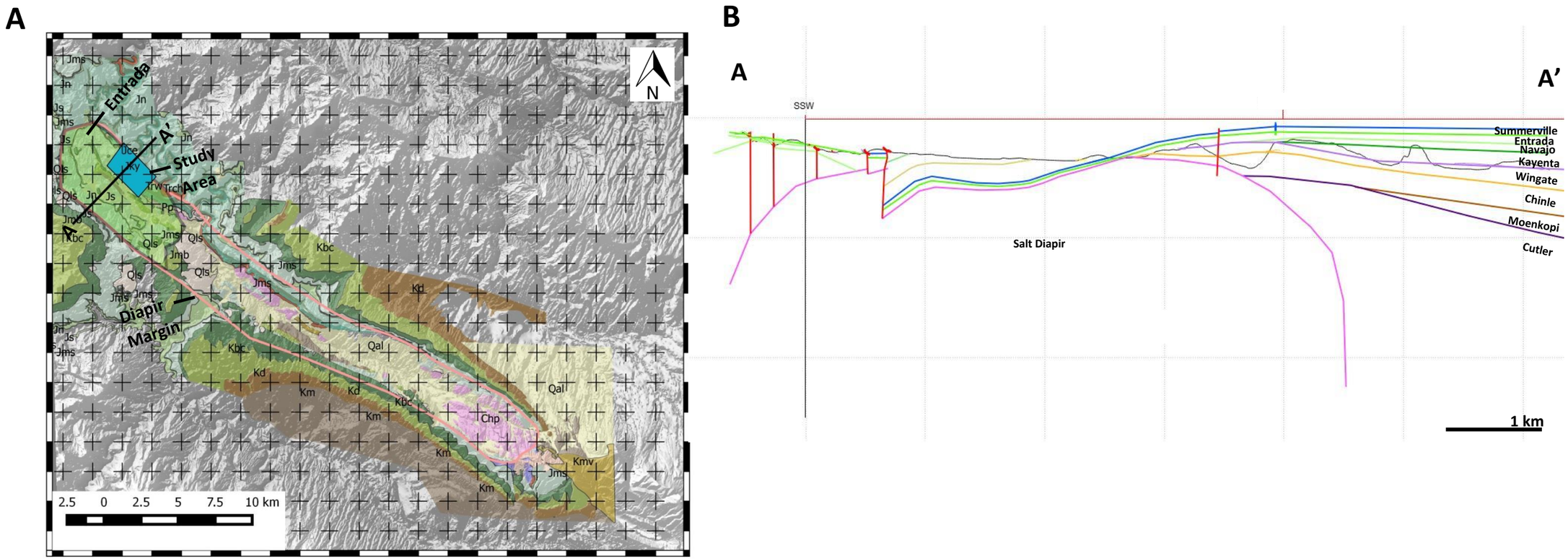

Figure 1.5: A) Map view from QGIS showing the extent of the Gypsum Valley Salt Wall outlined in pink, the extent of the Entrada over Little Gypsum Valley (green-yellow), the study area (blue box), and cross-section line (A-A') through the study area that corresponds with (B) B) A cross-sectional view across the study area showing the geometry of the Entrada and adjacent formations as they come into contact with and move over the salt shoulder eventually dipping below the surface. Line SSW to the left of the image is not relevant to this study (REF).

1.4 Methods

Detailed macroscopic descriptions and analysis of both typical and atypical facies, as well as alterations caused by fluid flow, were combined with a microscopic examination of 30 thin sections to best infer environments and sources of clasts. Surfaces were traced and correlated in the field with photo panoramas to illustrate and understand strategic changes associated with salt tectonics and facies variations (Fig. 1.5). This was done by taking photos on a computer tablet and later using Adobe Illustrator software to trace the geometries onto the images.

A detailed geologic map was created with Move software by Midland Valley to display the aerial geometries of the Entrada/Carmel and surrounding formations as well as strike/dip data, paleowind directions, and fault locations. Because the formations of interest are too steep and cliff forming in nature, displaying the individual facies changes in an aerial map view is not effective for this study. Nine stratigraphic sections were measured on the salt shoulder ranging from approximately 20-50 meters in thickness and their locations extend from the northeast margin of the diapir to its center (Fig. 3.1). Sections were measured and correlated using a Jacob staff, Field Move tablet software, and located using a GPS, and physically tracing marker horizons on photo panoramas to create a complete stratigraphic cross section to estimate thickness variations and document facies distributions. Sections include measurements of sedimentary structures, bedding geometries, and contact types. Eolian dune foreset dips were used to reconstruct paleowind direction. A combination of these observations was used to interpret depositional environments from genetically related facies. The grain size variations, facies percentages, and other features of each section were compared to evaluate the impact of the diapir on the Entrada Sandstone and Carmel Formation. One additional section was measured

in Slick Rock Canyon, 13 km to the southwest of the diapir, for comparison of equivalent units that remain unaffected by local salt tectonics (Fig. 1.1). Facies transitions across the area were also thoroughly documented to determine the stratal and environmental relationships between different facies associations.

In addition to facies and stratigraphic correlation, petrographic analysis of thin sections was used to document and compare the overall composition of samples both on the salt shoulder and those at Slick Rock Canyon. Diagenetic changes related to fluid flow in and adjacent to the diapir were also analyzed. Over fifty hand samples were collected in the field up stratigraphic sections and carefully chosen to encompass all of the key facies observed. Their locations were documented using a handheld GPS device. Thirty-three samples were subsequently cut to billet sized dimensions before being sent to Spectrum Petrographics to create the thin sections. Half of each sample was stained red for calcite and the entire sample was stained with a blue epoxy for porosity. Three-hundred points were counted on each sample to estimate their lithologies. Thirty of the samples were then classified into petrofacies based on their grain type, cement and porosity percentages. Compaction, roundness, and sorting were also verified microscopically.

Chapter 2: Entrada and Carmel Lithofacies and Facies Associations:

2.1 Lithofacies

Eleven lithofacies were classified during analysis of measured sections and outcrops in Little Gypsum Valley (Fig. 1.1 and 3.1). The facies were then grouped into eight facies associations. Lithofacies identified include: Siltstone with lag deposits, current ripple cross-stratified siltstone, flaser bedded sandstone, white reduced siltstone horizons, structureless/mottled bioturbated sandstone, thin ledge-forming trough cross-bedded sandstone, trough cross-stratified sandstone, wind ripple cross-stratified sandstone, wave ripple cross-stratified sandstone, poorly consolidated shale, and structureless/mottled bioturbated sandstone.

2.1.1 Siltstone with lag deposits-

This facies typically occurs at the base of the Carmel Formation and ranges in thickness from approximately 0.5 to 1.5m (Fig. 2.1 A). It rests in angular unconformity with a sharp contact atop the Kayenta and Navajo Formations (Fig 2.4). The facies is primarily composed of very-fine sand and silt-sized particles, and contains bands of coarse angular gravel throughout. It is predominantly a brick red color and its exposure is often only partial and irregular within a covered slope. Beds contain matrix supported clasts of distinctive white chert and rock fragments. The coarse grains are granular 2mm-1cm and make up approximately 20% of the unit. The beds are horizontally laminated, and near the top of the unit there is a 20 cm thick band composed of siltstone with spotted casts of evaporite with diffused boundaries (Fig. 2.1 B). The siltstones beds that alternate between the coarser beds are approximately 15 cm thick with irregular contacts.

2.1.2 Current ripple cross-stratified siltstone-

Current ripple cross-stratified siltstones and very-fine grained sandstones are found throughout the Carmel Formation (Fig. 2.1 C). Thickness ranges from 5-15cm. Beds weather smooth on rounded or spheroidal surfaces. Ripples internally exhibit an upward fining pattern indicating aqueous deposition (Shaw, et al. 1999). Grain size of the units that confine this facies is overall fine grained sandstone. Contacts with this facies are normally gradational. The color is typically a brick red except where altered and reduced by fluid flow along later fractures where units become yellow in color (Fig. 2.1 D). Ripple cross-strata are only visible within beds over distances of centimeters to a few meters.

2.1.3 Flaser bedded sandstones-

Flaser bedded sandstones can be found throughout the Carmel Formation (Fig. 2.1 E). Bed thicknesses range from 10 to 30 cm. Contacts between these beds appear to be scoured. Individual beds of silt and very-fine sandstone within these units themselves are typical of flaser beds (5mm-1cm) (Reineck and Singh 1980, Terwindt 1988). There is a color distinction between the fine-grained sand beds which are pink in color and the silt lenses that are the customary brick red of the Carmel. Although there are a few instances where flaser bedding is continuous across hundreds of meters, its presence is typically disrupted by bioturbation. In some places, the flaser beds have undergone soft sediment deformation distorting the subhorizontal deposition of the original layering (Fig. 2.1 E).

2.1.4 White reduced siltstone horizons-

Two extensive horizons within the Carmel Formation appear that can be distinguished by their irregularly shaped white reduced patches that contrast to the characteristic brick red color (Fig. 2.1 F). Although they are thin (~20 cm), they are surprisingly continuous in coutcrop. Therefore,

they can be correlated on the scale of at least a few kilometers. The facies consists of silt sized grains. They occur at unit boundaries above scoured surfaces. One is approximately in the middle of the Carmel, and the other is near the top. The contacts where these reduced beds form appear to be less resistant to weathering when compared to the surrounding rocks, which jut out above and below it (Fig. 2.1 F).

2.1.5 Structureless/mottled bioturbated siltstone –

Perhaps the most common facies within the Carmel formation are the massive beds where traces of the more defining sedimentary structures have been disrupted, or masked (Fig. 2.1 G). Patches of mottling and burrows can be observed sporadically throughout the unit signifying that the structureless beds are the result of bioturbation. At the base of the Carmel Rhizocorallium burrows are distinguishable amongst the basal lag portion of the Carmel which is consistent with a marine environment (Fig. 2.1 B) (Leckie and Walker 1982).

2.1.6 Thin ledge forming trough cross-bedded sandstone-

A few occurrences of a thin (0.5-1.5 m) white eolian facies with small trough cross-beds is present (Fig. 2.1 H). It is bound by sharp contacts and contains medium upper size grains. This facies has a consistent weathering style reminiscent of a popcorn ceiling texture (Fig. 2.1 I). It is generally a ledge former, being more resistant to weathering than the beds above and below it. However, in some places there is no differential weathering and it is only distinguishable by its texture, foresets that exhibit eolian wind ripples and grain flow deposits (Hunter 1977), and white coloring (Fig. 2.1 I). In most sections on the salt shoulder (except 3 and 4), there is a current-ripple cross-stratified pink silty sandstone bed at the top of the Carmel that is approximately 0.5m thick with silt sized to fine sand grains that shares the same popcorn weathering characteristic as the eolian component above it (Fig. 2.1 H).

2.1.7 Trough cross-stratified sandstone-

The most common facies encountered within the Entrada Sandstone formation are troughs that contain cross beds that exhibit wind ripple laminae and grain flow strata (Fig. 2.1 J). The foreset beds are 5-50cm thick. Cross stratified sets are bounded by sharp erosional surfaces. Grain size ranges from medium to coarse and are well-rounded and well-sorted. The coarser sediments are generally found as separate laminations within the grain flow deposits of the barchanoid dune formations and are slightly more resistant to weathering. These beds can range in color from pink to red-orange and white units. All of the marker beds within the Entrada contain cross-bedding, but it is more distinguishable in areas where less erosion has taken place. Another distinguishing feature of these eolian beds on the salt shoulder is the presence of small white chert grains throughout termed 'Entrada Berries' (Wright, et al. 1962) (Fig. 2.1 K).

2.1.8 Wind ripple cross-stratified sandstone-

Wind ripple cross stratified intervals are commonly found throughout all units of the Entrada and can be either well defined, or only hints may be present following heavy bioturbation (Fig. 2.1 L). Thickness ranges from 10 centimeters to upwards of a meter. Wind ripple facies coarsen upward (Reineck and Singh 1980) and their grain size is generally medium to coarse grained in contrast to the units confining the facies, which are overall more fine. Sometimes the coarser nature of the wind ripples makes them more resistant to weathering causing these thin beds to protrude slightly on an otherwise smooth surface (Fig. 2.1 L). Contacts can be either sharp, if in contact with another eolian facies, or gradational if in contact with an aqueous facies. They can be correlated laterally across most units that are on the salt shoulder except for 2, 6 and 7 where they experience intertonguing with current ripple cross-stratified sandstones (Fig. 2.10).

2.1.9 Wave ripple cross-stratified sandstone

Wave ripple cross-stratified sandstone beds generally have two stratigraphic occurrences within the Entrada Sandstone, except when affected by intertonguing (Fig. 2.1 M). Thickness ranges from 20 centimeters to over 3 meters. Wave ripple facies fine upward (Reineck and Singh 1980) ranging from medium to very-fine in contrast to the units confining the facies, which are overall fine grained. Eolian facies in contact with aqueous facies exhibit gradational contacts. Wave ripple cross-stratified bedding is difficult to correlate laterally since it often becomes disrupted by bioturbation, or eolian facies in units where they are interbedded (Fig. 2.1 M).

2.1.10 Poorly consolidated shale-

The Entrada Sandstone at the northeastern portion of the study area contains a thin, friable and dark purple shale layer (Fig. 2.1 N). Weathering is platy and it erodes more readily compared to the units that bound it. Thickness is moderately consistent at approximately 10 centimeters. It is laterally extensive for less than 100m before it becomes lost in outcrop. The bounding contacts are sharp. Below lies a dark red massive paleosol and above lies wave ripple cross stratified sandstone (Fig. 2.1 N). It is only present in measured Section 4 (Fig. 2.1.).

2.1.11 Structureless/mottled bioturbated sandstone-

A number of the eolian beds in the Entrada Sandstone lack distinctive bedding and sedimentary structures may be difficult to see, are discontinuous, or may not present at all (Fig. 2.1 O). These structureless textures result from bioturbation. Thickness ranges from approximately 2-3 meters. Grain size is generally fine sand, but there are often coarser grains included in the matrix. Units containing these facies are generally in contact with units that contain wet interdune facies. Burrows and mottling are sometimes visible, and disrupt the bedding patterns that are typically expected in eolian dune deposits (Fig. 2.1 O). Overall, these massive facies can be correlated

laterally, but they can be briefly interrupted by short intervals where sedimentary structures are still distinguishable.

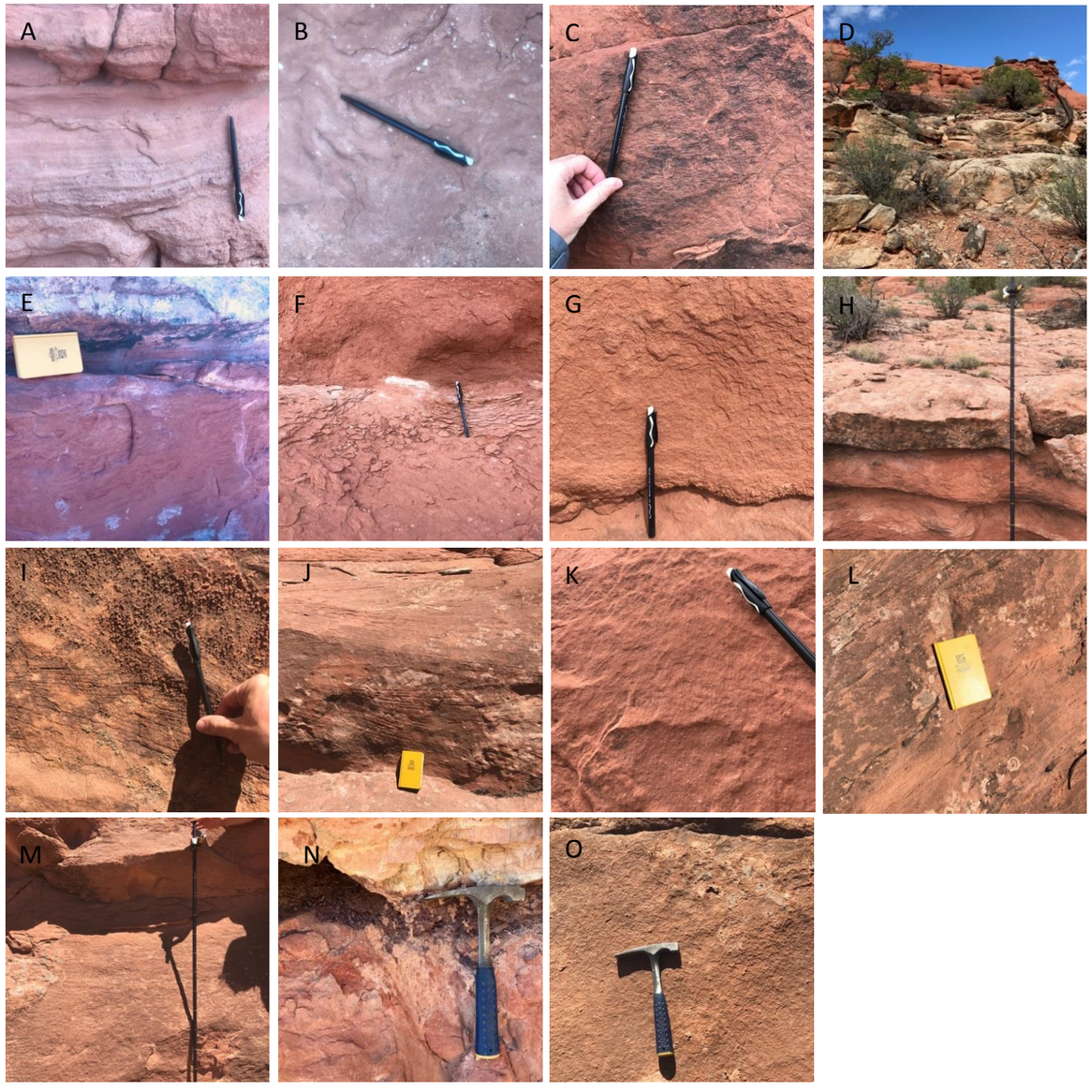

Figure 2.1: A) Lag deposits (Secion 2, C1) B) Rhizocorallium burrows and evaporate casts with diffused boundaries (Section 2, C1) C) Current Ripples (Section 1, C3) D) Yellowing from fluid alteration (Sectopm 9) E) Flaser bedding with soft-sediment deformation (Secion 2, C5) F) White reduced siltstone horizon (Section1, C6) G) Structureless siltstone (Section 4, C3) H) Small white ledge forming dunes and pink transitionary facies below (Section 1) I) Popcorn weathering and small foresets (Section 2, E1) J) Large trough cross-stratified sandstone (Section 1, E5) K) Entradaberries (Section 1, E5) L) Wind ripple cross-stratified sandstone (Section 5, E3) M) Wave ripple cross-stratified sandstone (Section1, E4) N) Poorly consolidated shale (Section 4, E2) O) Stuctureless sandstone (Section 9, E5)

2.2 Facies Associations

2.2.1 Facies association 1: Tidal flat deposits

2.2.1.1 Description-

This facies is found only within the Carmel interval. Beds of tidal flat strata are a distinct dark red color and range from 0.5-3 meters thick when fully exposed (Fig. 2.10). They are laterally extensive for hundreds of meters and contacts between them are typically scoured. Two of these beds display a horizon of dappled white reduction spots in the top. Well-defined bedding within these facies associations is often not visible due to the sediments having been reworked by bioturbation and soft-sediment deformation (Fig. 2.2). FA-TF can be distinguished from other facies associations on the basis of its finer grain size, which ranges from silt to very fine sands, and lack of eolian facies with a few minor exceptions. Grains also appear to be well sorted, except where coarse lag deposits and evaporate crystals are present. Based on petrographic analysis grains were determined to be rounded-subrounded. The primary sedimentary structures include flaser bedding, aqueous ripple cross-strata, lag deposits, mottling, and bioturbation that often disrupts the fabric of other sedimentary structures (Fig. 2.2).

2.2.1.2 Processes-

At the base of the Carmel Formation, bands of pebble lag deposits are present indicating ravinement during transgression (Cattaneo and Steel 2003). They are interbedded with fine silts, which suggest they were deposited in an environment with a lower energy setting (Cattaneo and Steel 2003). The red color of the silts indicates that the grains have been oxidized except at certain contacts where reduced white horizons are present and potentially form as a result of bacterial reduction activity (Jacobson 1994). The presence of scoured contacts is an expression of erosion by a strong current flow. Evaporite crystals that are present signify intermittent

desiccation of the tidal flat (Kinsman 1969). The presence of flaser bedding indicates considerable fluctuation of flow energy that accounts for the alternating layers of silt and sand that are often encountered in tidal settings, and sometimes interdune processes (Reineck and Wunderlich 1968, Nio and Yang 1991, Doelger 1987). The occurrence of small-scale ripple cross-stratification in siltstone indicates a waning subordinate current (Nio and Yang 1991). Disruption of flaser bedding, ripples, and other sedimentary structures by bioturbation and mottling is implies the presence of organisms reworking the sediments (Driese, et al. 1981).

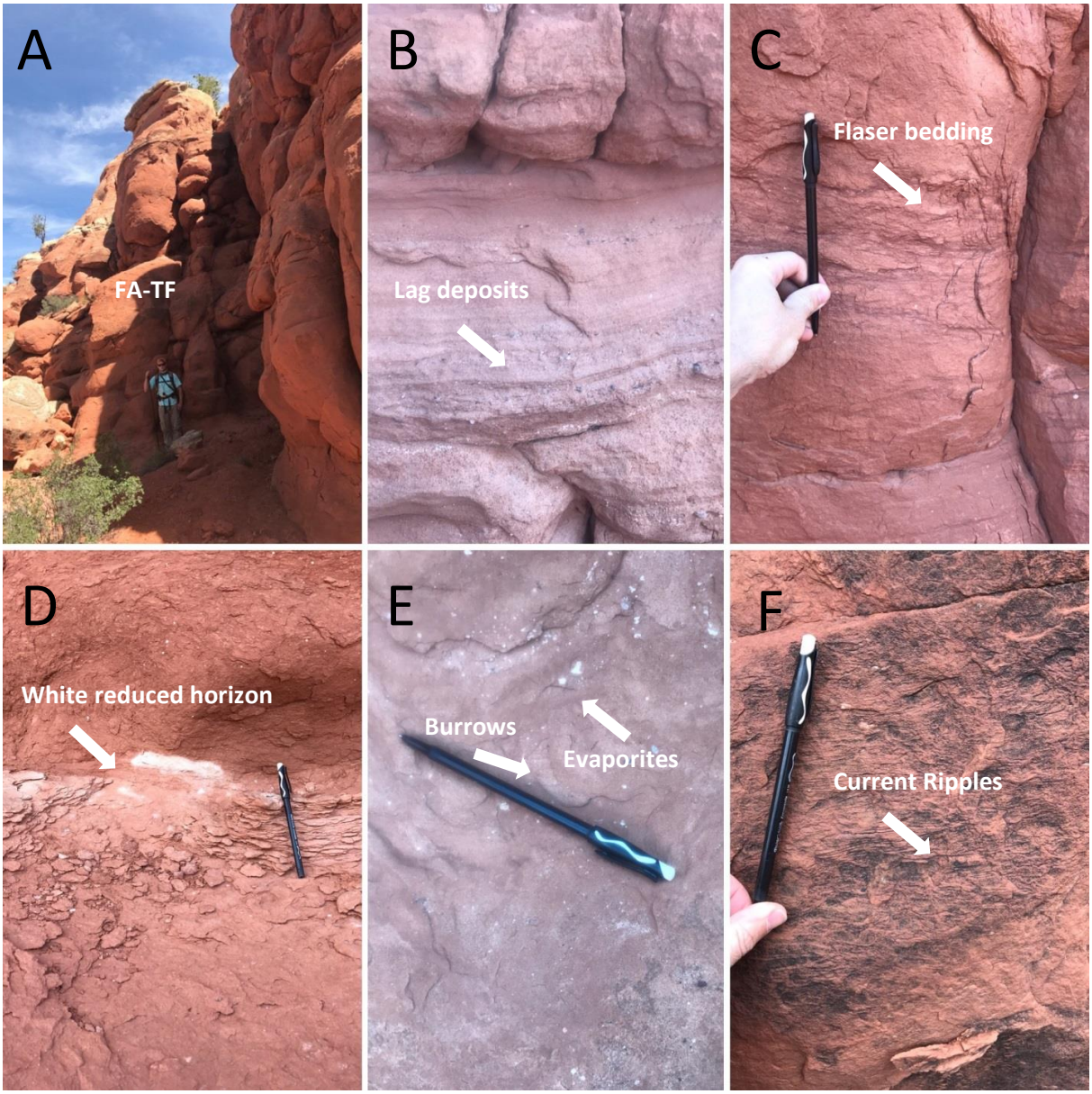

Figure 2.2: A) Outcrop photo of FA-TF (Section 6) B) Silt deposits with continuous bands of pebble lag (Section 2, C1) C) Laterally discontinuous band of flaser bedding (Section 2, C5) D) White reduced horizon experiencing differential weathering compared to rocks above and below (Section 1, C6) E) Sedimentary structures disrupted by burrows and coarse evaporite crystals (Section 2, C1) F) Current ripple cross-stratified silty sandstone (Section 1, C3)

2.2.2 Facies Association 2: Wet interdune deposits

2.2.2.1 Description-

Beds of aqueous facies occur between the classic eolian dunes of the Entrada Sandstone formation (Fig. 2.10). These aqueous facies are notably finer grained as compared to the typical eolian dune outcrops. Beds of aqueous ripples that are part of these facies range from 0.5-1m in thickness and generally display an asymmetrical wave ripple pattern (Fig. 2.3). The ripples are typically smaller at the bottom of these beds and increase in size towards the top as they transition back into eolian facies. Small amounts of flaser bedding in this facies association are sometimes found at the southern portion of the study area, but they are not a common occurrence. Bioturbation and burrowing is always present, but in varying degrees and, in some cases, increases either upwards or downwards. Burrows and mottling may occur alongside bioturbation, but are not as common. Soft-sediment deformation can be observed to affect the aqueous facies that are present within the Entrada (Fig. 2.3). Typical eolian facies are also present and interbedded with these aqueous facies (Fig. 2.3). Dune foresets with grain flows and wind ripples can also be observed, but are commonly disrupted by bioturbation.

2.2.2.2 Processes-

The grain size change in the aqueous facies to finer sediment is an indication that temporary standing water bodies with periodic flooding (Viega, et al. 2002). Aqueous depofacies found interbedded with terrestrial dune systems suggest a high water table (Langford and Chan 1988). These facies associations vary from pink to red in color indicating that they have been oxidized to different degrees. The presence of wave ripples implies open water that was stirred by the wind and that must have been relatively shallow. The upward increase in ripple size signifies the body of water is becoming progressively shallower (Evans 1942). Small amounts of flaser

bedding in some places may indicate tidal influence, and an open connection to the sea rather than an interdune setting (Reineck and Wunderlich 1968). Disruption of sedimentary structures from bioturbation, and burrows denotes the presence of organisms to rework the sediments. The presence of soft-sediment deformation indicates a higher deposition rate leading to loosely packed sediments that are more prone to distortion (Owen 1996).

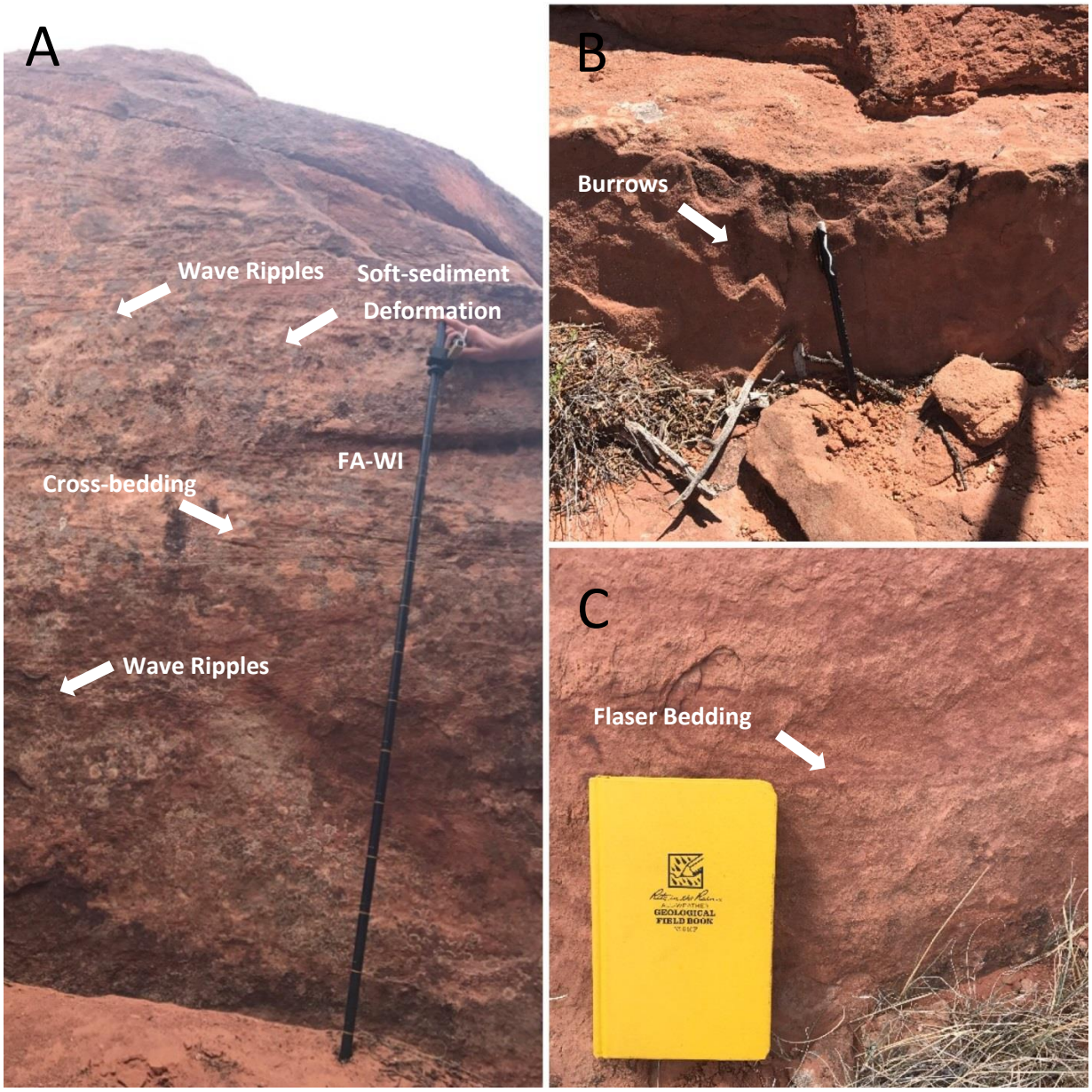

Figure 2.3: A) Outcrop photo of FA-WI. Wave ripples are interbedded with eolian dune foresets (Section 2, E5) B) Bioturbation and burrowing disrupt sedimentary structures (Section 1, E2) C) Flaser bedding is sometimes observed when at the southern end of the study area (Section 2, E5)

2.2.3 Facies Association 3: Small eolian dune deposits

2.2.3.1 Description-

This facies association consists of white trough cross-bedded fine to medium grained sandstone (Fig. 2.4). Sand grains are well sorted and well-rounded. Dune foresets are small-scale (<10cm), but well-defined. It is bounded by sharp contacts and is generally more resistant to weathering than the surrounding facies associations forming a blocky ledge and displaying a rough popcorn texture. The member is present in all measured sections and has a relatively consistent thickness across the study area (0.4-0.6m) and is extensive for hundreds of meters (Fig. 2.10). Weathering makes observation of sedimentary structures difficult to see, but well-defined upward coarsening laminae can be found in most outcrops (Fig. 2.4).

2.2.3.2 Processes-

The upward coarsening laminae are interpreted as deposits of migrating wind ripples (Hunter 1977) (Fig. 2.4). The dune foresets are made up of slightly finer sand representing grain flows from wind driven processes. Slightly coarser grained cross-beds result from the development of wind ripples (Langford, et al. 2016). Small barchanoid dune foresets indicate that there was enough sand present for barchan type dunes to become adjoined, but not abundant enough for them to form large features (McKee 1979). The mode of development in barchanoid dunes consists of a unidirectional wind regime (Ford, et al. 2010). Contacts bounding FA-SE are abrupt meaning they are conformable and are likely flooding surfaces due to the aqueous nature of the surrounding facies associations (Zerfass, et al. 2003).

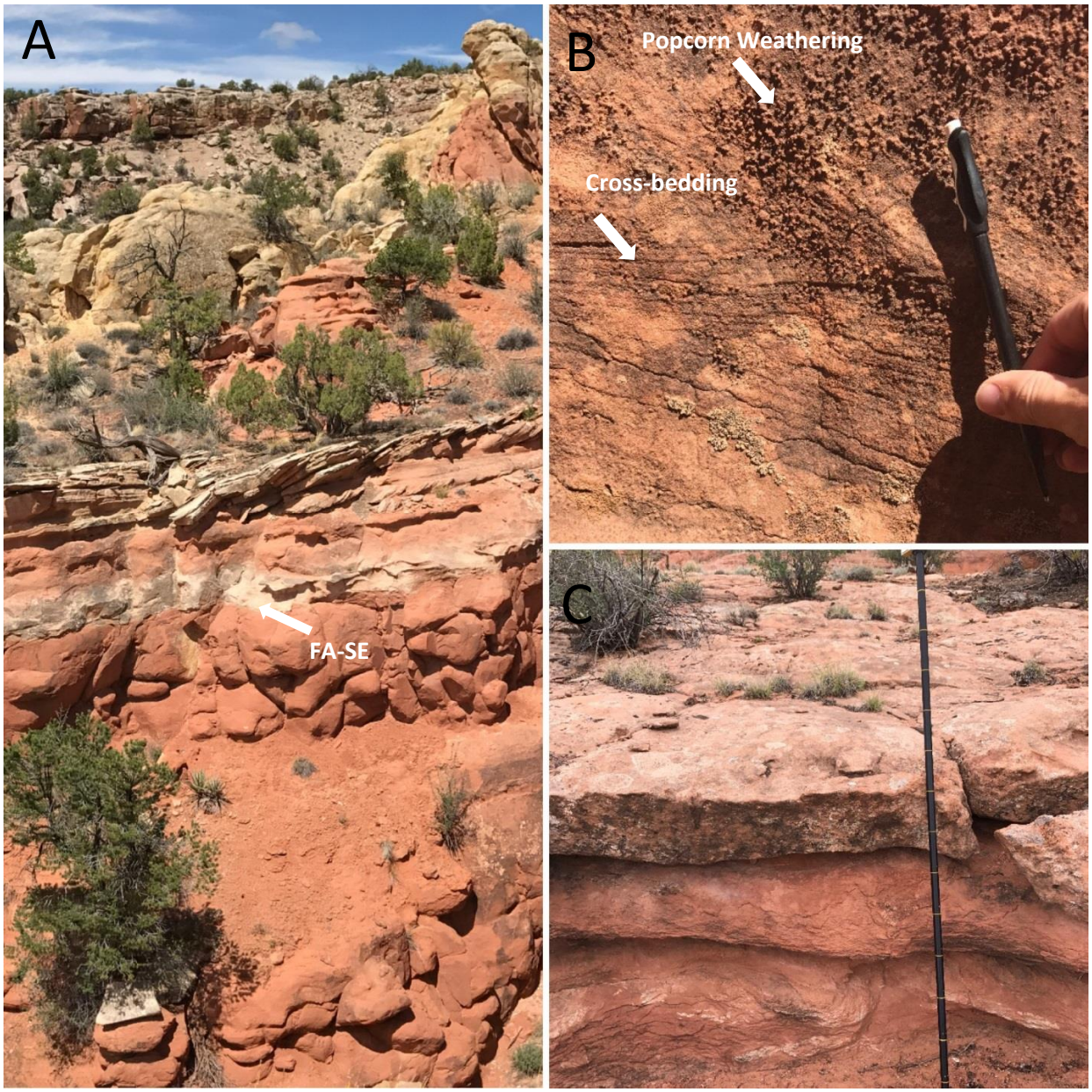

Figure 2.4: A) Outcrop photo showing stratigraphic position of FA-SE above the Carmel Formation (Section 3) B) Small barchanoid dune foresets made difficult to see because of popcorn weathering (Section 2, E1) C) Jacob staff for scale showing the relative thickness of FA-SE (Section 1)

2.2.4 Facies Association 4: Paleosol deposits

2.2.4.1 Description-

This facies association has an overall massive texture that has been heavily bioturbated, and exhibits mottling with some sparse evidence of potential root traces (Fig. 2.5). Its color is a light pink to dark clay-red and is overlain by a very thin dark purple friable structureless shale (<10cm). The dark red portion of the facies association displays rutted weathering and consists of silt sized particles with a small amount of medium sand sized grains. The bottom contact is scoured in contrast to the top contact, which is sharp. FA-PS is only present in stratigraphic section four at the northeastern portion of the research area and is laterally extensive for less than one-hundred meters before it becomes obstructed, or buried without resurfacing elsewhere (Fig. 2.10).

2.2.4.2 Processes-

A lack of aqueous facies suggests that this member formed as part of a terrestrial setting, but the aqueous facies directly below indicate that it was modified from what was likely a wet interdune (Kraus 1999). The fact that it is laterally discontinuous suggest that the facies we expect to see in this part of the Entrada Sandstone have been altered either physically, chemically, or a combination (Kraus 1999, Demko, et al. 2004, Retallack 1986). The thin dark purple clay layer grades down into a dark red silty clay layer followed by a fine-grained pink and white heavily mottled portion with numerous burrows (Retallack 1986; Brown and Kraus 1987). These characteristics are consistent with the formation of a paleosol. Conditions that formed this ancient soil would have involved minimal erosion, nondeposition, and at least some precipitation and vegetation, although no root traces are apparent (Demko, et al. 2004).

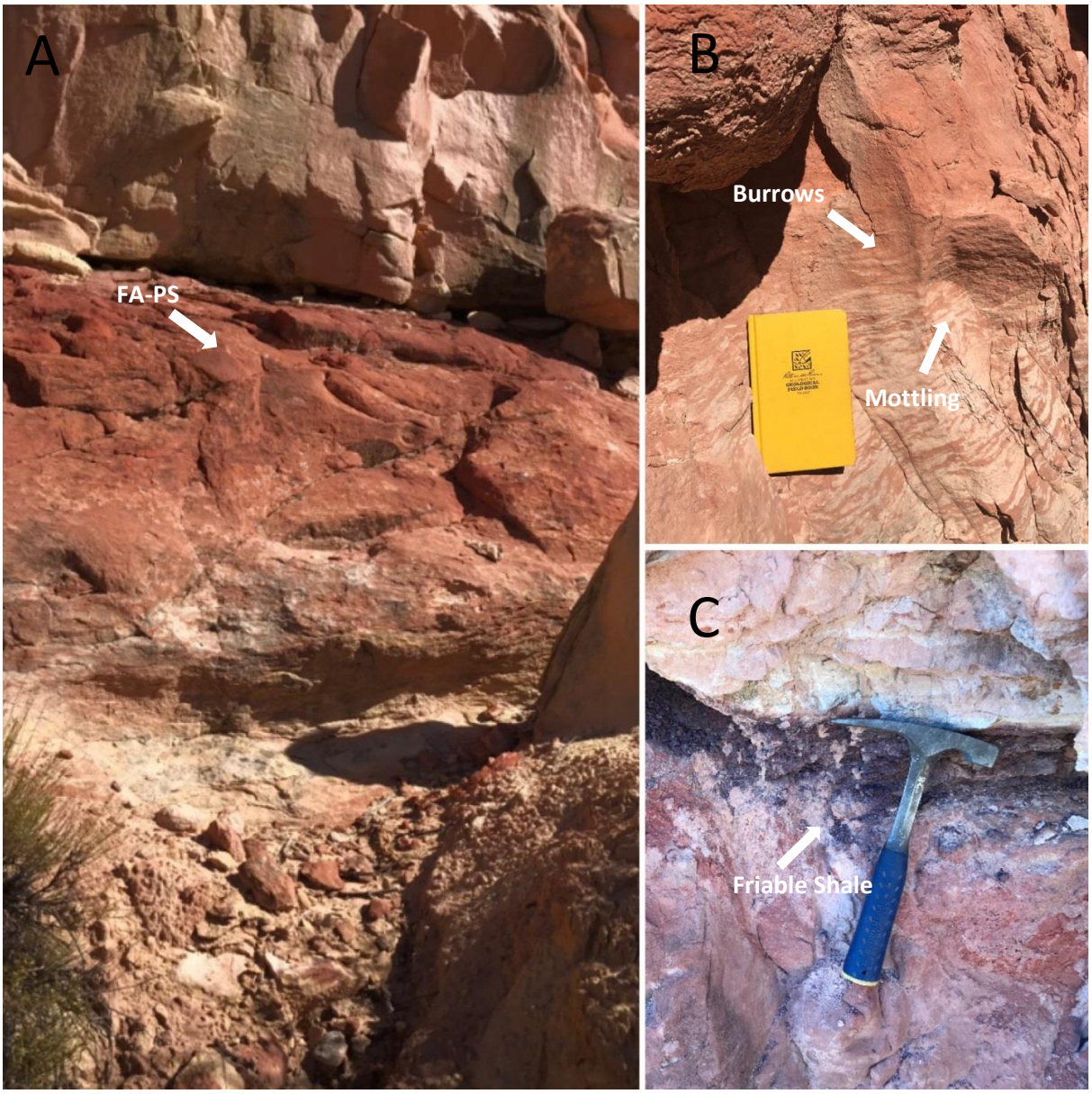

Figure 2.5: A) Outcrop photo of the FA-PS; a dark red paleosol grading down to lighter pink in color and sitting on top of the first occurrence of FA-WI (Section 4) B) Extensive mottling and large burrows are visible just below the dark red layer (Section 4, E2) C) A thin and friable dark purple shale sits above the dark red silty layer (Section 4, E2)

2.2.5 Facies Association 5: Large eolian dune deposits

2.2.5.1 Description-

This facies association consists of both low and high angle trough cross-bedded white to light pink sandstones that weathers to a light grey (Fig. 2.6). The overall grain size of this facies association is generally fine to medium sand. Wind ripples are present alternating from fine grained laminations to medium grained laminations with some coarse grains present. The grains are moderately sorted and well rounded. This member exhibits either a steep surface or is cliff forming. Weathering is smooth except where small portions of the coarser laminations stick out from the surface. Dune foresets and bedding range in thickness from about 0.5-1m. The overall thickness of the facies association does not fluctuate significantly ranging from 3.5-4.8m with a geometry that appears to thicken slightly in the northerly direction of the study area. FA-LE is present in all measured sections and is extensive for hundreds of meters (Fig. 2.10).

2.2.5.2 Processes-

Processes for FA-LE are similar to FA-SE. Key disparities include a greater sediment supply necessary for the formation of larger dune features. There are also both low and high angle cross-bedding, which suggest this is possibly becoming more of a transverse dune type (Werner; 1995; Tsoar and Blumberg 2002). The moderately-sorted texture and presence of coarse grains indicated that deposition occurred more rapidly, wind speeds during the time of deposition were higher than normal, and potentially a spacing increase between dunes (Lancaster 1988). The pink portions of FA-LE reveal that oxidation occurred in these members and that anoxic conditions prevailed in the white portions (Chan, et al. 2000). As cliff formers with smooth surfaces these facies are also more resistant to erosional processes than others.

Figure 2.6: A) Outcrop photo showing the stratigraphic position of FA-LE as a thick white horizon (Section 3) B) Close up photo of the white dune facies showing high and low angle cross-bedding, coarse-grained wind ripples and avalanche deposits (Section 3, E3) C) Pink eolian facies analogous to (B), sits stratigraphically higher (Section 1, E5)

2.2.6 Facies Association 6: Dry interdune deposits

2.2.6.1 Description-

This facies association consists of horizontally to subhorizontally discontinuous beds, or lenses of fine grained sandstones that alternate with medium grained wind ripple laminations (Fig. 2.7). These sandstones are pink and weather to a dark grey. The grains are moderately sorted and well-rounded. They typically have a lateral continuity of <100m and range in thickness from ~30-50cm. Weathering makes the laminations more prominent, but is otherwise flush with the steep faces of the surrounding facies associations. Contacts above and below beds of FA-DI are abrupt. FA-DI is present in stratigraphic sections 1 and 9 and are normally found below depofacies consistent with FA-WI (Fig. 2.10).

2.2.6.2 Processes-

The thin well-developed horizontally laminated bedding of FA-DI is an indication of surface creep and saltation movement of sand grains (Reineck & Singh 1980). These smaller features compared to the larger dune formations suggest an area of active deflation although some sedimentation does take place (Reineck & Singh 1980). The presence of wind ripples indicates the presence of interdune hallows between dune forms (Mountney 2004). The thickness of the interdune beds, and that they are not extensively continuous laterally is consistent with the unimodal wind regime determined from the barchanoid dune formations (Ahlbrandt & Fryberger 1981).

Figure 2.7 A) Outcrop photo of FA-DI showing a several meters long lens of horizontally bedded sandstone (Section 3) B) Discontinuous horizontally bedded fine grained sandstone alternating with beds of medium grained wind ripple laminations (Section 1, E2)

2.2.7 Facies Association 7: Eolian deposits with shallowly scoured bedding

2.2.7.1 Description-

This facies association consists of a white fine to medium grained sandstone with wavy irregular bedding formed by shallow scouring that distinguishes it from other facies associations. There are also hints of cross-bedding, but an otherwise a lack of distinct sedimentary structures (Fig. 2.8). Grains appear to be well-sorted and well-rounded. It appears to erode more readily than the facies associations below it; wearing away into a slope as outcrops become intermittently covered in some places. The surfaces of the exposed outcrops are usually rough and sometimes have lumpy nodular-like concretions (Fig. 2.8). Two sets of beds belonging to this member that dip westward into the Gypsum Valley salt diapir and are heavily altered appearing more red than white in color. The fundamental characteristics of this facies association, however, are comparable to the other sections. FA-SC appears in all stratigraphic sections except for 2 and 9 where it has been eroded away and varies greatly in thickness due to differential erosion (6-14.1m) (Fig. 2.10).

2.2.7.2 Processes-

The lack of distinct sedimentary structures makes it difficult to determine some of the potential processes that may have occurred in this facies association. In the majority of the measured sections the white sand suggest reduced conditions. However, in the westward dipping beds the predominantly red coloring suggests they have been subject to oxidation (Chan, et al. 2000). Wavy irregular bedding is interpreted shallow scours that occur as a result of local turbulence, changes in wind speed, changes in local topography, and fluctuations in surface wetness, or sediment supply (Grotzinger et al. 2005).

Figure 2.8: A) Outcrop photo of upper most portion of the Entrada Sandstone. It has been heavily fractured and altered at this location. (Section 3) B) Bedding of FA-SC that dips towards the salt diapir becomes mottled and predominantly red in color, but otherwise maintain the same characteristics (Section 7, E7) C) Hints of dune foresets are sometimes visible, but weathering and erosion make them difficult to see in most places (Section 3, E7) D) Lumpy nodular weathering occurs in most outcrops (Section 1, E7) E) Wavy irregular bedding is present throughout due to shallow scouring from wind processes (Section 1, E7)

2.2.8 Facies Association 8: Mottled eolian deposits

This facies association consists of a pink medium to coarse grained sandstone with traces of dune foresets, but for the most part is mottled and lacks sedimentary structures (Fig. 2. 9). Grains are moderately sorted and well rounded. This member is bounded by sharp contacts and exhibits smooth erosional surfaces and steep faces, which are often cliff forming. FA-ME is only present in stratigraphic sections 2 and 6 at the southeastern portion of the study area an appears to be laterally continuous for a few hundred meters slightly thickening to the south (3.4-4.2m) (Fig. 2.10).

2.2.8.2 Processes-

The lack of sedimentary structures in FA-ME makes it difficult to determine many of the potential processes that have occurred in this member. Mottled and massive bedding suggest that this facies association has been heavily reworked as a result of bioturbation (Stewart and Walker 1980). Traces of dune foresets suggest eolian driven deposition, however the type of dunes and whether or not aqueous faces were at some point present cannot be determined. The moderately sorted texture and presence of coarser grains suggest more rapid deposition likely due to wind speeds being higher than normal at the time (Lancaster 1988). The cliff forming nature of this member along with smooth surfaces indicates that it is more resistive to weathering. This facies association is most prominant in the southeast portion of the study area, but appears throughout stratigraphic Unit E5 (Fig. 2.3).

Figure 2.9 A) Outcrop photo of FA-ME. Structures are indistinctive compared to other facies associations (Section 9) B) Massive texture devoid of any distinguishable sedimentary structures (Section 2, E5) C) Hints of cross-bedding occasionally, but overall mottled and lacking any sedimentary structures (Section 2, E5)

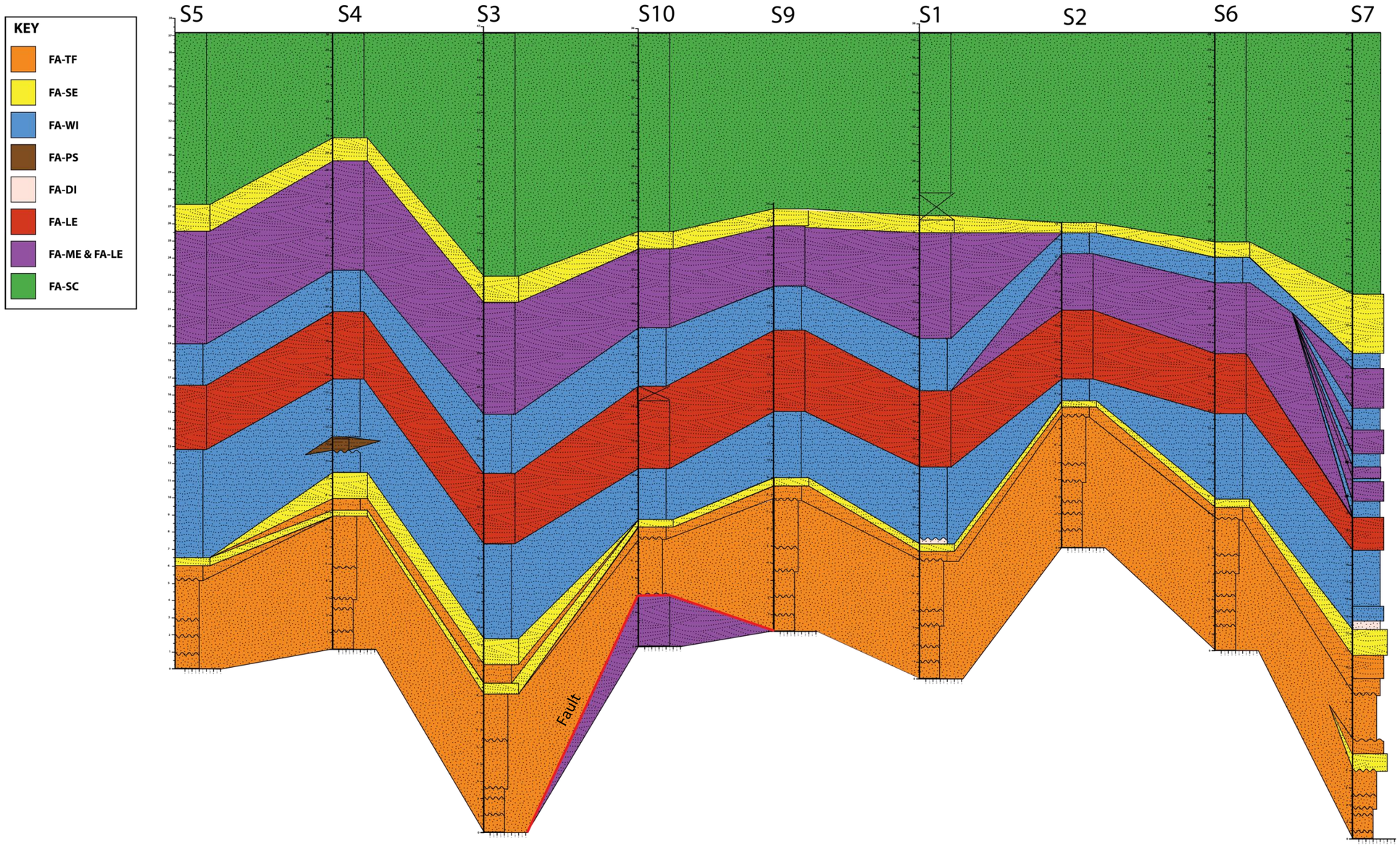

Figure 2.10: A cross-section showing the stratigraphic position of facies associations based on measured sections at Little Gypsum Valley. The repetition of FA-ME and FA-LE in Section 10 is due to the northeasternmost fault shown in figure 3.4, which covers the base of the Entrada in this location.

Chapter 3: Stratigraphy and Unit Descriptions

3.1 Stratigraphic Results

Nine sections were measured through the Carmel and Entrada Sandstone formations on the salt shoulder at Little Gypsum Valley (Fig. 3.1). Seven stratigraphic units were identified in each of these formations totaling fourteen units (Figure 3.2). Units tend to strike NE-SW and dip in a northwesterly direction (Fig. 3.4). Paleocurrent direction indicates a predominant NW-SE wind (Fig. 3.4).

These units and how their facies change across the study area is detailed below. One of the most notable of these changes within the study area is unit thickness. Thickness of complete stratigraphic sections ranges from approximately 30-50 meters. Thickness changes that occur within Entrada units tend to be greater than those in the Carmel and sections overall experience maximum thickness variation of just under 20 meters (Fig. 3.3). Units E2, E5, and E7 experience the greatest thickness changes (Fig. 3. 3). In general, sections that dip west into the diapir (Sections 3, 4, 5, and 7) demonstrate notable thickness changes that occur over mere tens of meters, but overall thin away from the crest of the diapir shoulder (Fig. 3.1 and Fig. 3.3). Thickness changes observed on the crest of the diapir occur more gradually (Sections 1, 2, 6, 9, and 10) (Fig. 3.1 and Fig. 3.3). Units towards the south and dipping west of Section 7 experience notable thinning as they gradually dip below ground (Fig. 3.1 and Fig. 3.7). Intertounging relationships are observed over a short distance in the northern portion of the study area at Section 3 between FA-TF and FA-SE (Fig. 3.1 and Fig. 3.6). Intertonguing is also observed in the southern portion in Sections 2, 6, and 7 between FA-WI and FA-ME (Fig. 3.1 and Fig. 3.5). Grain size is another unit property that is uniform across the study area; however, there are some Entrada Units (E3, E4, E5, E6, and E7) where grain size is observably finer on, or near the crest

of the diapir; particularly in the north part of the study area (Sections 1, 2, 9, and 10) where it ranges from very-fine to fine compared to the other sections where it ranges from fine to medium (Fig. 3.1) (Appendix 1).

The section at Slick Rock Canyon, about thirteen kilometers west of the diapir was measured through the Carmel and Entrada formations to be compared more generally with those that are on and adjacent to the diapir (Fig. 1.1 and Fig. 3.3). Seven units were identified in the Carmel and four additional units were recognized in the Entrada totaling eleven units (Fig. 3.3). A brief description of these units is also detailed below. The most obvious discrepancy observed is that overall thickness is greater in the Slick Rock Canyon section; especially within the uppermost unit of the Entrada (Fig. 3.3). Differences are more subtle when it comes to grain size; however, Slick Rock Canyon units have much less variation and coarsen upward from very-fine sands in the Carmel to fine sands in the Entrada. Little Gypsum Valley units experience more grain size variations moving up through the sections. Many of the units on the salt shoulder, both Carmel and Entrada, contain notably coarser sediments when compared to the Slick Rock Canyon section.

3.2 Carmel Stratigraphic Units (Salt Shoulder):

Unit C1 is recognized by facies consistent with FA-TF, which include basal lag deposits, soft-sediment deformation, hints of aqueous ripples, mottling, burrows, and bioturbation. Grain size is very-fine to fine and is uniform across the study area. Grains are rounded and moderately-sorted. Poorly-sorted bands of medium to very-coarse pebbles and rip up clasts are present and are generally continuous laterally although they are sometimes disrupted by the bioturbation. This unit is only intermittently exposed, if present at all, and can be found in Sections 2, 6, and 7 (Fig. 3.1). The lower contact is erosional and unconformable atop the Jurassic Kayenta and

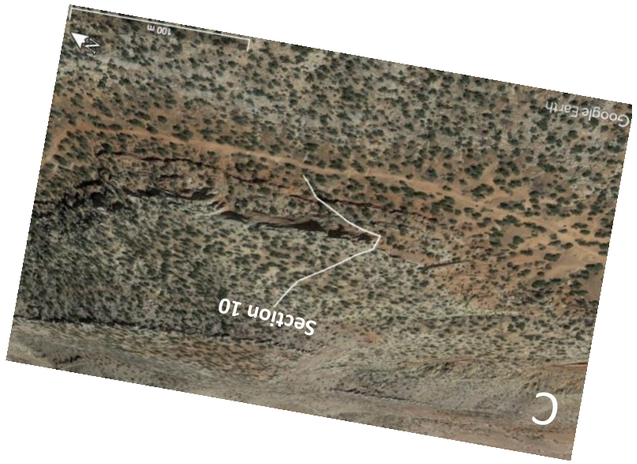

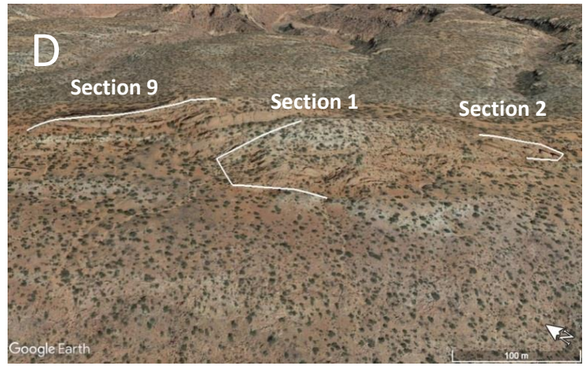

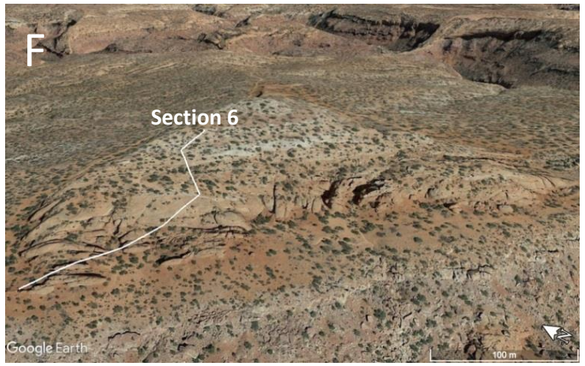

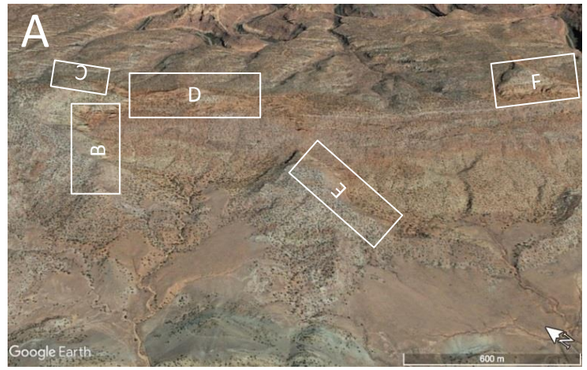

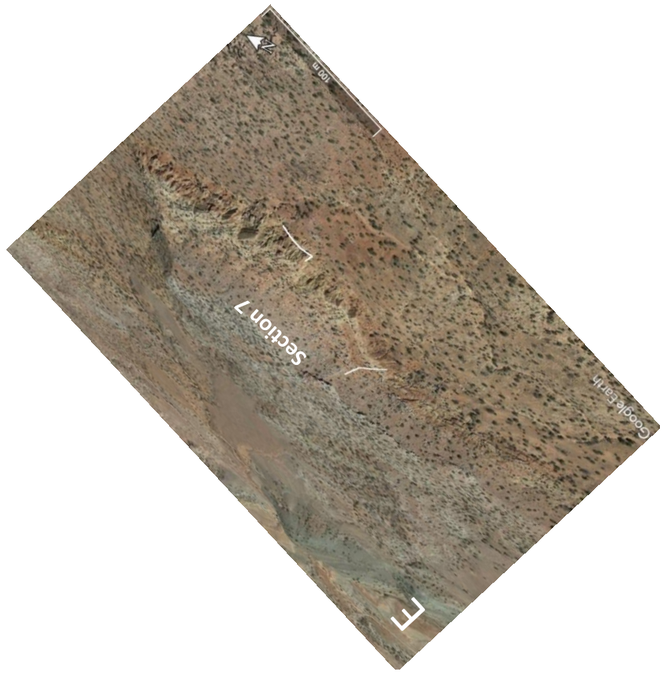

Figure 3.1: Google Earth images rotated relative to where the north arrow points on image (A). Displayed on each photo are the positions of sections measured throughout the Little Gypsum Valley. A) Aerial view of the Little Gypsum Valley study area. Boxes represent the locations for subsequent images B-F B) Aerial view displaying the paths for Sections 3, 4, and 5 C) Aerial view displaying the path for Sections 10 D) Aerial view displaying the paths for Sections 1, 2, and 9 E) Aerial view displaying the path for Section 7 F) Aerial view displaying the path for Section 6

Navajo Formations (Fig. 3.1, 3.2, and 3.4). The upper contact is scoured. Thickness ranges from 0.5 to 1.5 meters, but the unconformity makes it impossible to determine actual thickness (Fig. 3.3).

Unit C2 is recognized by facies consistent with FA-TF, which include flaser bedding and aqueous ripple cross-strata near the bottom and becomes more poorly expressed above due to mottling and bioturbation, which results in an otherwise structureless unit. Grain size is very-fine with occasional medium to coarse grains and is consistent across the study area. Grains are well-sorted and subrounded. Spheroidal weathering is present and characteristic of most Carmel units (Fig. 3.2). The upper contact is scoured (Fig. 3.2). Thickness is uniform ranging from 1-1.2 meters and is present in all section except 5 and 10 (Fig. 3.1 and 3.3).

Unit C3 is recognized by facies consistent with FA-TF, which inlcude burrows, mottling, hints of aqueous ripple cross-strata, 20-40 centimeters of continuous flaser bedding near the top; except in Sections 1 and 2 where there is none, a small amount of soft-sediment deformation in Sections 3 and 5 only, but is otherwise structureless (Fig. 3.1). Grain size is very-fine with some medium grains present and is consistent across the study area. Grains are overall well-sorted and rounded. The upper contact is scoured (Fig. 3.2). Thickness ranges from 0.7-1.4 meters. It is thickest in Section 4 (1.4 meters) and thinnest in Section 2 (0.7 meters) and Section 6 (0.8 meters), but is of uniform thickness in other sections (Fig. 3.3). Unit C3 is present in all sections except 10 (Fig. 3.1 and 3.3).

Unit C4 is recognized by facies consistent with FA-TF, which include aqueous ripple-cross strata, approximately 15-20 centimeters of continuous flaser bedding near the top, but is otherwise structureless from bioturbation. Grain size is fine in most sections. However, Section 7 is also fine grained, but contains laterally continuous bands of medium to coarse grains (Fig.

3.1). The grains are well-sorted and rounded. The upper contact is scoured (Fig. 3.2). Thickness ranges from 0.7-1.2 meters and is thickest in sections on the crest of the diapir; particularly Sections 1, 2, and 9 (Fig. 3.1 and 2.3). Unit C4 is present in all sections except 10 (Fig. 3.1 and Fig. 3.3).

Unit C5 is recognized by facies consistent with FA-TF, which include aqueous ripple cross-strata, bioturbation, and an approximately 5-10 centimeter thick horizon with white reduced 'patches' at the top contact. Small amounts of flaser bedding and soft-sediment deformation are present in this unit in Section 6 only. Grain size is fine with dispersed coarse grains sometimes appearing as discontinuous bands and is consistent in all sections. Grains are well-sorted and rounded. The upper contact is scoured (Fig. 3.2). Thickness ranges from 0.8-1.1 meters and is relatively uniform across the study area (Fig. 3.3). Unit C5 is present in all sections except 10 (Fig. 3.1).

Unit C6 is recognized by facies consistent with FA-TF, which include flaser bedding, aqueous ripple cross-strata mottling, bioturbation, and an approximately 5-10 centimeter thick horizon with white reduced 'patches' at the top contact. Soft-sediment is present, but only in Section 2 (Fig. 3.1 and 3.3). Grain size is very-fine with some medium grains present only in the lower portion of the unit and is uniform in all sections. Grains are well-sorted and rounded. The upper contact is sharp (Fig. 3.2). Thickness ranges from 2.3-3.3 meters (Fig. 3.3). It is thinnest in Section 6 at the most southern portion of the study area, but is uniform across the rest of the area (Fig. 3.1 and 3.3). Unit C6 is present in all sections (Fig. 3.1).

Unit C7 is recognized as a pink ledge former that is transitionary between aqueous Carmel and eolian Entrada facies exhibiting facies consistent with FA-TF and FA-SE, which include include aqueous ripple cross-strata and mottling in some sections, and eolian foresets

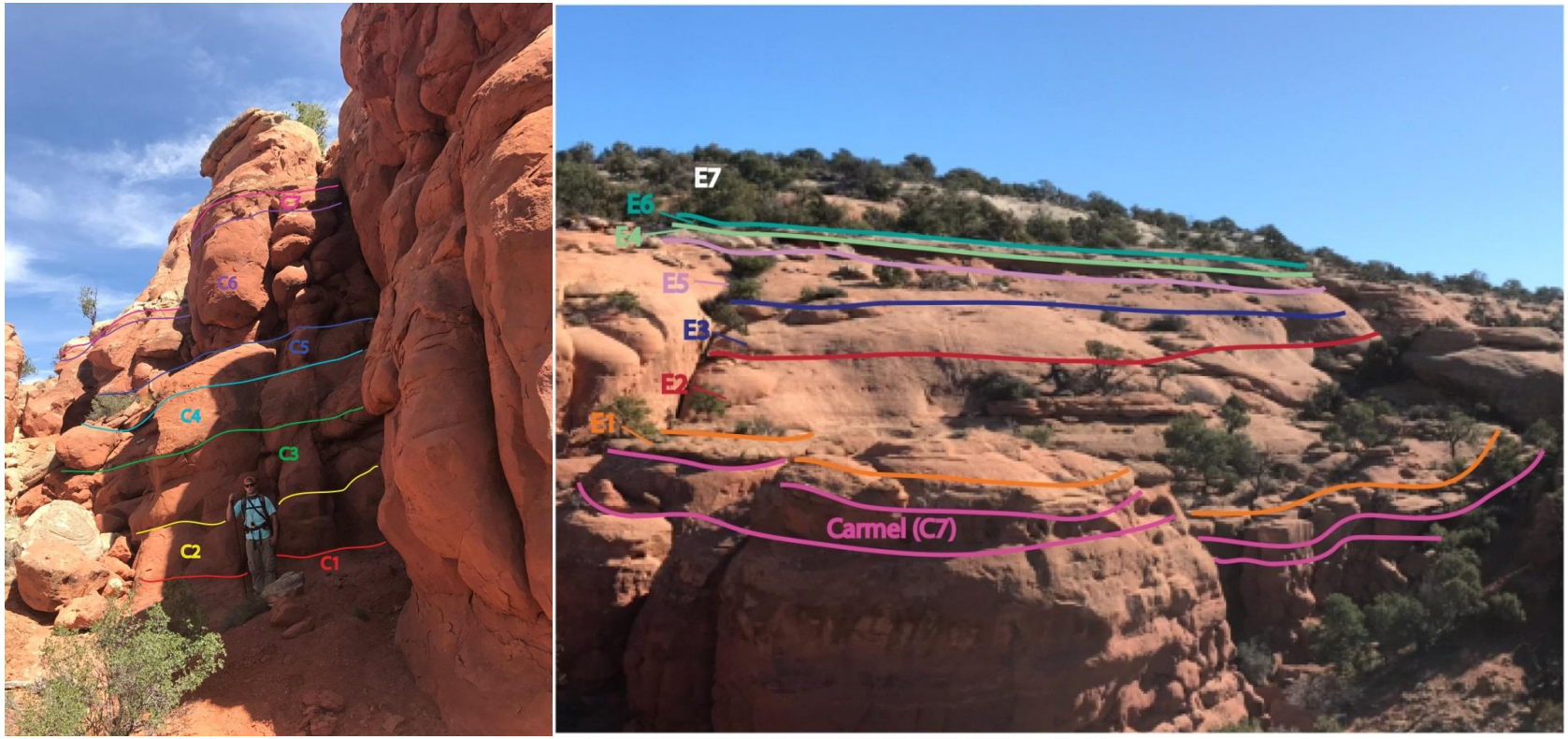

Figure 3.2: Images showing the stratigraphic position of each unit in outcrop at Section 6 (Fig. 3.1). On the left are Units C1-C7 of the Carmel Formation with field assistant and Jacob staff for scale. On the right are Units E1-E7 of the Entrada Formation. In this particular section, as well as sections towards the southern portion of the study area, Unit E4 atypically lies on top of Unit E5. This is attributed to an intertonguing relationship between these units that is most apparent in Section 7 (Fig. 3.1 and Fig. 3.5).

with coarse grained wind ripples in others. ‘Popcorn’ weathering is characteristic of this unit as well. Grain size is fine and is consistent across the study area. Grains are well-sorted and rounded. The upper contact is sharp (Fig. 3.2). Thickness ranges from 0.5-1 meter remaining relatively uniform across the area (Fig. 3.3). Unit C7 is present in sections all sections except 3 and 4 (Fig. 3.1).

3.3 Entrada Stratigraphic Units (Salt Shoulder):

Unit E1 is recognized as a white ledge forming unit consistent with FA-SE, which includes popcorn weathering, small barchanoid dune foresets, and coarse grained wind ripples. In Sections 3 and 4 it briefly intertongues with Unit E2 as is apparent by the atypical repetition of these strata (Fig. 3.1, 3.3, and 3.6). In Section 7 it briefly intertongues with upper Carmel units (Fig. 3.1, 3.3, and 3.5). Grain size is fine to medium and is uniform across the study area. Grains are well-sorted and well-rounded. The upper contact is sharp (Fig. 3.2). Thickness is uniform across the study area and ranges from 0.4-0.6 meters (Fig. 3.3). It is present in all sections (Fig. 3.1).

Unit E2 is recognized as a wet interdune consistent with FA-WI, which includes interbedded aqueous ripples and dune foresets. Wave ripples are smaller at the bottom and become progressively larger upwards as they transition back into eolian facies. Coarse grained wind ripples, and mottling are also present. It is difficult to see many sedimentary structures otherwise as features have been disrupted by bioturbation. Horizontally bedded sands can be observed at the base of the unit (FA-DI), but only in sections 1, 7, and 9. In section 4, the base is heavily burrowed and a discontinuous paleosol (FA-PS) also appears in this unit at 1.5 meters (Fig. 3.1). Some soft-sediment deformation is present in Section 7 only (Fig. 3.1). Grain size is fine to medium and is uniform across the study area. Grains are moderately-sorted and rounded.

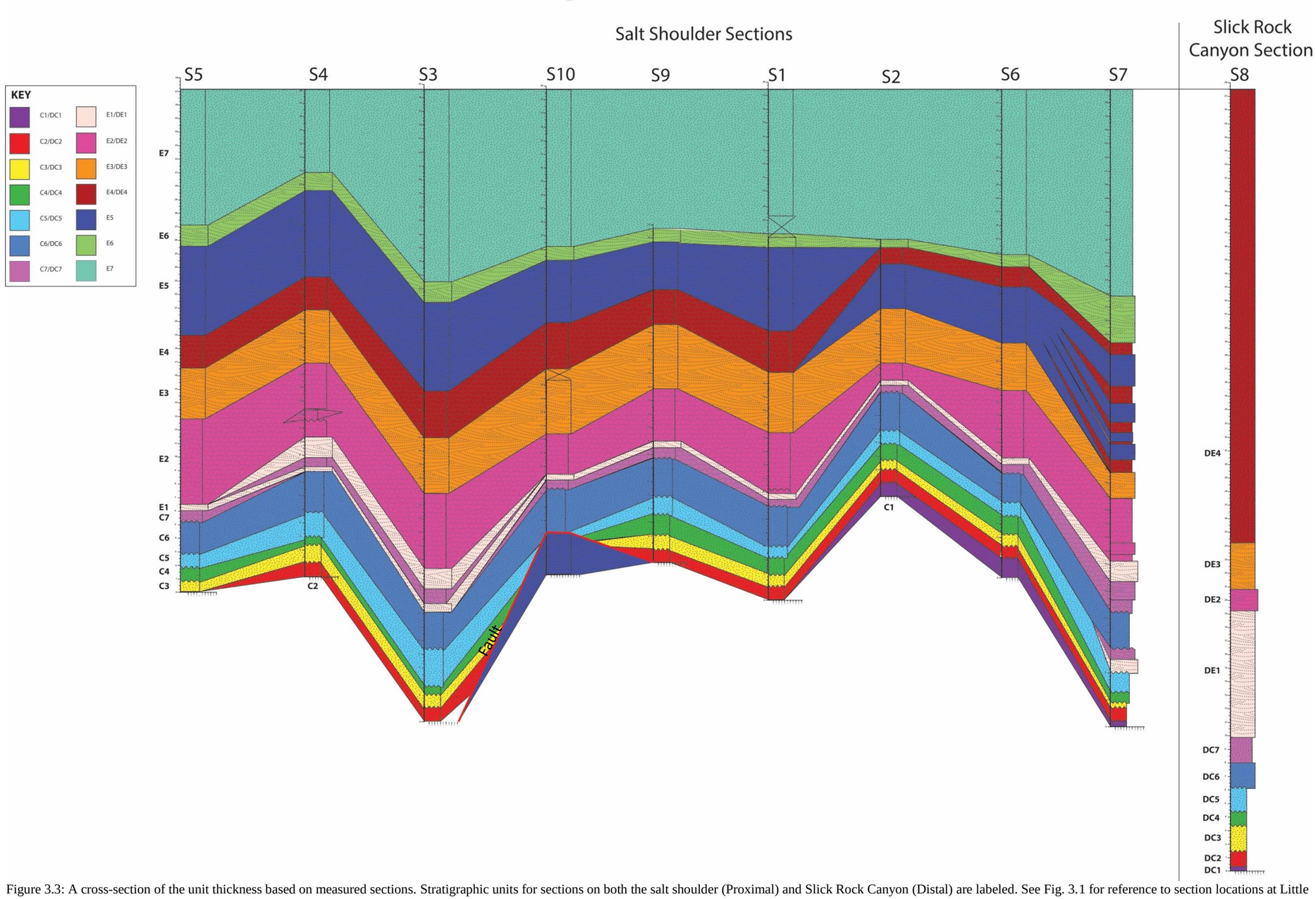

Figure 3.3: A cross-section of the unit thickness based on measured sections. Stratigraphic units for sections on both the salt shoulder (Proximal) and Slick Rock Canyon (Distal) are labeled. See Fig. 3.1 for reference to section locations at Little Gypsum Valley. The fault shown in Section 10 is the northernmost fault in Fig. 3.4, which offsets the Entrada by 20 m. The down-dropped block covers units C1-C4 in Section 10.

The upper contact is gradational (Fig. 3.2). The unit is generally thinnest in select sections (2, 9, and 10) on the crest of the diapir where they range from 1.3-3.7 meters (Fig. 3.3). The remaining sections are thicker varying from 4.5 -6.3 meters (Fig. 3.3).

Unit E3 is recognized by facies consistent with FA-LE, which include large well-defined barchanoid dune foresets, grain flows, and coarse-grained wind ripples. It can usually be distinguished by its white color, or light pink color with a gray varnish. Grain size is typically fine to medium except for some sections on the crest of the diapir where it is finer overall; particularly Sections 1, 2, and 9. Grains are moderately-sorted and well-rounded. The upper contact is gradational at the top with the exception of Sections 2 and 6 where this is sharp (Fig. 3.2). Units are thinnest as they dip into the diapir away from the crest (Sections 4, 5, and 7) ranging from 2-3.9 meters (Fig. 3.1 and Fig. 3.3). The only exception is Section 3 which measures 4.3 meters. Units on the crest of the diapir (Sections 1, 2, 9, 10) are thickest ranging from 4-4.7 meters (Fig. 3.1 and Fig. 3.3). The only exception is Section 6 at the southernmost part of the study area which measures 3.5 meters.

Unit E4 is recognized as a wet interdune consistent with FA-WI, which includes wave ripple bedding, soft sediment deformation, and bioturbation. Grain size is fine in most sections, but coarsensin this unit as it dips further into the diapir as can be observed in Sections 4, 5, and 7 where grain size is fine to medium compared to other sections were it is fine (Appendix 1). Unit E4 is present in all sections (Fig. 3.1). It does; however, sit atypically atop Unit E5 in sections 2 and 6 at the southern part of the study area and intertongues with Unit E5 in section 7 (Fig. 3.1, 3.2, and 3.3). Grains are moderately-sorted and rounded. The upper contact is gradational with the exception of Sections 2 and 6 where this is sharp (Fig. 3.2). Sections appear to thicken from

the southern end of the study area to the north ranging from 1.1-3.5 meters (Fig. 3.1 and Fig. 3.3).

Unit E5 is recognized as a pink colored eolian dune consistent with FA-LE, which includes with large barchanoid dune foresets, coarse grained wind ripples, grain flows and avalanche deposits. Distinctive eolian structures are often disrupted by varying amounts of mottling (FA-ME). Bioturbation and mottling is much heavier in sections that are closer to the south side of the study area, particularly in Sections 2 and 6 on the crest of the diapir (Fig. 3.1). This unit also sits atypically below Unit E4 in these sections as a result of an intertonguing relationship exclusively present at the southern portion of the area that is even more apparent in Section 7 (Fig. 3.1, 3.3, and 3.5). Grain size is typically fine to medium, however it appears to be finer overall in the northern part of the area on the crest of the diapir; particularly Sections 1, 9, and 10. Grains are well-sorted and subrounded. The upper contact is sharp with the exception of Sections 2 and 6 where this is gradational (Fig. 3.2). Thickness is generally uniform ranging from 6.3-6.6 meters in most sections; however, significant thinning occurs on the diapir crest in the north at Section 9 as well as at the southern portion in Sections 2, 6, and 7 where thickness ranges from 2.3-4.2 meters (Fig. 3.1 and Fig. 3.3).

Unit E6 unit has similar primary features to that of Unit E1 (FA-SE). It is also recognized as a white ledge forming eolian unit, but has slightly larger well-defined dune foresets, grain flows, and coarse grained wind ripples. Small amounts of popcorn weathering are sometimes found on this unit. Grain size is typically fine to medium in most sections, but is finer overall in the north part of the study area on and near the crest of the dipair; particularly Sections 3, 9 and 10 where grain size is fine compared to the other sections where it is fine to medium. Grains are moderately-sorted and well- rounded. The upper contact is sharp (Fig. 3.2). Thickness of units

that dip towards the diapir ranges from approximately 1.4-1.6 meters (Fig. 3.3). Units on the crest of the diapir are thinner than those that dip into the diapir and gradually continue to thin towards the southern portion of the study area ranging from0.5 to1 meter in thickness (Fig. 3.1 and Fig. 3.3).

Unit E7 is recognized by facies consistent with FA-SC, which include wavy irregular beds, hints of foresets, coarse-grained wind ripples, and horizontal bedding, lumpy nodule-like concretions exposed in weathering, but overall sedimentary structures are indistinctive. Portions of this unit are intermittently covered in some places from erosion. This unit is present in all section except 2 and 9 where it has been removed by erosion (Fig. 3.1 and Fig. 3.3). Unit E7 is typically white to beige in color although its appearance changes drastically in Sections 5 and 7 where units dip into the diapir and are furthest away from its crest (Fig. 3.1). In these sections Unit E7 is iron-stained and is, therefore, a predominantly a deep red color, which displays both small and large reduced white patches giving it a mottled appearance. Otherwise the features and appearance are the same as in other sections. Grain size is fine to medium in most sections, but is finer overall in sections 1 and 10 on the crest of the diapir at the north part of the study area. Grains are moderately-sorted and well-rounded. The upper contact is scoured with the Summerville formation above. Unit E7 experiences many thickness variations over the confines of the study area (Fig. 3.3). Sections on the crest of the diapir seem to be most consistent ranging from 11.7- 12.2 meters for section unaffected by erosion (Fig. 3.1 and Fig. 3.3). Units dipping into the diapir fluctuate rapidly and range anywhere between 6-15.1 meters in thickness (Fig. 3.1 and 3.3).

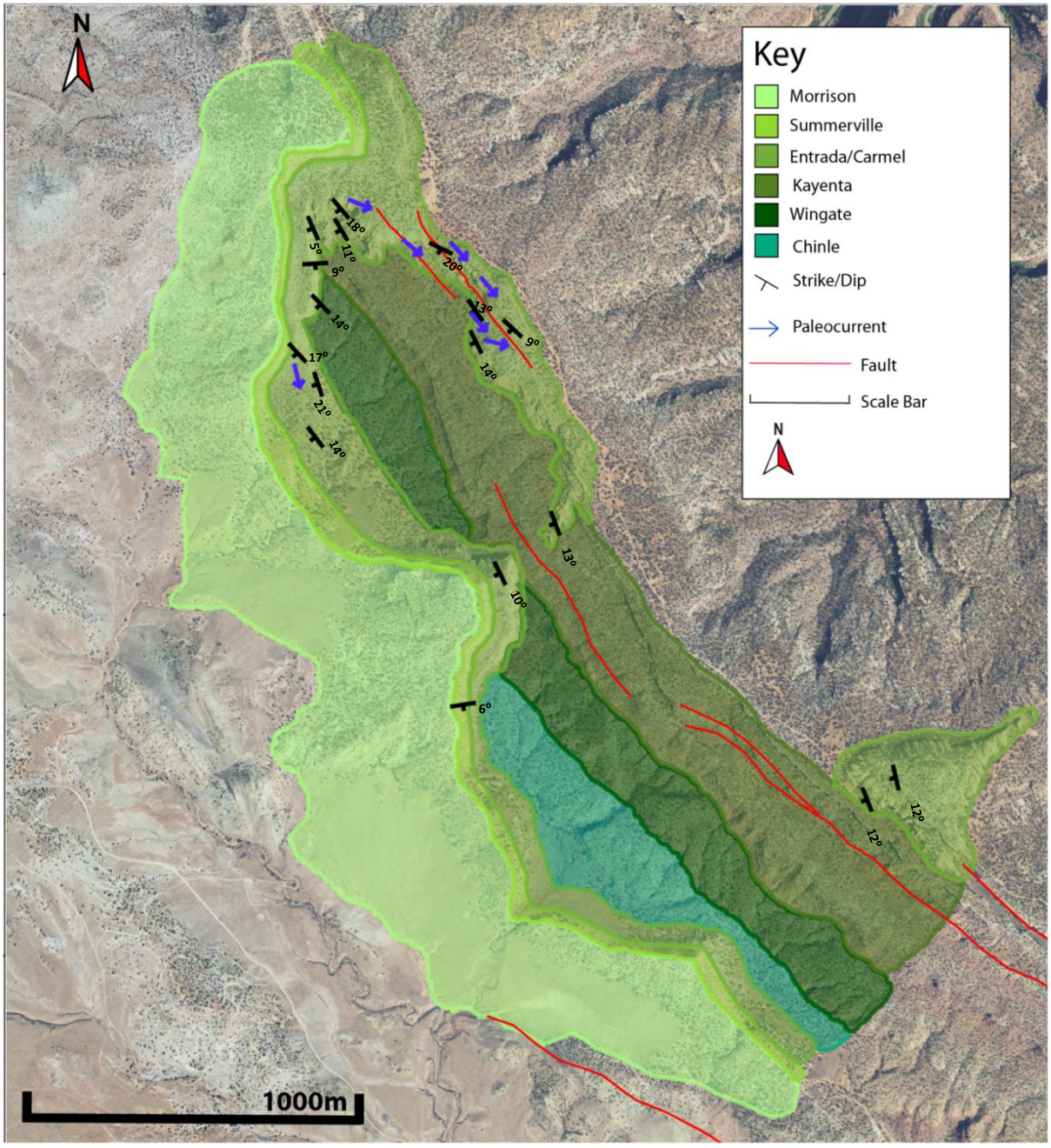

Figure 3.4: Geologic map showing the geometry of the Entrada/Carmel with respect to adjacent formations. Strike and dip data, paleowind directions, and faults are also displayed. Paleowind directions were taken in units E3, E5 and E7 when cross-bedding allowed for accurate measurements.

3.4 Carmel Stratigraphic Units (Slick Rock Canyon):

The facies associations and stratigraphic position of the following Carmel units (DC1-DC7) are equivalent to those seen at Little Gypsum Valley (C1-C7).

Unit DC1 is recognized by bioturbation, mottling, soft-sediment deformation, and flaser bedding. Grain size is very-fine and grains are moderately-sorted and subrounded. The lower contact is sharp and lies conformably on top of the Navajo Sandstone formations. The upper contact is scoured (Fig. 3.2). Weathering in the Slick Rock Canyon Carmel units are brick red in color with spheroidal, but slightly more 'blocky' than the units on the salt shoulder. Thickness is 0.6 meters (Fig. 3.3).

Unit DC2 is recognized by indistinctive sedimentary structures, hints of flaser bedding and aqueous ripple cross-strata, bioturbation, mottling, and a white reduced horizon near the lower contact approximately 10 centimeters in thickness. Grain size is very fine and grains are moderately-sorted and subrounded. The upper contact is scoured (Fig. 3.2). Thickness is 0.9 meters (Fig. 3.3).

Unit DC3 is recognized by ripple cross-strata, a 40 centimeter thick continuous layer of flaser bedding near the top as well as discontinuous 'patches' throughout, bioturbation, and mottling. Grain size is very-fine and grains are moderately-sorted and subrounded. The upper contact is scoured (Fig. 3.2). Thickness is 1.9 meters (Fig. 3.3).

Unit DC4 is similar to Unit DC3, but its structures have been disrupted to a greater degree by bioturbation, so there are only hints of aqueous ripple cross-strata and no laterally continuous flaser bedding. Grain size is very-fine and grains are moderately-sorted and subrounded. The upper contact is scoured (Fig. 3.2). Thickness is 1.3 meters (Fig. 3.3).

Unit DC5 is similar to Unit DC4, but also displays soft-sediment deformation. Grain size is very-fine and grains are moderately-sorted and subrounded. The upper contact is scoured (Fig. 3.2). Thickness is 1.6 meters (Fig. 3.3).

Unit DC6 is similar to Unit DC5, but its structures are less distinguishable as a result of heavy weathering, which is more blocky than the units below it. The upper contact is scoured (Fig. 3.2). Grain size is very-fine and contains some medium grains. Grains are moderately-sorted and subrounded. Thickness is 1.7 meters (Fig. 3.3).

Unit DC7 is recognized as a cliff forming unit that displays aqueous facies similar to those in Unit DC1. Grain size is very-fine with some medium grains. Grains are moderately sorted and subrounded. The upper contact is gradational as it transitions into eolian facies (Fig. 3.2). Thickness is 2 meters (Fig. 3.3).

3.5 Entrada Stratigraphic Units (Slick Rock Canyon)

Unit DE1 does not correlate with any stratigraphic units in the Entrada observed at Little Gypsum Valley. It is recognized by indistinctive pink eolian dune facies, which include foresets, coarse grained wind ripples, mottling, and wavy irregular beds (Fig. 3.2). Grain size is fine and grains are well-sorted and rounded. The upper contact is sharp (Fig. 3.2). Thickness is 9.2 meters (Fig. 3.3).

Unit DE2 may correlate with Unit E3 at Little Gypsum Valley on the basis of relative stratigraphic position, similar facies and color. It is recognized as a beige ledge forming eolian unit with facies that include dune foresets, coarse grained wind ripples (Fig. 3.2). Unit DE2 also displays popcorn weathering and small vugs. Grain size is fine and grains are well-sorted and rounded. The upper contact is sharp (Fig. 3.2). Thickness is 1.6 meters (Fig. 3.3).

Unit DE3 may correlate with Unit E5 at Little Gypsum Valley on the basis of relative

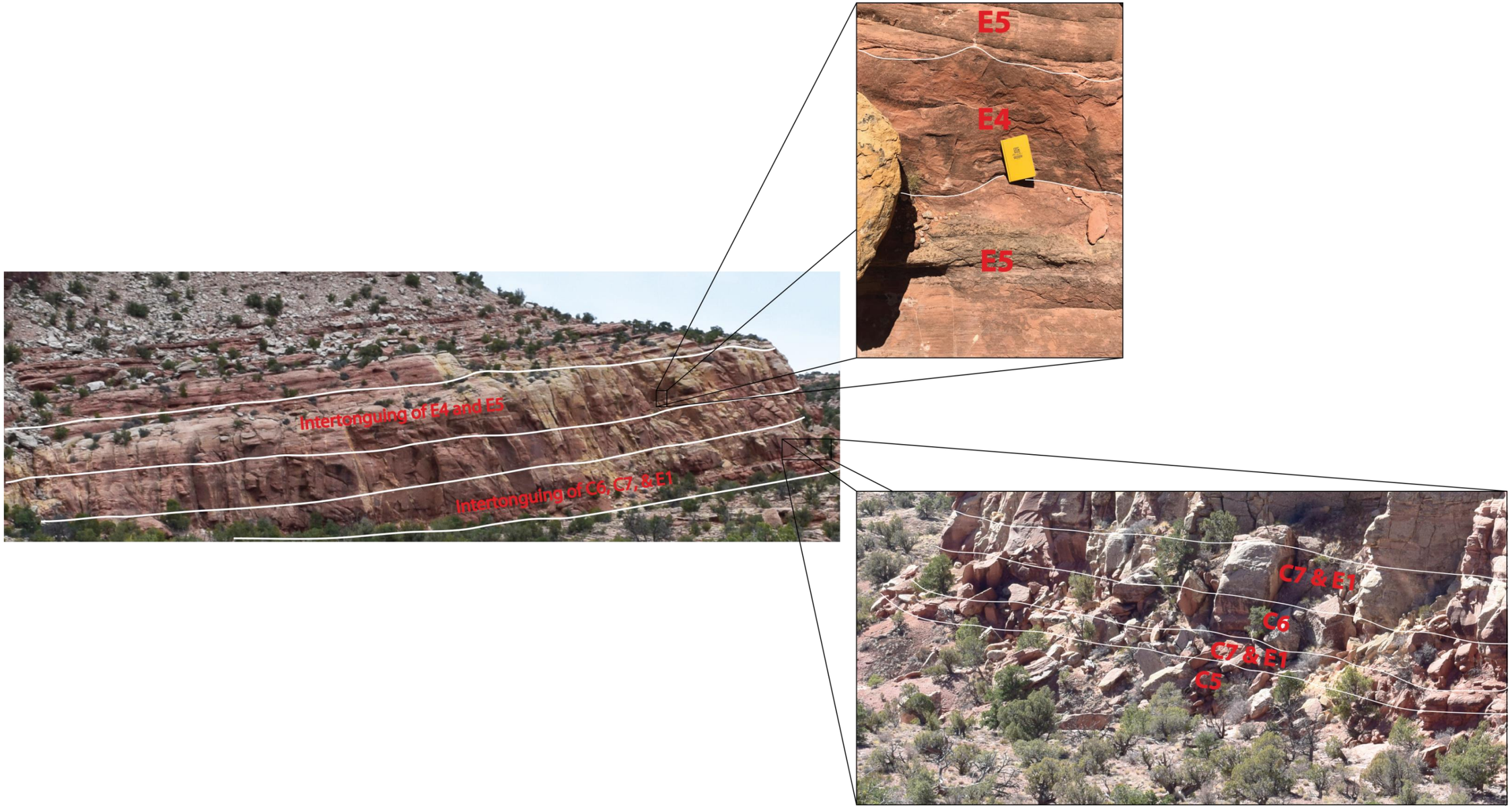

Figure 3.5: The group of images above show two sets of intertonguing relationships within Section 7 units dipping into the diapir at the southern portion of the study area. The first set of intertonguing involves Units C7 and E1 sitting unconformably atop Unit C5 and then a repetition of these units above C6 where they are expected to be stratigraphically. The second set involves intertonguing between Units E4 and E5, which alternate every 0.5-2 meters.

stratigraphic position, facies and color. It is recognized as pink eolian dunes with an overall lack of sedimentary structures, mottling, and hints of dune foresets (Fig. 3.2). Grain size is fine and grains are well-sorted and rounded. The upper contact is sharp (Fig. 3.2). Thickness is 3.4 meters (Fig. 3.3).

Unit DE4 may correlate with Unit E7 at Little Gypsum Valley on the basis of relative stratigraphic position and color, but has few distinctive facies in common. It is recognized as a white to gray eolian dunes with large well defined dune foresets, coarse-grained wind ripples, avalanche deposits, and grain flows (Fig. 3.2). Nodular concretions similar to those in Unit E7 are present near the top. Grain size is fine and grains are well-sorted and rounded. The upper contact with the Jurassic Summerville is scoured. Thickness is 33.3 meters (Fig. 3.3).

Figure 3.6: This image shows the intertonguing relationship that occurs at the northern portion of the study area between Sections 3 and 4. Unit C7 is missing from these sections and Units E1 and E2 repeat in a single consecutive occurrence.

Figure 3.7: Photo panorama taken at the base of Section 7 (Fig. 3.1). Thinning is noticeable in all units as they dip westward (left) into the diapir over approximately 300 meters. Such drastic thinning is not observed at locations away from the diapir and is not mentioned in any previous studies.

Chapter 4: Petrographic Facies Analysis and Diagenesis

Collected samples were selected carefully to cover the study area and encompass as many lithologies as possible making up the Carmel and Entrada formations (Fig. 4.1). Of the 33 samples that were gathered, 30 samples were point counted to estimate their lithologies, cement types, and porosity (Fig. 4.20). Three-hundred points were counted on each thin-section.

Eleven samples are from FA-TF, three from FA-WI, four from FA-SE, three from FA-PS, three from FA-LE, three from FA-SC, and three from FA-ME. All thirty of the samples came from fine to medium grained sandstones. Most are fine grained although some contain notable amounts of silt sized particles, especially within FA-TF and FA-PS. Clastic grains formed 49-72% of the samples. Grain composition varied from 77-94% quartz, 2-12% feldspar, and 2-13% lithics. Classification of samples is determined by the location of where each is plotted on a ternary diagram (Fig. 4.13).

Samples were classified into petrofacies on the basis of detrital grain types, cements, and pore fabric. Restoration of paragenetic history was accomplished using the relationships among cement formation, dissolution, and compaction events.

Several diagenetic elements are apparent as color variations in the Entrada Sandstone and Carmel outcrops. These colors include dark red, orange-red, pink, buff and white both on the salt shoulder and at Slick Rock Canyon. The color changes originate from disparities with the amount of hematite cement present in each unit. In some areas on the salt shoulder, especially those that dip away from the crest, heavy fracturing has resulted in reduction from red to yellow as fluids have passed through these conduits making it more difficult to distinguish the stratal differences that are usually obvious in other parts of the study area. Twenty-two of the samples analyzed were taken on the salt shoulder. These intervals were similar to the ones at Slick Rock

Canyon thirteen miles away from the diapir, but had more lithofacies changes. Eight additional samples were acquired at this location.

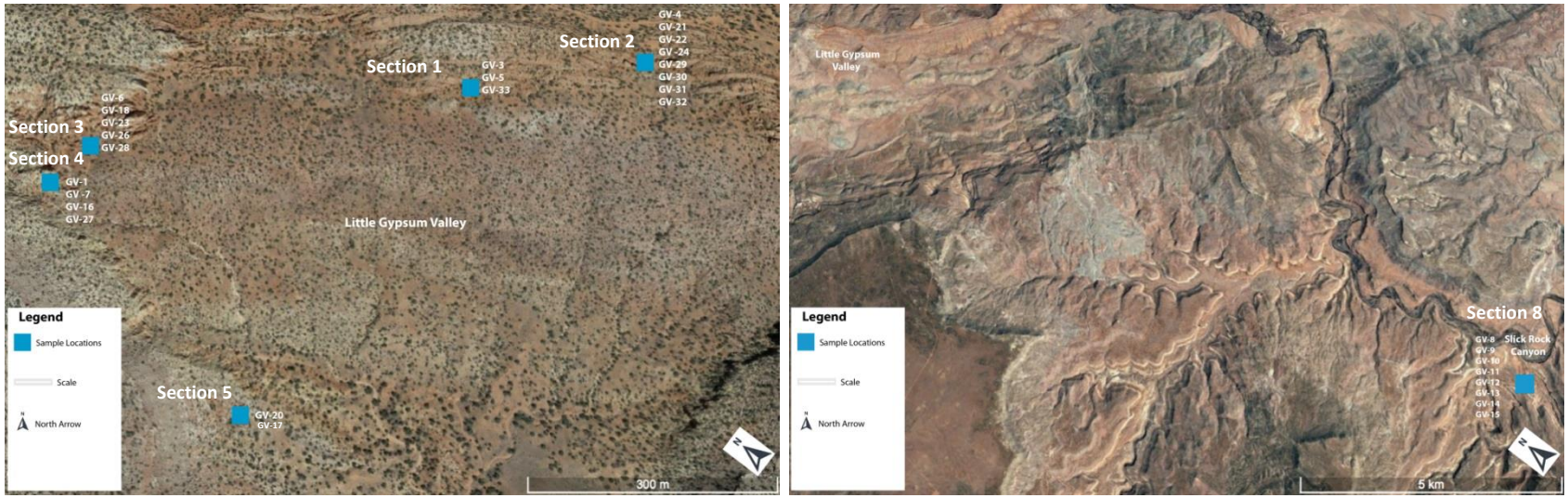

Figure 4.1: Location map for thin section samples acquired at Little Gypsum Valley and Slick Rock Canyon.

4.1 Petrofacies Associations (PFA)

Eleven petrofacies were identified from 30 microscopically analyzed thin sections. They were classified on the basis of grain composition, cement, and porosity.

4.1.1 PFA1: PFA1 is present in samples GV-1, GV-7, and GV16 (Fig. 4.1). These samples were derived from FA-PS, and units in direct contact with the paleosol. All three were gathered in Section 4 unit E2 (Fig. 3.1 and 2.10) at the northern portion of the study area where units dip south a few hundred meters away from the crest of the diapir and towards the valley. It lies stratigraphically above the first occurrence of FA-SE (Fig. 3.2). Grains comprise 50-55% of this petrofacies. Monocrystalline quartz is the most abundant ranging from 84-87% of the clasts. Feldspar and chert make up an additional 13-16% of the grains in the samples. A majority of the grains in the samples touch and, in some cases, the contacts are embayed, or sutured indicating moderate to heavy amounts of compaction. Cements compose 28-38% of the overall constituents including 79-89% hematite (pore-lining and pore-filling) and a presence of calcite, gypsum, dolomite, clay and chert cements in much lesser amounts. Secondary porosity accounts for 10-18% of the sample's volume resulting from the dissolution of both cement and detrital grains. The texture of the grain fabric is moderately to well-sorted with sub-rounded to rounded grains. Most are generally between 30-100μm (Fig. 4.2).

PFA1 is characterized by a high amount of hematite cement along with relatively moderate amounts of secondary porosity and moderate to heavy amount of compaction. Early cementation of hematite appears to both predate and postdate compaction events. Irregular pores and dissolution fabrics on some grains indicate late stage secondary porosity.

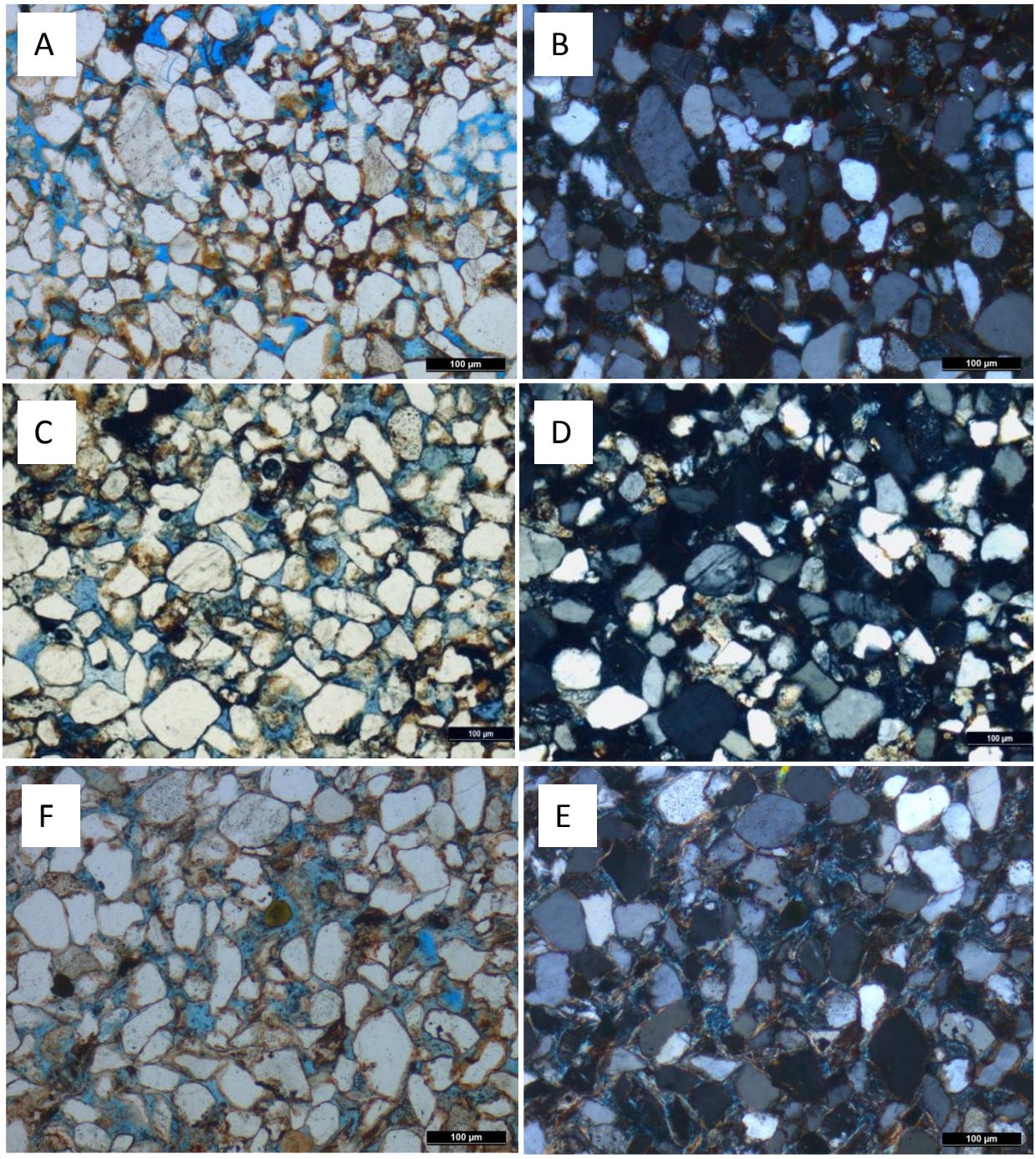

Figure 4.2: PFA1 thin section photos taken under PPL (left) and XPL (right) of samples GV-1 (A&B), GV-7 (C&D), and GV-16 (E&F). Gathered from measured section 4, and part of FA-PS. These samples are primarily characterized by their relatively high amounts of hematite cement that generally lines and sometimes fill pores (H), and moderate amounts of porosity stained blue (P). The scale is set to 100 microns in all photographs.

4.1.2 PFA2: PFA2 is present in samples GV-3, GV-4, GV-31, and GV-33 (Fig. 4.1). These samples were derived from FA-TF in the Carmel formation. They were gathered from Sections 1 and 2 within the units sitting at or near the crest of the diapir in the stratigraphically lowest part of the units studied. Grains comprise 59-63% of this petrofacies. Monocrystalline quartz is the most abundant ranging from 82-88%. Accessory minerals dominated by feldspar and chert make up an additional 12-18% of the grains in the samples. High amounts of compaction in these samples are apparent based on the fact that the majority of grains are in contact with each other and numerous are embayed, or sutured. Cements compose 30-38% of the overall constituents including 44-63% hematite cement (pore-lining and pore filling), 31-47% calcite cement (pore-filling) and a presence of dolomite, clay, chert and gypsum cements in much lesser amounts. Secondary porosity accounts for 1-8% of the sample's total composition resulting from partial and complete dissolution of detrital grains and parts of cements lining those grains. The texture of the grain fabric is poorly to moderately sorted with sub-rounded grains. Most are generally between 30-70μm (Fig. 4.3).

PFA2 can be distinguished from other petrofacies on the basis of its high quantity of hematite cement, moderate amount of calcite cement, and low to absent secondary porosity. Early cementation of both hematite and calcite appear to predate compaction events as growths are either deformed by surrounding grains, or only a small amount of cement remains confined by sutured contacts. Later cementation of both cement types occurred as well. The small amount of irregular pores and dissolution on some of the grains indicates late stage secondary porosity.

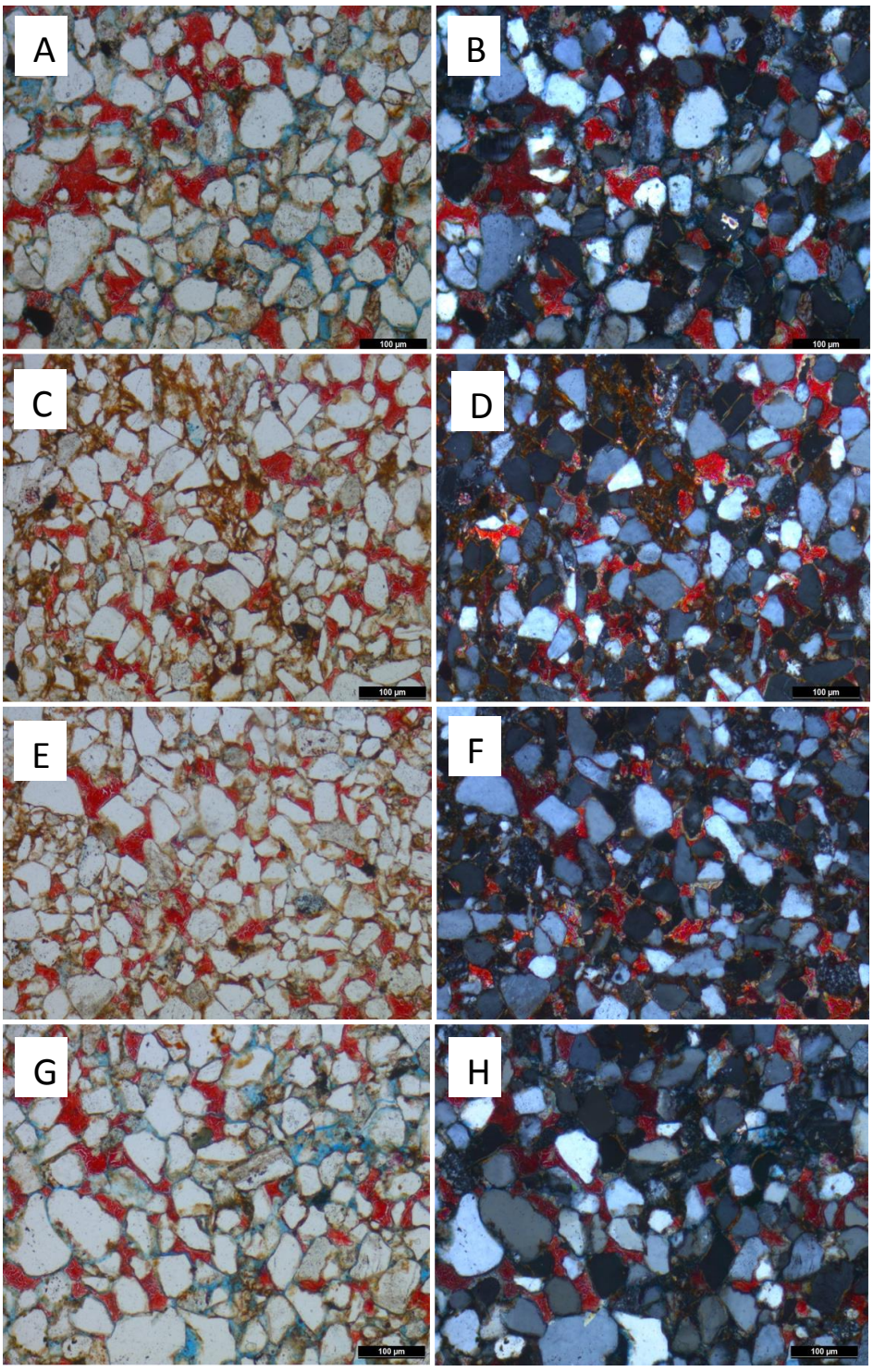

Figure 4.3: PFA2 thin section photos taken under PPL (left) and XPL (right) of samples GV-3 (A&B), GV-4 (C&D), GV-31 (E&F), and GV-33 (G&H). Gathered from measured sections 1 and 2, and part of FA-TF. These samples are primarily characterized by their relatively high amounts of hematite cement that generally lines and sometimes fill pores (H), moderate amounts of calcite cement stained red (C), and low amounts of porosity stained blue (P). The scale is set to 100 microns in all photographs.

4.1.3 PFA3: PFA3 is present in samples GV-18, GV-21, GV-22, GV-24, and GV-26 (Fig. 4.1). These samples were derived from FA-SE, FA-LE, and FA-SC within the Entrada formation. They were gathered within Sections 1 and 3 from units deposited near the crest of the diapir as well as ones that dip away from it towards the south. Stratigraphically the sampled units sit above FA-TF, the first occurrence of FA-WI, FA-ME, and the second occurrence of FA-SE. Grains comprise 63-70% of this petrofacies. Monocrystalline quartz is the most abundant ranging from 90-94%. Accessory minerals, dominated by feldspar, make up an additional 7-10% of the grains in the samples. Low amounts of compaction are evident from a fabric of relatively sparser grains where the majority do not touch each other and boundaries lack embayment and sutured contacts. Cements compose 7-16% of the overall constituents including 33-61% calcite cement (pore-filling), 13-27% hematite, and the presence of quartz overgrowths, dolomite, clay, chert, gypsum, and ferroan calcite cements in much lesser amounts. Secondary porosity accounts for 15-22% of the sample's total composition resulting from both complete and partial dissolution of detrital grains and the cements between them. The texture of the fabric is moderately to well-sorted with sub-rounded to well- rounded grains. Most are generally between 50-120μm (Fig. 4.4).

PFA3 can be distinguished from other petrofacies on the basis of its low quantity of cement, higher porosity, and low amounts of compaction. Hematite and calcite cements formed in an early event prior to any compaction event. A second formation of these cements occurred after minor compaction as well as a minor amount of quartz overgrowths in a few of the samples. The irregular grain sized pores and microcrystalline dissolution on some grains indicates late stage secondary porosity.

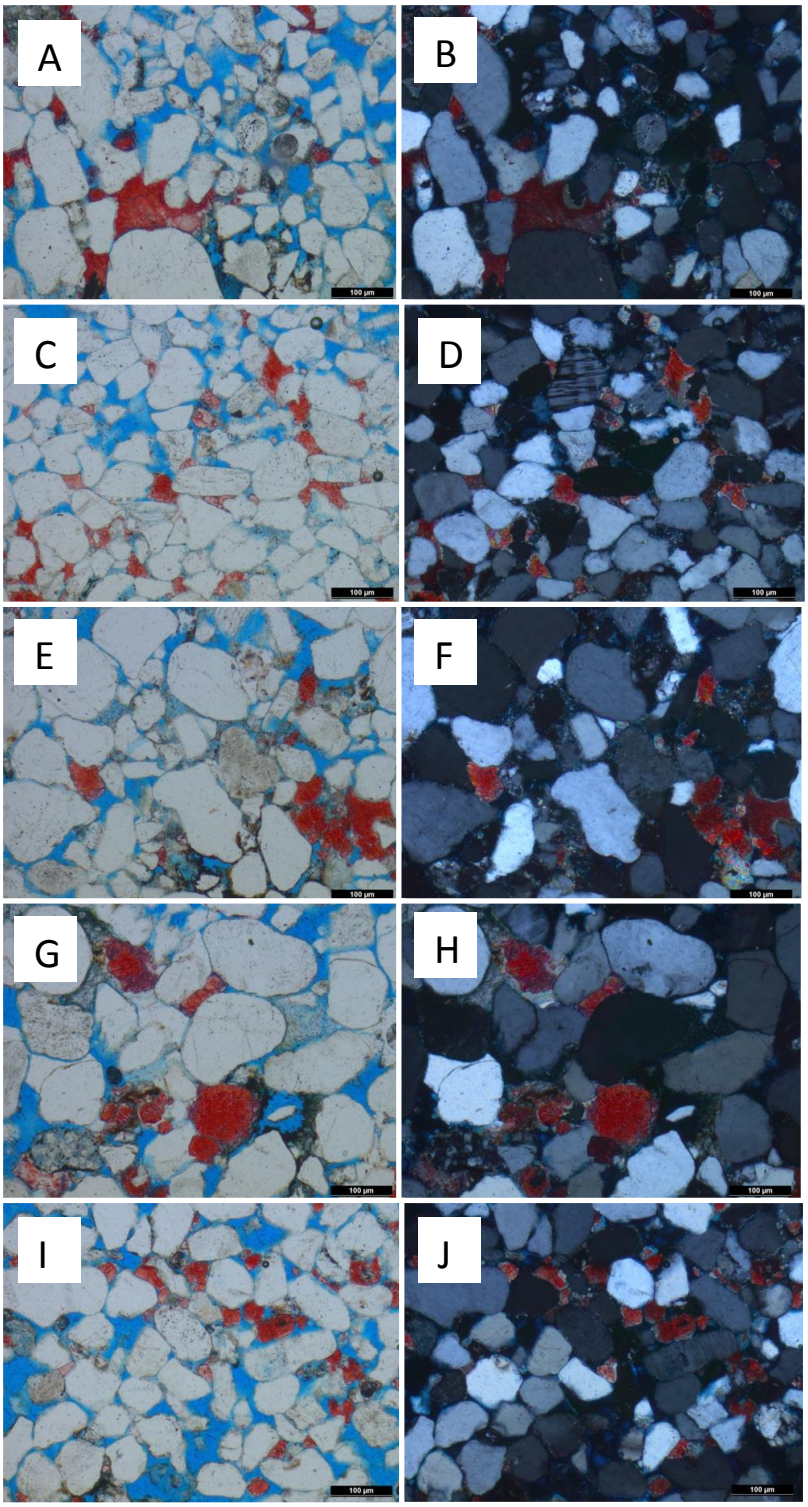

Figure 4.4: PFA3 thin section photos taken under PPL (left) and XPL (right) of samples GV-18 (A&B), GV-21 (C&D), GV-22 (E&F), GV-24 (G&H) and GV-26 (I&J). Gathered from measured sections 2 and 3, and part of FA-SE, FA-LE and FA-SC. These samples are primarily characterized by their relatively low amount amounts of cement and high amounts of porosity stained blue (P). The scale is set to 100 microns in all photographs.

4.1.4 PFA4: PFA4 is present in samples GV-30 and GV-32 (Fig. 4.1). These samples were derived from FA-TF and FA-WI within the Carmel and Entrada formations (Fig. 4.1, 3.1 and 2.10). They were gathered from Section 2 within untis deposited near the crest of the diapir. Stratigraphically the sampled units sit at the bottom portion of FA-TF and the first occurrences of FA-SE and FA-LE. Grains comprise 49-50% of this petrofacies. Monocrystalline quartz is the most abundant ranging from 77-91%. Accessory minerals dominated by feldspar and chert make up an additional 9-23% of the grains in the samples. Low to moderate amounts of compaction are apparent in portions of the samples where grains are in contact with each other, but have fewer sutured contacts and lack embayment of the grains comparatively. Cements compose 40-44% of the overall constituents including 55-63% calcite cement (pore-filling), 34-37% hematite cement (pore-lining and pore-filling), and the presence of dolomite, clay, gypsum, chert and ferroan calcite cements in much lesser amounts. Secondary porosity accounts for 7-10% of the sample's total composition resulting from both partial and complete dissolution of detrital grains and the cements between them. The texture of the fabric is moderately to well sorted with sub-rounded grains. Most are generally between 30-70μm (Fig. 4.5).

PFA4 can be distinguished from other petrofacies on the basis of its very high quantity of cement, low amounts of secondary porosity, and low to moderate level of compaction. Hematite and calcite cements formed in an early event prior to any compaction activity. Additional formations of both these cement types also occurred post compaction. The irregular grain sized pores and microcrystalline dissolution on some grains indicates late stage secondary porosity.

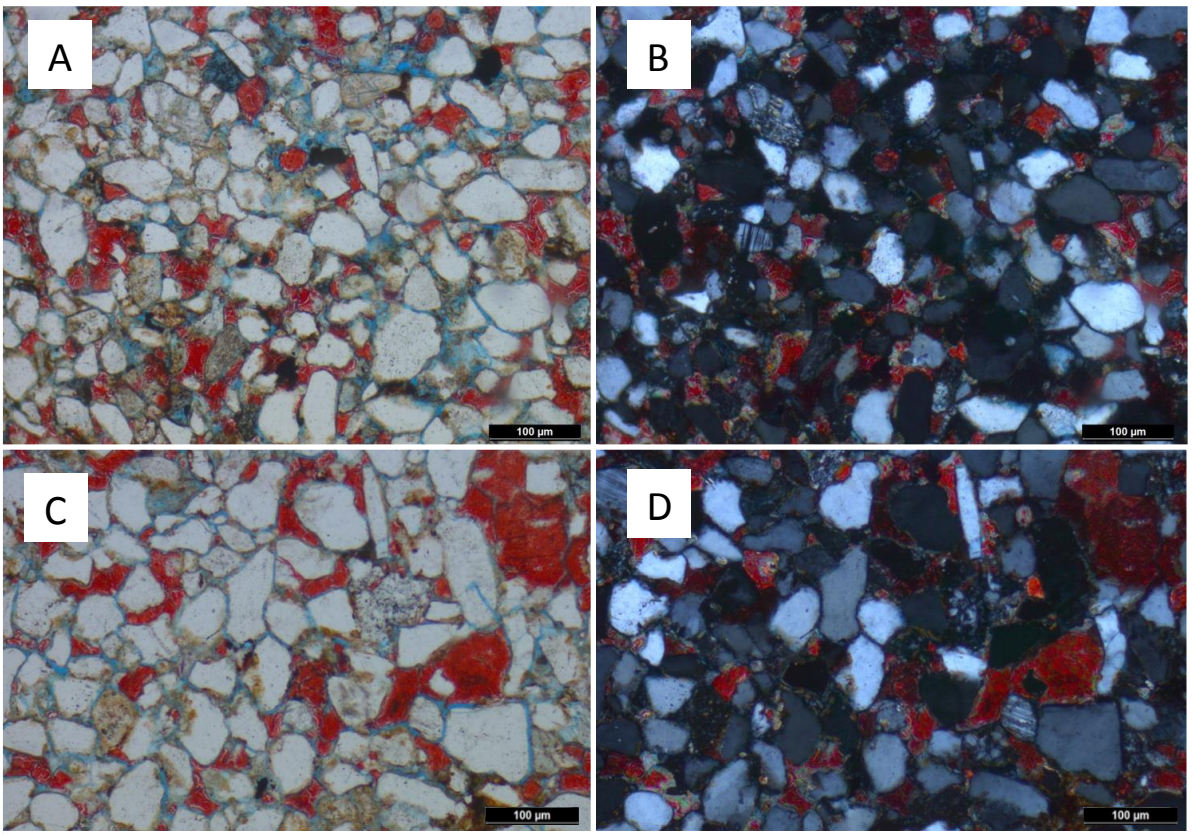

Figure 4.5: PFA4 thin section photos taken under PPL (left) and XPL (right) of samples GV-30 (A&B) and GV-32 (C&D). Gathered from measured section 2, and part of FA-TF and FA-WI. These samples are primarily characterized by their relatively high amounts cement, and low amounts of porosity stained blue (P). The scale is set to 100 microns in all

4.1.5 PFA5: PFA5 is present in samples GV-23, GV-28, and GV-29 (Fig. 4.1). These samples were derived from FA-TF, FA-SE, and FA-ME within the Carmel and Entrada formations (Fig. 4.1, 3.1 and 2.10). They were gathered from Section 2 and Section 3 within units deposited near the crest of the diapir as well as ones that dip away from it towards the south. Stratigraphically the sampled units sit towards the top of FA-TF and above the second occurrence of FA-WI. Grains comprise 55-63% of this petrofacies. Monocrystalline quartz is the most abundant ranging from 85-87%. Accessory minerals dominated by chert and feldspar make up an additional 13-15% of the grains in the samples. Low to moderate amounts of compaction are apparent in portions of the samples where grains are in contact with each other, but have fewer sutured contacts and lack embayment of the grains comparatively. Cements comprise 19-29% of the overall constituents including 43-64% calcite cement (pore-filling), 23-45%, hematite cement (pore-lining and pore-filling), and the presence of dolomite, clay, gypsum, chert, and ferroan calcite cements in much lesser amounts. Secondary porosity accounts for 13-18% of the samples total composition resulting from both partial and complete dissolution of detrital grains and the cements lining them. The texture of the fabric is well sorted with sub-rounded to rounded grains. Most are generally between 40-120µm (Fig. 4.6).

PFA5 can be distinguished from other petrofacies on the basis of its relatively moderate amounts of cement, porosity, and level of compaction. Hematite and calcite cements formed in an early event prior to any compaction activity. Additional formations of both these cement types also occurred post compaction. The irregular grain sized pores and microcrystalline dissolution on some grains indicates late stage secondary porosity.

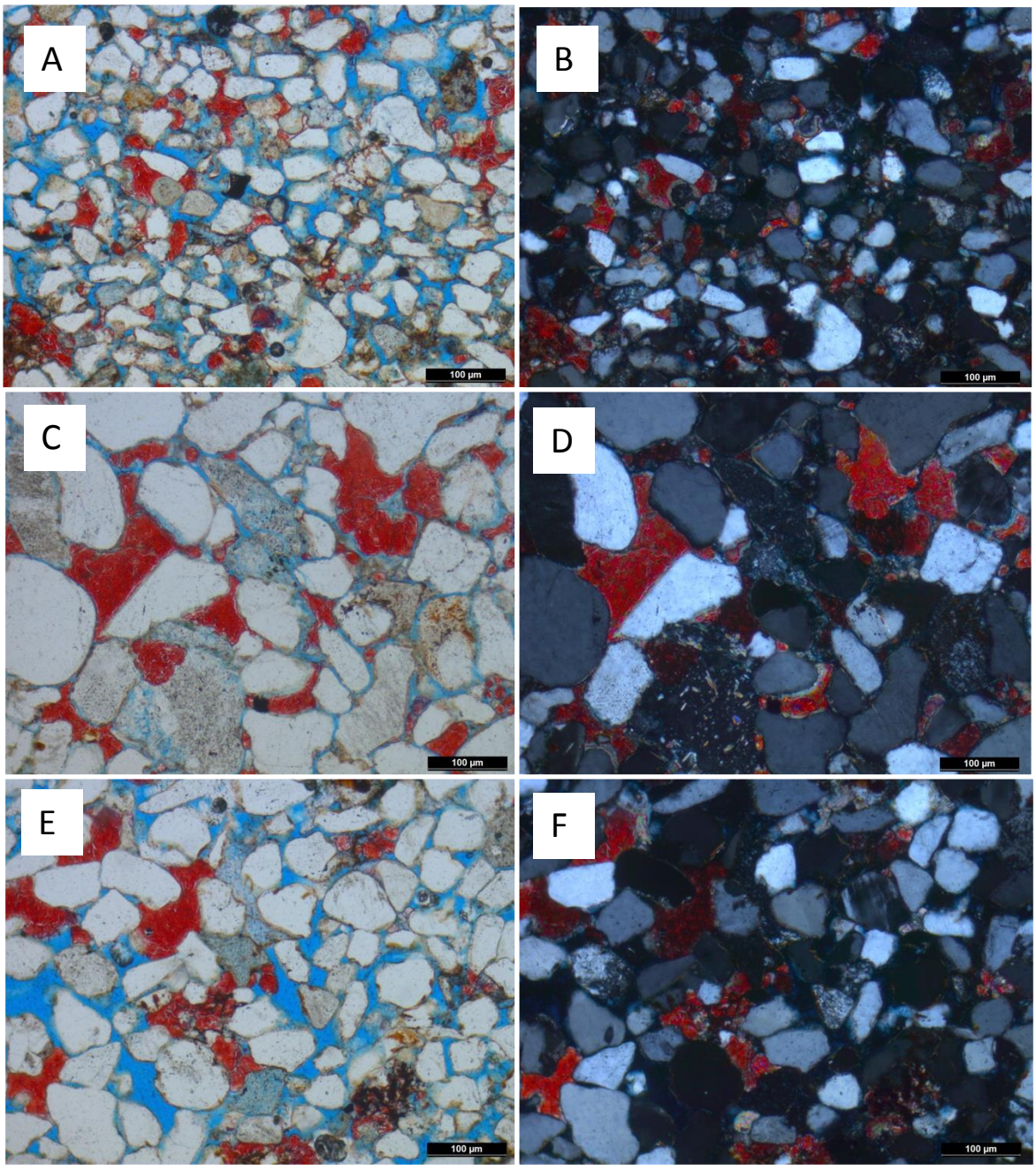

Figure 4.6: PFA5 thin section photos taken under PPL (left) and XPL (right) of samples GV-23 (A&B), GV-28 (C&D), and GV-29 (E&F). Gathered from measured section 2 and 3, and part of FA-TF, FA-SE, and FA-ME. These samples are primarily characterized by their relatively moderate amounts of cement, and moderate amounts of porosity stained blue (P). The scale is set to 100 microns in all photographs.

4.1.6 PFA6: PFA6 is present in samples GV-5, GV-17 and GV-20 (Fig. 4.1). These samples were derived from FA-WI and FA-LE from the Entrada formation having been fractured and subsequently altered by fluid flow. They were gathered from Section 1 and 5 from units deposited near the crest of the diapir as well as ones that dip away from it towards the south. Stratigraphically these units sit above the first occurrences of FA-WI, FA-SE, and FA-LE (Fig. 4.1, 3.1 and 2.10). Grains comprise 63-72% of this petrofacies. Monocrystalline quartz is the most abundant ranging from 76-89%. Accessory minerals dominated by feldspar and chert make up an additional 11-24% of the grains in the samples. Low to moderate amounts of compaction are apparent in portions of the samples where grains are in contact with each other, but have fewer sutured contacts and lack embayment of the grains comparatively. Cements comprise 13-24% including 22-28% calcite cement, 0-70% hematite cement, 0-64% clay cement, 24% dolomite cement exclusive to sample GV-5 and the presence of chert and gypsum cements in much lesser amounts. Secondary porosity accounts for 12-17% of the samples total composition resulting from partial and complete dissolution of detrital grains and the cements lining them. The texture of the fabric is moderate to well-sorted with sub-rounded to rounded grains. Most are generally between 50-100μm (Fig. 4.7).

PFA6 can be distinguished from other petrofacies on the basis of its relatively low cement content, moderate porosity, and low to moderate amounts of compaction. Early formation of hematite cement in samples GV-5 and GV-20 and clay cement in sample GV-17 occurred before any compaction activity. Calcite cement formed post compaction in all samples. The irregular grain sized pores and microcrystalline dissolution on some grains indicates late stage secondary porosity.

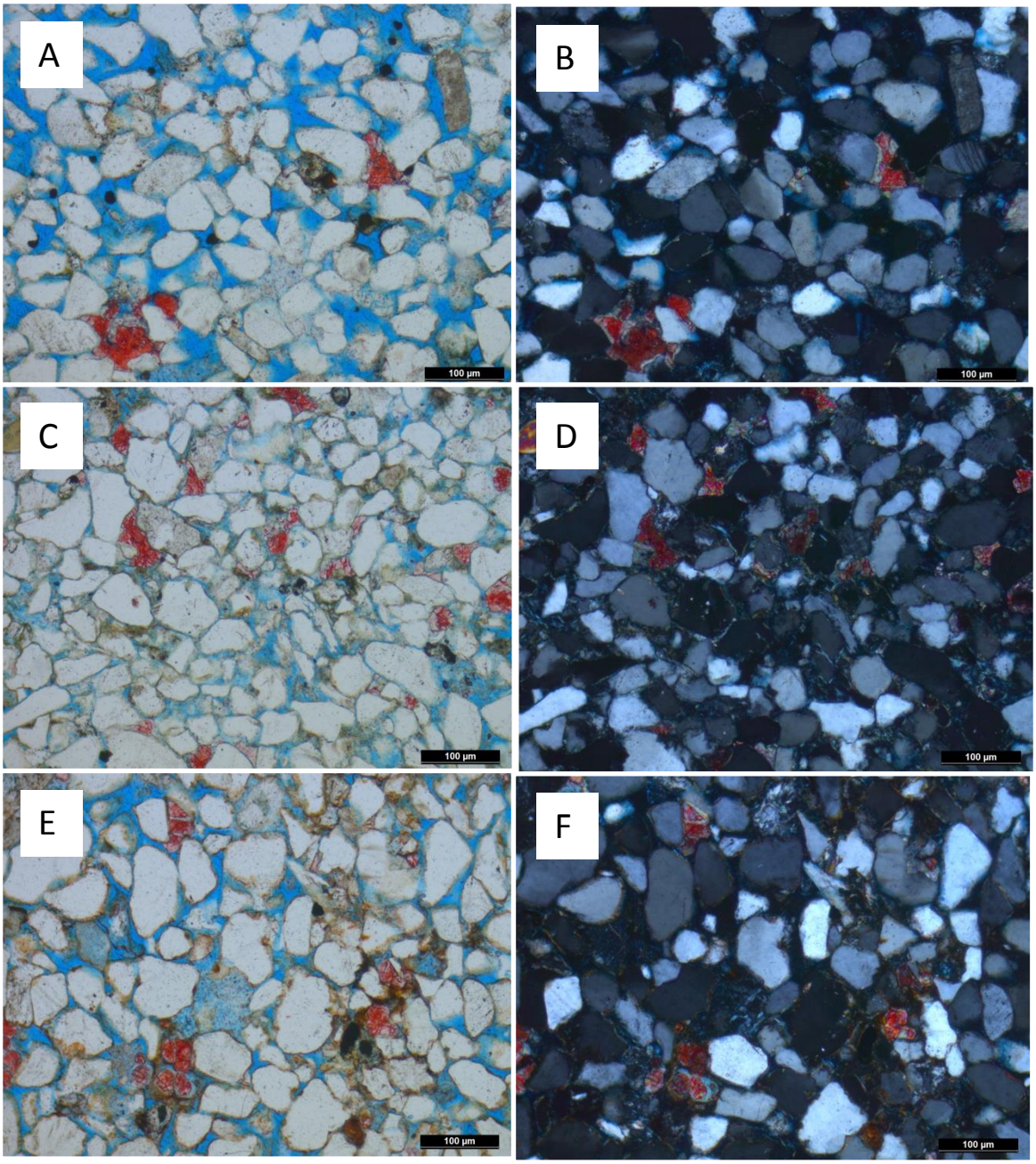

Figure 4.7: PFA6 thin section photos taken under PPL (left) and XPL (right) of samples GV-5 (A&B), GV-17 (C&D), and GV-20 (E&F). Gathered from measured section 1 and 5, and part of FA-WI and FA-LE. These samples are primarily characterized by their relatively low amounts of cement, and moderate amounts of porosity stained blue (P). The scale is set to 100 microns in all photographs.

4.1.7 PFA7: PFA7 is present in sample GV-6 (Fig. 4.1). This sample was derived from FA-TF within the Carmel Formation having been fractured and subsequently altered by fluids flowing through the conduits. It was gathered from Section 3 from a unit deposited near the crest of the diapir. Stratigraphically this unit sits at the Carmel/Entrada section. Grains comprise 56% of this petrofacies. Monocrystalline quartz is the most abundant at 90%. Accessory minerals dominated by chert and feldspar make up an additional 10% of the grains in the samples. Moderate to high amounts of compaction are apparent as many of the grains are in contact with each other and, in some cases, the grains are embayed, or the contacts between them are sutured. Cements comprise 36% including 70% hematite cement (pore-lining and pore-filling), 27% calcite cement (pore-filling), and the presence of clay and gypsum cements in much lesser amounts. Secondary porosity accounts for 8% of the samples total composition resulting from both partial and complete dissolution of detrital grains and the cements lining them. The texture of the fabric is moderately sorted with rounded grains. Most are generally between 30-80μm (Fig. 4.8).

PFA7 can be distinguished from other petrofacies on the basis of its relatively high amount of hematite cement, low porosity and moderate to high amounts of compaction. Hematite cement formed in an early event prior to any compaction activity. Additional formation of both calcite and hematite cement types also occurred post compaction. The irregular grain sized pores and microcrystalline dissolution on some grains indicates late stage secondary porosity. Porosity is also slightly higher in parts of the sample where hematite cement has been leached by the altering fluid.

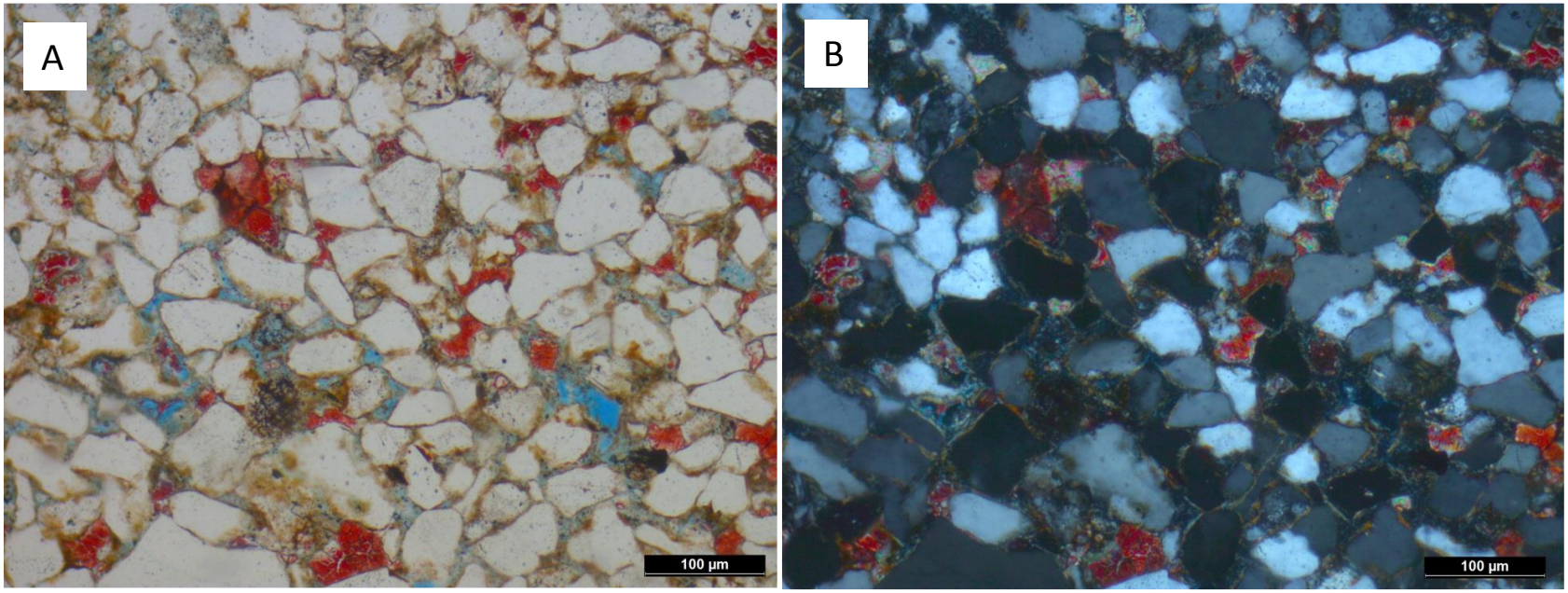

Figure 4.8: PFA7 thin section photos taken under PPL (left) and XPL (right) of samples GV-6 (A&B). Gathered from measured section 3, and part of FA-TF. These samples are primarily characterized by their relatively high amounts of hematite cement that generally lines and sometimes fill pores (H), low amounts of calcite cement (C) and moderate amounts of porosity stained blue (P). The scale is set to 100 microns in all photographs.

4.1.8 PFA8: PFA8 is present in sample GV-27 (Fig. 4.1). This sample was derived from FA-SC within the Entrada Formation having been fractured and subsequently altered by fluids flowing through the conduits. It was gathered from Section 4 from a unit deposited within units that dip to the south approximately 200 meters from the crest of the diapir (Fig. 2.1 and 2.10). Stratigraphically this is the top Unit E7. Grains comprise 67% of this petrofacies. Monocrystalline quartz is the most abundant at 90%. Accessory minerals dominated by feldspar make up an additional 10% of the grains in the samples. Low to moderate amounts of compaction are apparent as many of the grains are in contact with each other and, in a few cases, the grains are embayed, or the contacts between them are sutured. Cements comprise 28% including 85% calcite cement (pore-filling), 10% dolomite cement (pore-filling), and the presence of hematite, chert, and clay cements in much lesser amounts. Secondary porosity accounts for 4% of the samples total composition resulting from mostly partial dissolution of detrital grains and the cements lining them. The texture of the fabric is well-sorted with rounded grains. Most are generally between 80-150μm (Fig. 4.9).

PFA8 can be distinguished from other petrofacies on the basis of its relatively high amount of calcite cement, low porosity and low to moderate amounts of compaction. Calcite cement present formed late and is post compactional. Small amounts of irregular shaped and grain sized pores as well as microcrystalline dissolution on some grains indicates late-stage secondary porosity.

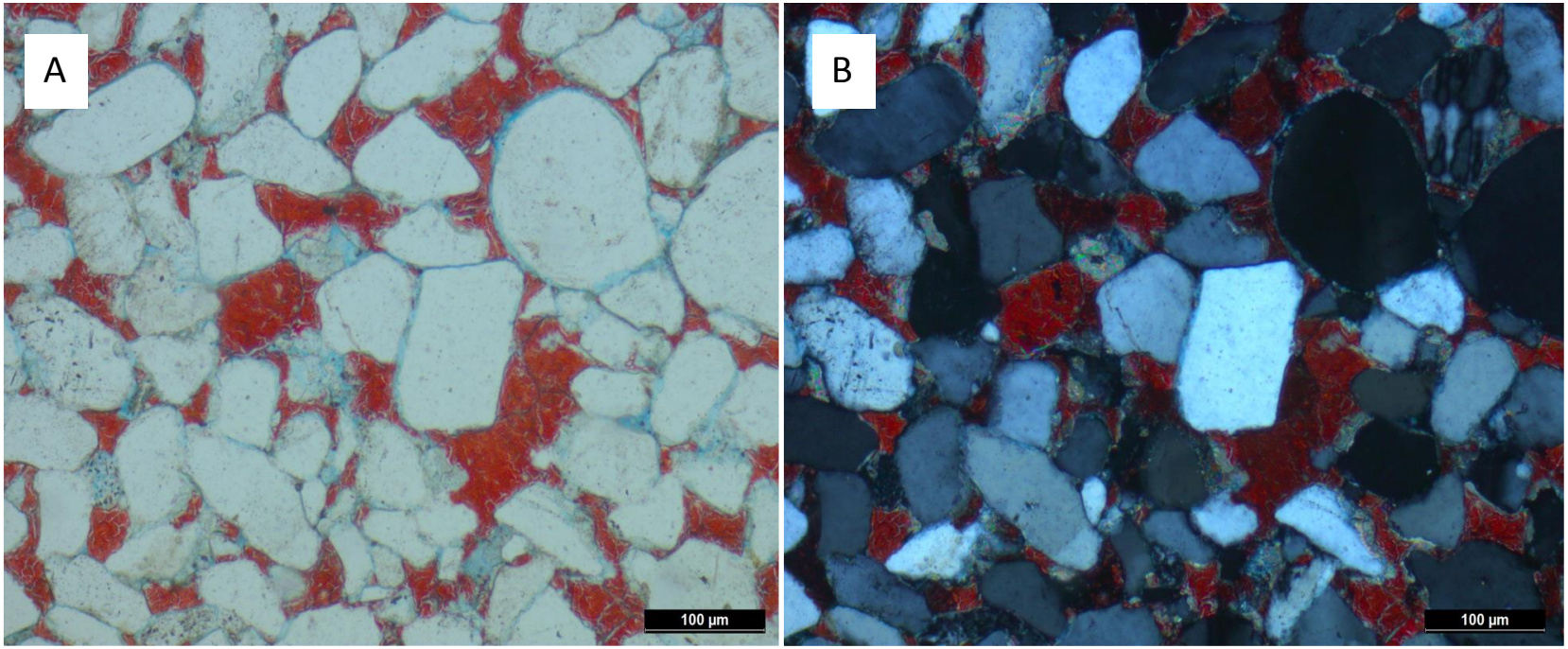

Figure 4.9: PFA8 thin section photos taken under PPL (left) and XPL (right) of samples GV-27 (A&B). Gathered from measured section 4, and part of FA-SC. These samples are primarily characterized by their relatively high amounts of calcite cement (C), and moderate amounts of porosity stained blue (P). The scale is set to 100 microns in all photographs.

4.1.9 PFA9: PFA9 is present in samples GV-8 and GV-10 (Fig. 4.1). These samples were derived from FA-TF within what is considered typical Carmel formation. They were gathered from Section 8 within units deposited 13km to the southwest of the Gysum Valley salt wall (Fig. 4.1, 3.1 and 2.10). Stratigraphically the sampled units sit at the lowest portion of the section of the section studied. Grains comprise 59-60% of this petrofacies. Monocrystalline quartz is the most abundant ranging from 86-88%. Accessory minerals dominated by chert and feldspar make up an additional 12-14% of the grains in the samples. Moderate amounts of compaction are apparent in the samples as many of the grains are in contact with each other, and some have sutured contacts. Cements comprise 35-37% of the overall constituents including 69-80% hematite cement (pore-filling and pore-filling), 15-21%, dolomite cement (pore-filling), and the presence of clay, gypsum, chert, and ferroan calcite cements in much lesser amounts. Secondary porosity accounts for 2-4% of the samples total composition resulting from both partial and complete dissolution of detrital grains and the cements lining them. The texture of the fabric is poorly to moderately sorted with sub-rounded grains. Most are generally between 20-60μm (Fig. 4.10).

PFA9 can be distinguished from other petrofacies on the basis of its relatively high amount of hematite cement, moderate amount of dolomite cement, low porosity, and moderate level of compaction. Hematite cement formed in an early event prior to any compaction activity. Additional formation of hematite and dolomite cement types also occurred post compaction. Small amounts of irregular shaped and grain sized pores as well as microcrystalline dissolution on some grains indicates late stage secondary porosity.

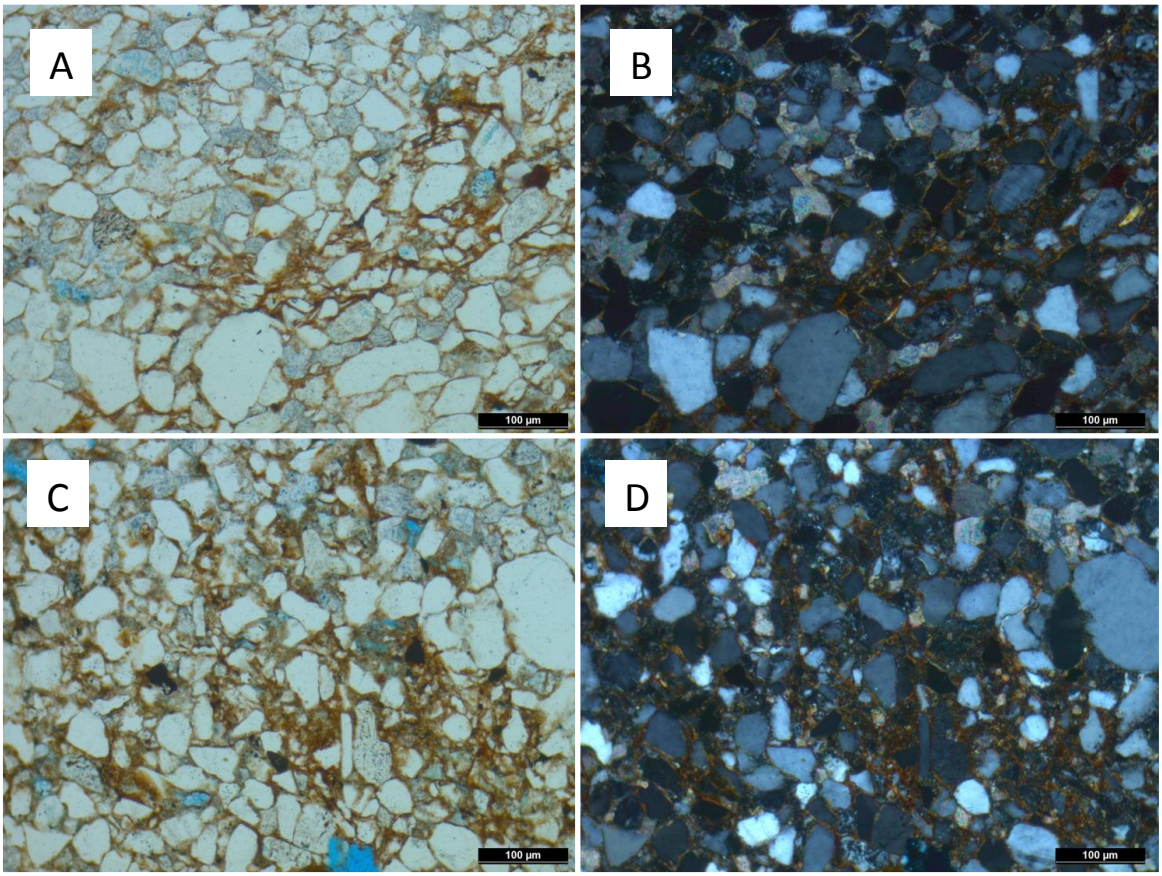

Figure 4.10: PFA9 thin section photos taken under PPL (left) and XPL (right) of samples GV-8 (A&B), GV-10 (C&D). Gathered from measured section 8, and part of FA-TF. These samples are primarily characterized by their relatively high amounts of hematite cement that generally lines and sometimes fill pores (H), moderate amounts of dolomite cement (D), and low amounts of porosity stained blue (P). The scale is set to 100 microns in all photographs.

4.1.10 PFA10: PFA10 is present in samples GV-9 and GV-11 (Fig. 4.1). These samples were derived from FA-TF within what is considered typical Carmel formation. They were gathered from Section 8 within units deposited 13km to the southwest of the Gysum Valley salt wall (Fig. 4.1, 3.1, and 2.10). Stratigraphically the sampled units sit at the lowest portion of the section studied. Grains comprise 51-59% of this petrofacies. Monocrystalline quartz is the most abundant ranging from 88-90%. Accessory minerals dominated by chert and feldspar make up an additional 10-12% of the grains in the samples. Moderate amounts of compaction are apparent in the samples as many of the grains are in contact with each other, and some have sutured contacts. Embayment of grains is minimal. Cements comprise 39-41% of the overall constituents including 35-57% hematite cement (pore-filling and pore-filling), 37-39%, dolomite cement (pore-filling), 2-7% ferroan calcite cement, and the presence of clay and chert cements in much lesser amounts. Secondary porosity accounts for 2-5% of the samples total composition resulting from both partial and complete dissolution of detrital grains and the cements lining them. The texture of the fabric is moderately to well-sorted with sub-rounded to rounded grains. Most are generally between 20-80μm (Fig. 4.11).

PFA10 can be distinguished from other petrofacies on the basis of its relatively high amount of dolomite cement, moderate amount of hematite cement, low porosity, and moderate level of compaction. Hematite cement formed in an early event prior to any compaction activity. Additional formation of hematite and dolomite cement types also occurred post compaction. Small amounts of irregular shaped and grain sized pores as well as microcrystalline dissolution on some grains indicates late stage secondary porosity.

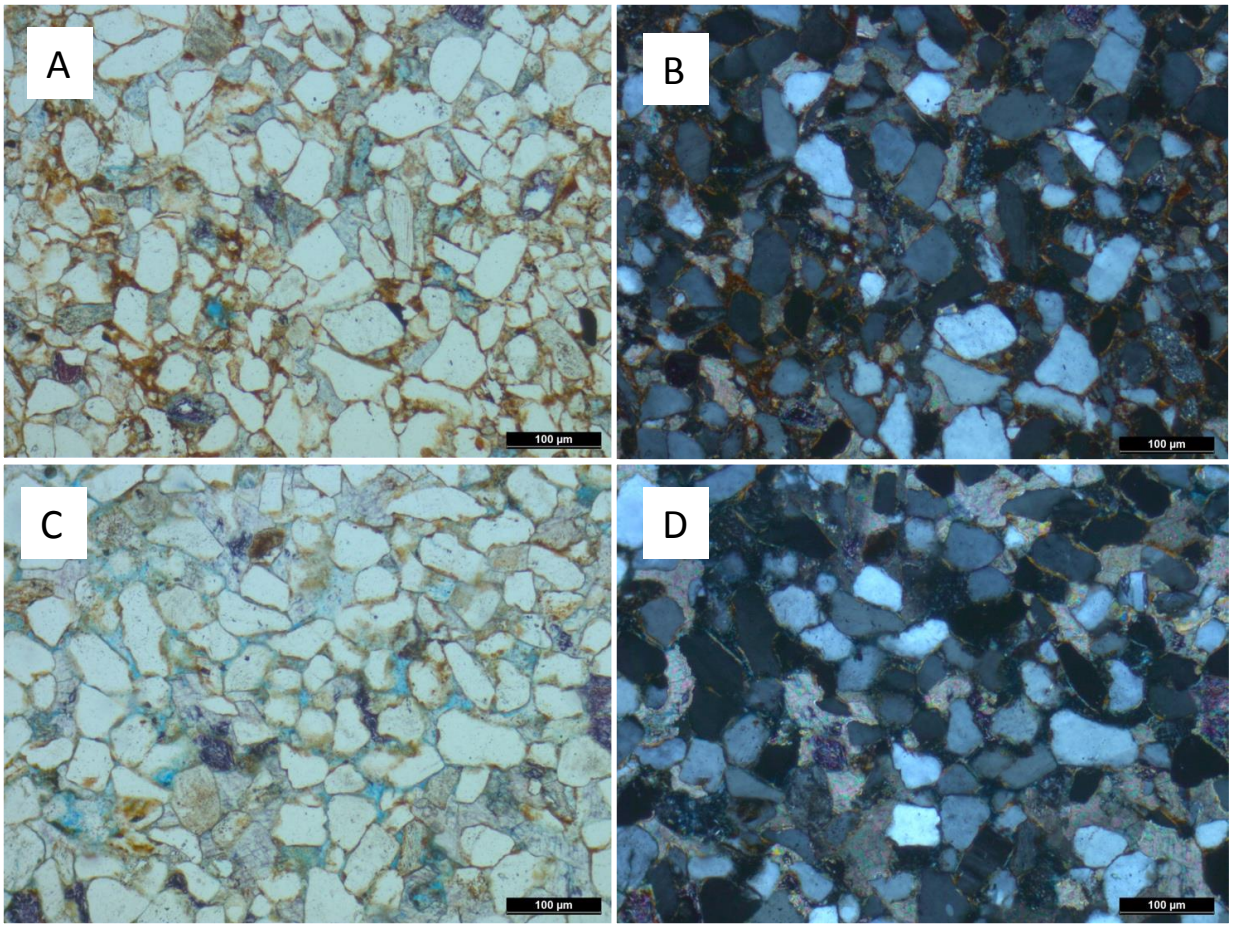

Figure 4.11: PFA10 thin section photos taken under PPL (left) and XPL (right) of samples GV-9 (A&B), GV-11 (C&D). Gathered from measured section 8, and part of FA-TF. These samples are primarily characterized by their relatively moderate amounts of hematite cement that generally lines and sometimes fill pores (H), high amounts of dolomite cement (D), and low amounts of porosity stained blue (P). The scale is set to 100 microns in all photographs.

4.1.11 PFA11: PFA11 is present in samples GV-12, GV-13, GV-14, and GV-15 (Fig. 4.1). These samples were derived from FA-SE, FA-LE, and FA-ME within what is considered typical Entrada formation. They were gathered from Section 8 within units deposited 13km to the southwest of the Gysum Valley salt wall (Fig. 4.1 and 3.1). Stratigraphically the sampled units sit in the upper portion of the section in units DE1-DE4. Grains comprise 56-59% of this petrofacies. Monocrystalline quartz is the most abundant ranging from 89-94%. Accessory minerals dominated by chert and feldspar make up an additional 6-11% of the grains in the samples. Low amounts of compaction are apparent in the samples as there is much more space between the grains and there are minimal signs of sutured contacts. Cements comprise 19-29% of the overall constituents including 15-49% hematite cement (pore-filling and pore-filling), 39-74%, dolomite cement (pore-filling) and the presence of clay and chert, gypsum, and calcite cements in much lesser amounts. Secondary porosity accounts for 10-20% of the samples total composition resulting from both partial and complete dissolution of detrital grains and the cements lining them. The texture of the fabric is moderately to well-sorted with rounded to well-rounded grains. Most are generally between 30-120μm (Fig. 4.12).

PFA11 can be distinguished from other petrofacies on the basis of its relatively high amount of dolomite cement, moderate to high amount of hematite cement, moderate porosity, and low level of compaction. Hematite cement formed in an early event prior to any compaction activity. Additional formation of hematite and dolomite cement types also occurred post compaction. Small amounts of irregular shaped and grain sized pores as well as microcrystalline dissolution on some grains indicates late stage secondary porosity (Fig. 4.3).

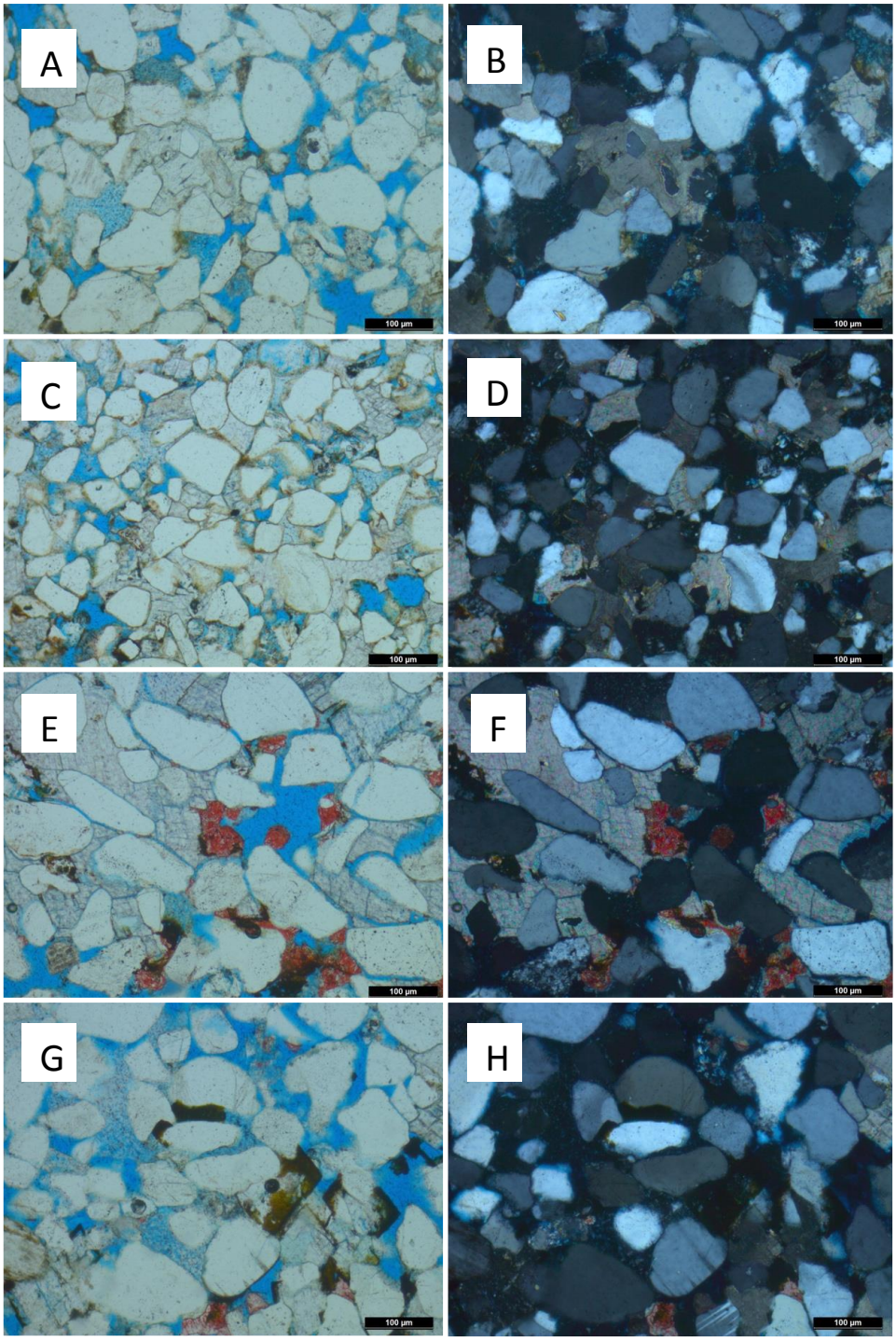

Figure 4.12: PFA11 thin section photos taken under PPL (left) and XPL (right) of samples GV-12 (A&B), GV-13 (C&D), GV-14 (E&F), and GV-15 (G&H). Gathered from measured section 8, and part of FA-SE, FA-LE, and FA-ME. These samples are primarily characterized by their relatively moderate amounts of hematite cement that generally lines and sometimes fill pores (H), moderate amounts of dolomite cement (D), and moderate amounts of porosity stained blue (P). The scale is set to 100 microns in all photographs.

4.2 Petrographic Interpretation

Detrital grain composition in the Entrada and Carmel samples, both on the salt shoulder and at Slick Rock Canyon, suggest a distant source of recycled sedimentary and granitic rocks (Otto & Picard 1976) with hardly any direct influence from the diapir. Primary sediment sources have been interpreted with relation to tectonic activity associated with the Uncompahgre Uplift and the Colorado Front Range of the Ancestral Rocky Mountain Highlands (ARM) (Otto & Picard 1976; Peterson 1989; Trudgill & Paz 2009). Lower amounts of feldspar in these samples compared to others farther north suggest this part of the Entrada/Carmel isn't as proximal to the source of feldspar. Small, but relatively consistent amounts of chert throughout the samples indicates the presence of preexisting sedimentary rock in the source areas (Otto & Picard 1976).

Cater (1970) reported the mean composition of the Entrada/Carmel formations by R. A. Cardigan (1967) as 76% quartz, 9% feldspar, calcite 9%, 3% chert, 3% quartz overgrowth, and 1%> accessory minerals. Individual records of the Carmel Formation's composition as an individual unit are not well documented otherwise. Otto and Picard (1976) recorded the mean composition of the subaerial sandstone facies of their Entrada samples as 67.4% quartz, 15.9% pore space, 7.1% feldspar, 3.9% matrix, 2.5% lithic fragments, 1.8% authigenic carbonate, 1.1% quartz overgrowth (silica), and 1%> accessory minerals. In addition, they recorded the mean composition of subaqueous sandstone facies of their Entrada samples as 63.1% quartz, 14.2% authigenic carbonate, 9.2% pore space, 5.3% feldspar, 4% matrix, 2.2% lithic fragments, 1% silica, and 1%> accessory minerals. They classified most of their samples as subarkose having over 75% quartz grains and the majority of the remaining grains being feldspar rich. Netoff (2002) also recorded a similar mean composition for his samples with 80.6% quartz and 16.1% feldspar likewise classifying as subarkose. The overall mean feldspar composition of the samples

documented in this study is approximately 3.2% suggesting that the plutonic or metamorphic source rock is further away from this region than in the comparative studies. Of the samples that were analyzed 14 can be classified as subarkose, 11 as quartzarenite, and 5 as sublitharenite based on their plotted position on the Ternary diagram after Folk (1980) (Fig. 4.13).

Quartz grains are, for the most part, nonundulatory, or slightly undulatory, which is common of typical quartz. Small amounts of strongly undulose and polycrystalline quartz are present having undergone post depositional stresses, but are not necessarily metamorphic in nature (Blatt & Christie 1963; Folk 1961; Krynine 1940). Round grains amongst more angular ones suggest they may originate from recycled sedimentary rock, while the rest likely eroded from various igneous sources (Otto & Picard 1976). Quartz overgrowths are rare within the Entrada/Carmel samples examined in this study. This is consistent with other studies referenced.

PFA2-PFA6 appear to contain detrital material that could be interpreted as originating from the diapir (Fig. 4.19). PFA2 and PFA5 have large clasts composed almost entirely of fine grained crystalline calcite and are a much larger pebble size in contrast to the fine-grained sand that surrounds them. They were sampled at Sections 2 and 3 in stratigraphic units C1 and C2 (Fig. 4.1 and Fig. 3.1). Smaller very-fine sized grains of carbonate material can be observed in the other petrofacies sampled in Sections 1,2, 3, and 5 (Fig. 4.19).

In general, samples that are on the salt shoulder tend to have relatively higher porosities in the Entrada formation (7-20%), however, the opposite is true of samples from Slick Rock Canyon where the Carmel has higher porosity values (8-18%). Porosity is present in most samples and is almost entirely secondary as a result of dissolution of cements and partial to complete dissolution of detrital grains.

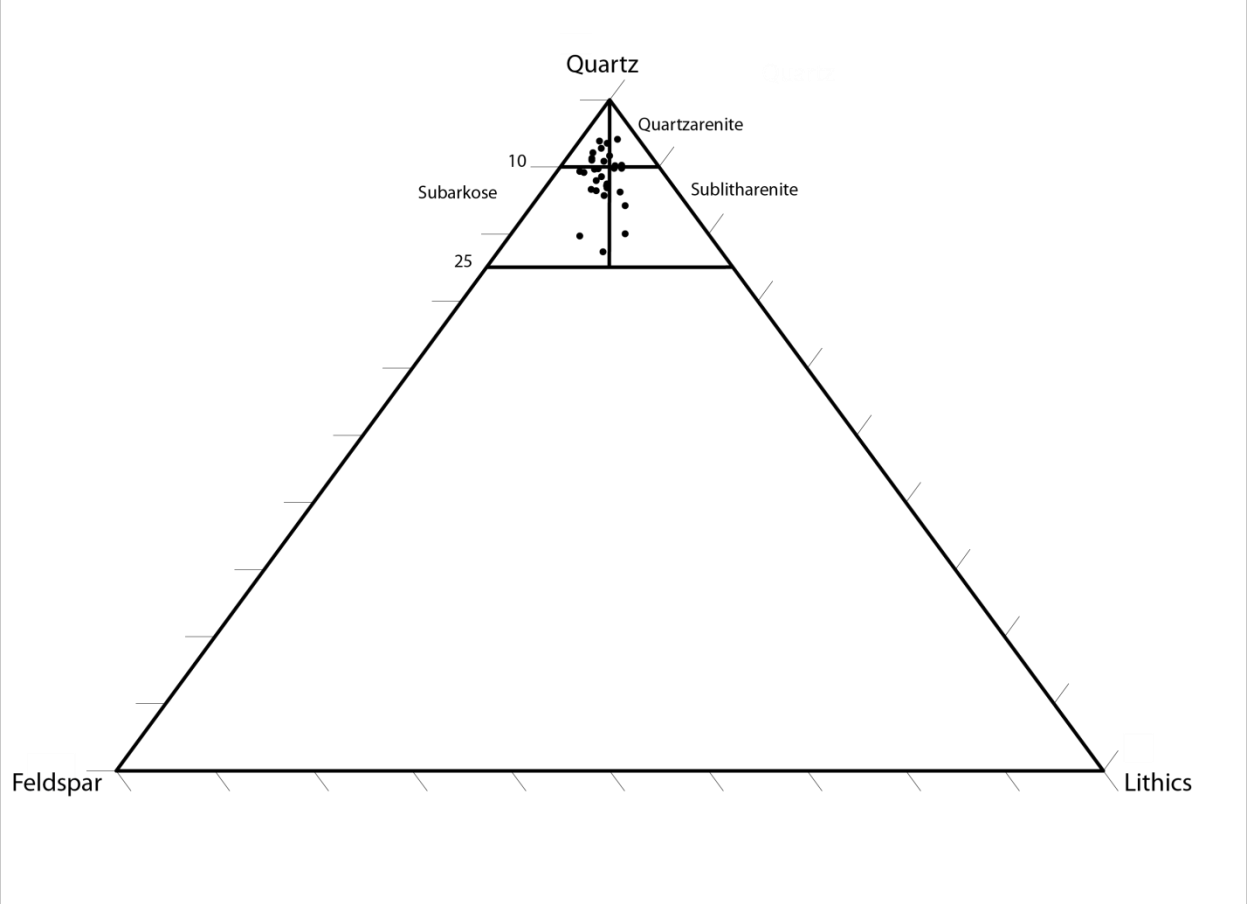

Figure 4.13: Ternary composition diagram after Folk (1980) for all 30 samples analyzed. No compositional discrepancies are apparent between samples at Slick Rock Canyon and those on the salt shoulder.

4.3 Diagenetic Sequences

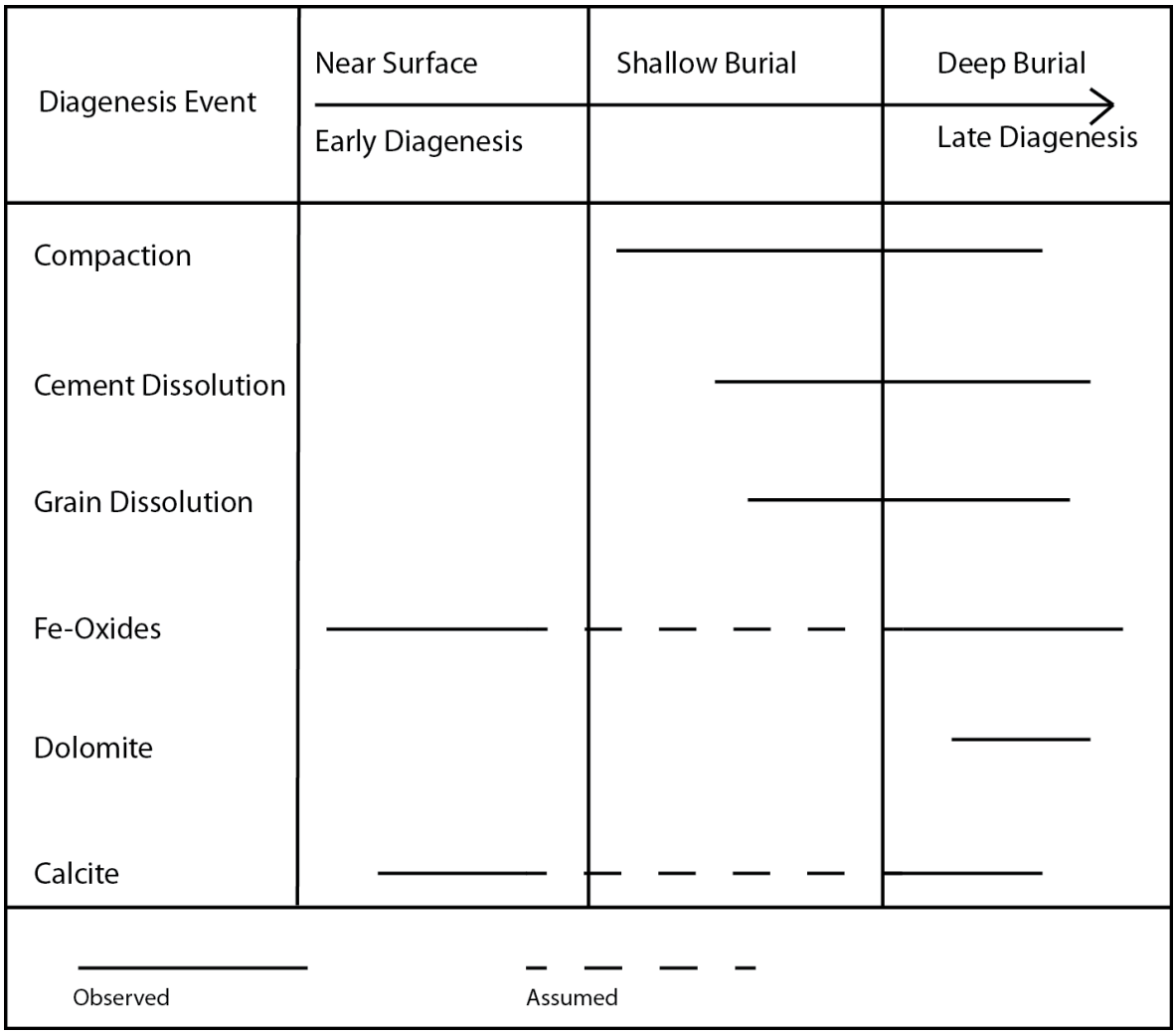

Figure 4.34: Diagenesis event chart based on petrographic analysis

Authigenic Mineralogy

The most common authigenic cements in the Entrada and Carmel Formations are hematite, calcite, and dolomite. Hematite cement is the most abundant and comprises 1-30% of the thin sections and is present in all thin sections. Textural characteristics suggest that precipitation has occurred in at least two stages. Calcite cement comprises 0-28% of the thin sections and is only absent in samples (GV-13 and GV-16). Petrographic analysis indicates that the calcite cement generally occurs in one stage of calcite precipitation, but in few cases there is evidence of two stages. Dolomite cement is the least abundant comprising 0-19% of the thin sections and is present in all samples (except GV-7, GV-16, GV-17, GV-20, and GV-26). Dolomite occurs in one stage replacing earlier calcite in very small amounts on the salt shoulder and almost completely replacing it in samples at Slick Rock Canyon.

Hematite is the earliest cement type present often observed in as confined between compacted grains in small amounts (Fig. 4.15 & 4.17). It is most typically an opaque lining that surrounds the detrital grains and sometimes appears as small irregular dark patches completely filling in pore space between them. A later stage of hematite precipitation is apparent in thin sections where it obscures portions late stage calcite cement, or fills small gaps previously dissolved within calcite cement (Fig. 4.15 & 4.17). This cement type is most prevalent in petrofacies associated with FA-TF and FA-PS and, which is consistent with the dark red color of these units in outcrop.

Early calcite cements can be observed where small amounts have been deformed and enclosed between grains after compaction. Only small amounts from this first stage of calcite precipitation remain if they are present at all (Fig. 4.15 & 4.17). The majority of existing calcite precipitated at a later stage is represented as void filling or mosaic void filling textures from

partial dissolution (Fig. 4.15 & 4.17). Manifestation of calcite cement as patches indicates porosity must have been lower at an earlier stage, but that fluids dissolved away some of the cement over time. In the most recent stage there are varying instances of dolomite replacement that have taken place with respect to the proximity of the diapir. In the Slick Rock Canyon section, early and late stage calcite present in the Carmel is exclusively ferroan based on the purple stain, which is not the case in Carmel samples that are from the main study area (Fig. 4.16).

Dolomite cement is the youngest and least prevalent of the major cement types. On the salt shoulder only small amounts of dolomite replacement are observed. However, in the petrofacies at Slick Rock Canyon (PFA9, PFA10, and PFA11) calcite has almost been entirely replaced to dolomite (Fig. 4.17 & 4.18). Rhombic crystals fill voids in with similar textures to those of the calcite cement (i.e. void filling and mosaic void filling). Similar to the calcite cements, partial dissolution of the dolomite suggests that porosity was lower prior to being affected by fluid.

Secondary porosity is present in all samples to varying degrees based on the unit and location (Fig. 4.16 & 4.17). Higher porosities are observed in the Entrada formation on the salt shoulder and at Slick Rock Canyon than in the Carmel samples.

Paragenetic Sequence of Samples On and Adjacent to the Diapir Shoulder

Samples on the salt shoulder (Little Gypsum Valley) differ slightly from those at the diapir (Slick Rock Canyon ~13km to the southwest of the diapir) (Fig. 4.1). The major authigenic cements present are hematite, calcite and dolomite. Calcite cement is much higher at the main study area. Secondary porosity is also higher in the Entrada units at Little Gypsum Valley. Of the samples taken at Gypsum Valley, five had been altered by fluid flow through

heavy fracturing in the area and were analyzed to see if there was any effect on the petrology. The samples did not appear to differ much in composition; however, the porosity appears to be influenced by the altering fluid flow in some cases.

The paragenetic sequence is as follows: 1) Early iron cementation 2) Calcite cementation 3) Compaction event 4) Late void filling calcite cementation 5) Partial dissolution of calcite cement 6) Late iron cementation 7) Localized dolomitization of calcite (Fig. 4.14).

Paragenic Sequence of Samples from Slick Rock Canyon

The main authigenic cements in the Slick Rock Canyon samples also include hematite, dolomite, and calcite. The quantities of dolomite are much higher at this location, however. Secondary porosity is also higher in the lower Carmel units.

The paragenetic sequence is as follows: 1) Early iron cementation 2) Calcite cementation 3) Compaction event 4) Late void filling calcite cementation 5) Near complete dolomitization of calcite 6) Partial dissolution of dolomite and calcite cements 7) Late iron cementation (Fig. 4.14).

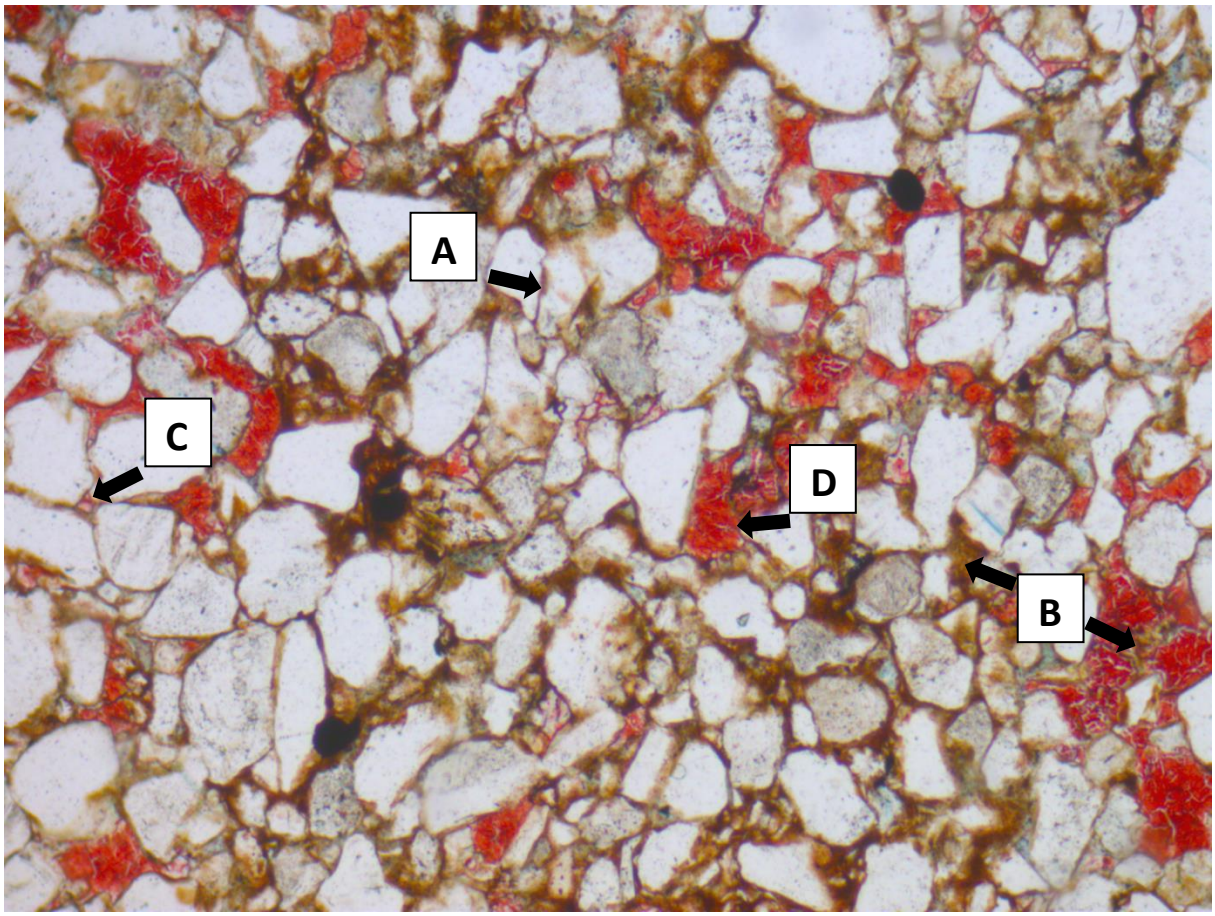

Figure 4.15: Thin section photo taken from GV-31 (On the salt shoulder). A) Early stage hematite confined by a compaction event between detrital grains. B) Late stage hematite lining detrital grains and forming on void filling calcite cement. C) Early stage calcite cement (stained red) deformed and by a compaction event and confined by detrital grains. D) Late stage void filling calcite cement (stained red).

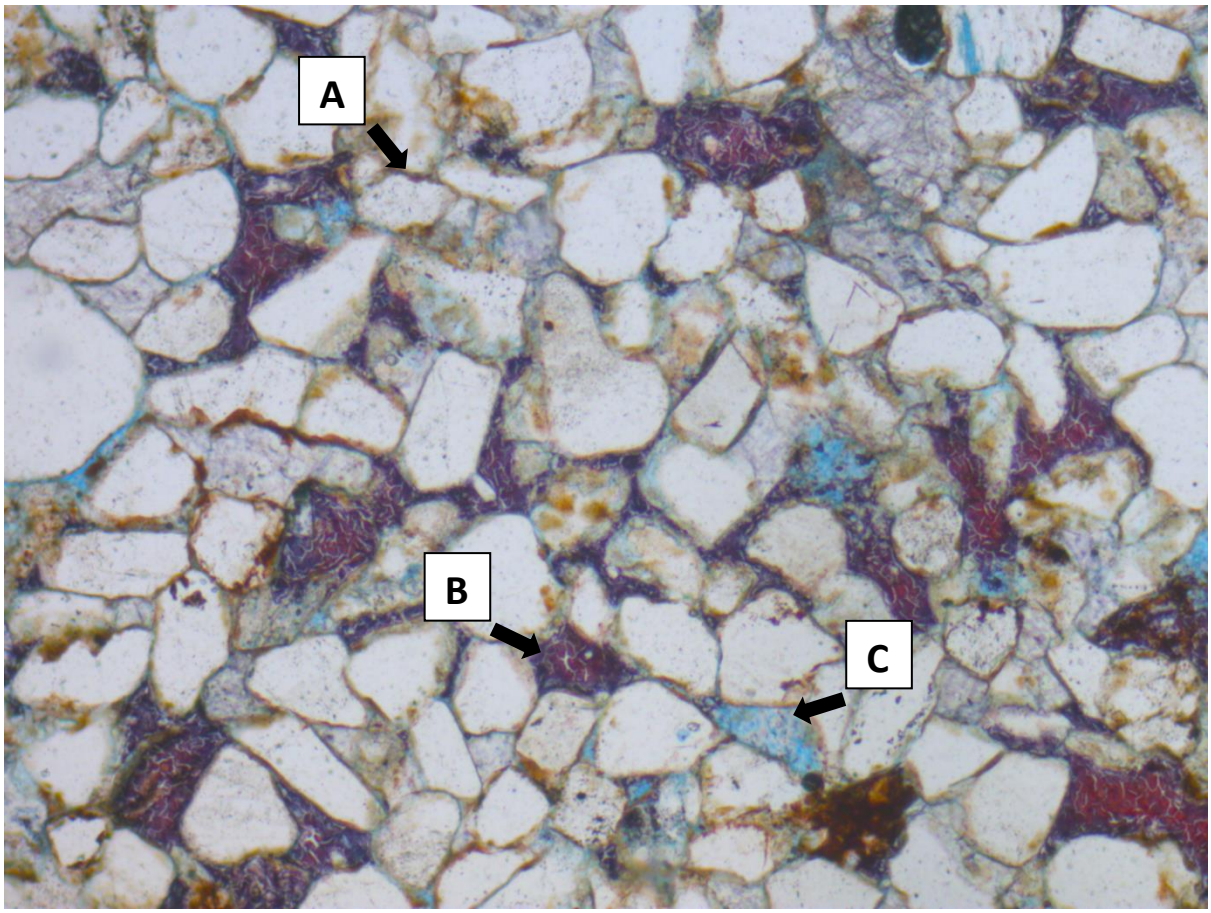

Figure 4.16: Thin section photo taken from GV-11 (Slick Rock Canyon). Ferroan calcite cement is a rare occurence, however all calcite cement in Carmel samples gathered at Slick Rock Canyon is ferroan. A) Early stage ferroan calcite cement (stained purple) confined by a compaction event between detrital grains. B) Late stage void filling ferroan calcite cement (stained purple) C) An example of secondary microporosity on a chert grain than has undergone partial dissolution.

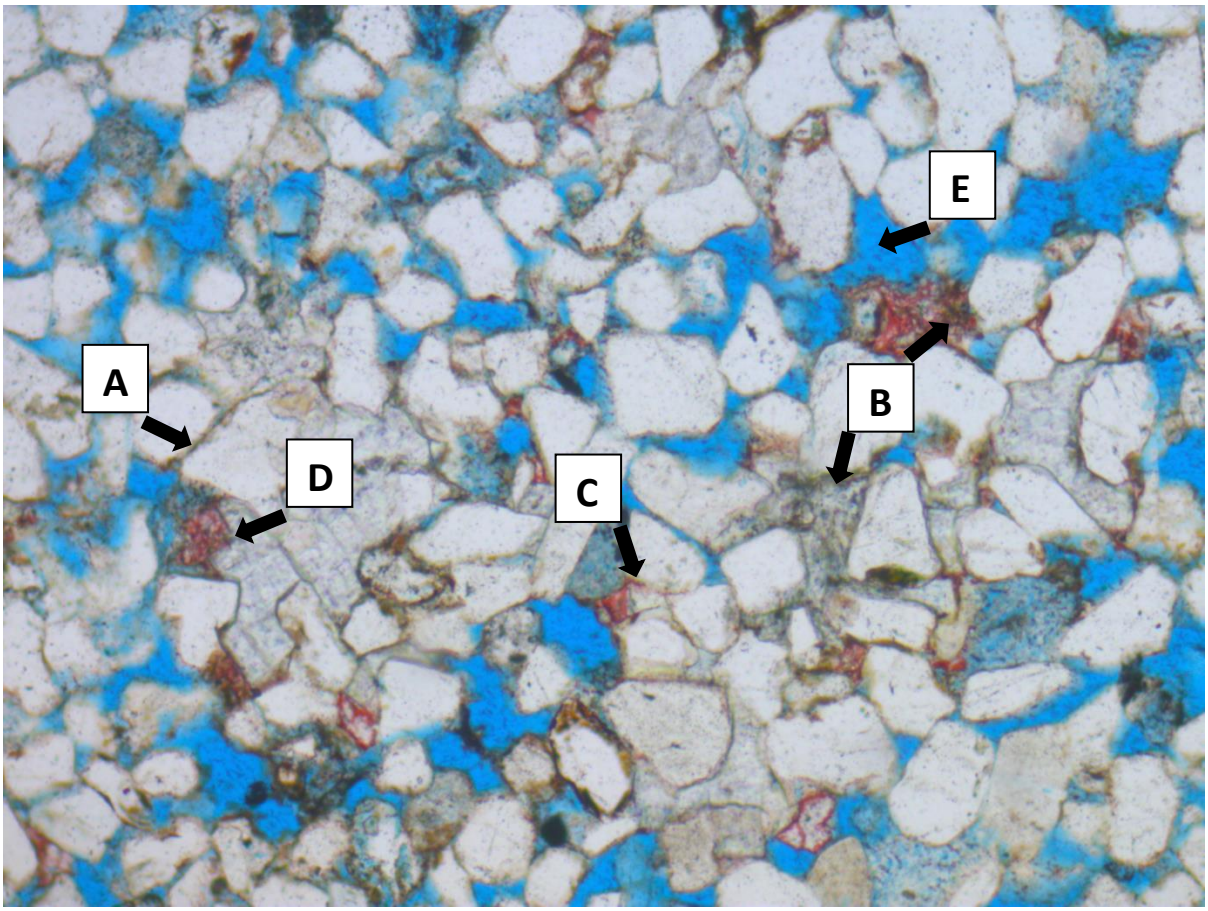

Figure 4.17: Thin section photo taken from GV-15 (Slick Rock Canyon). A) Early stage hematite confined by a compaction event between detrital grains. B) Late stage hematite lining detrital grains and forming on void filling calcite cement. C) Early stage calcite cement (stained red) deformed and by a compaction event and confined by detrital grains. D) Dolomite replacing late stage void filling calcite cement (stained red). E) An example of secondary porosity from the dissolution of both detrital grains and cements.

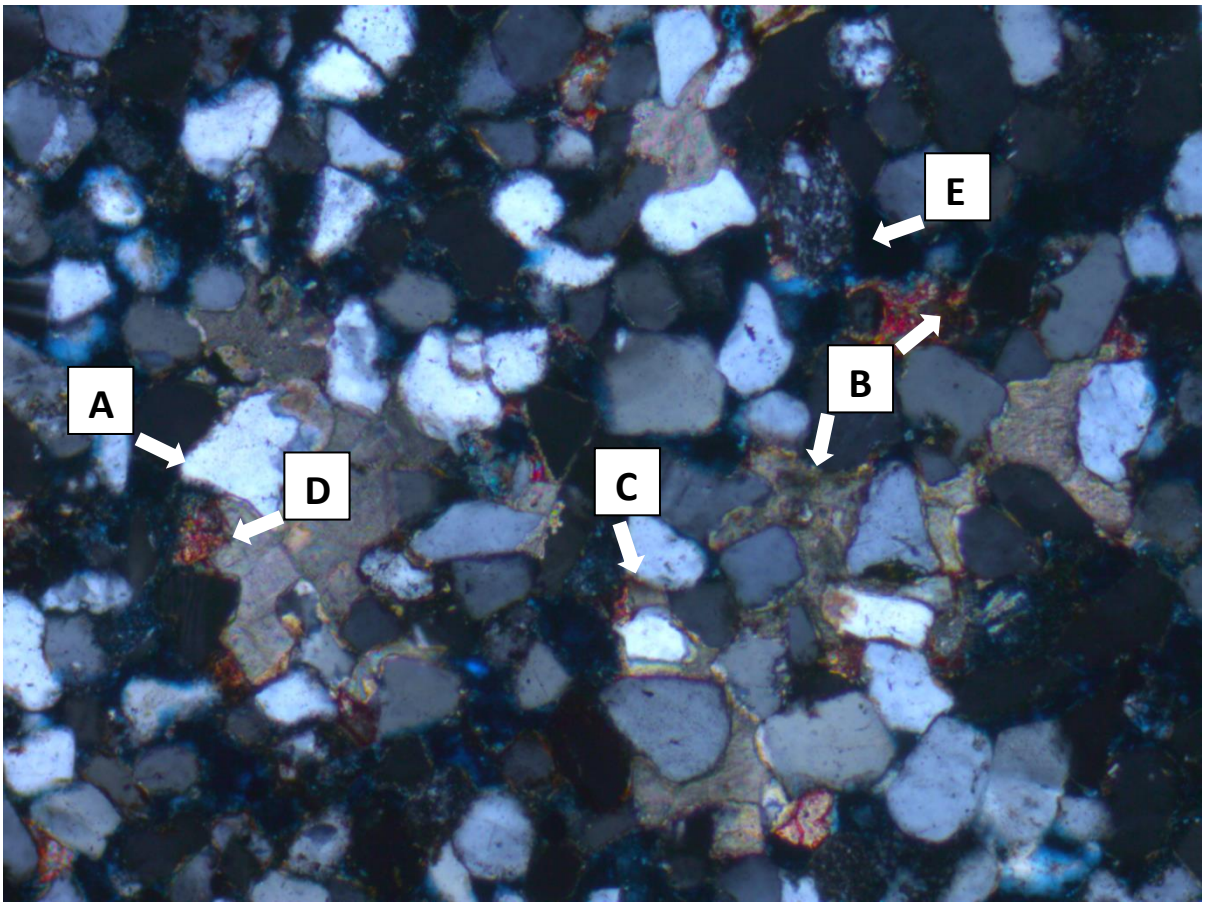

Figure 4.18: Thin section photo taken from GV-15 under cross-polarized light to better distinguish the dolomite cement, which remains unstained and has a high birefringence. Letters correspond with those from Fig. 4.17.

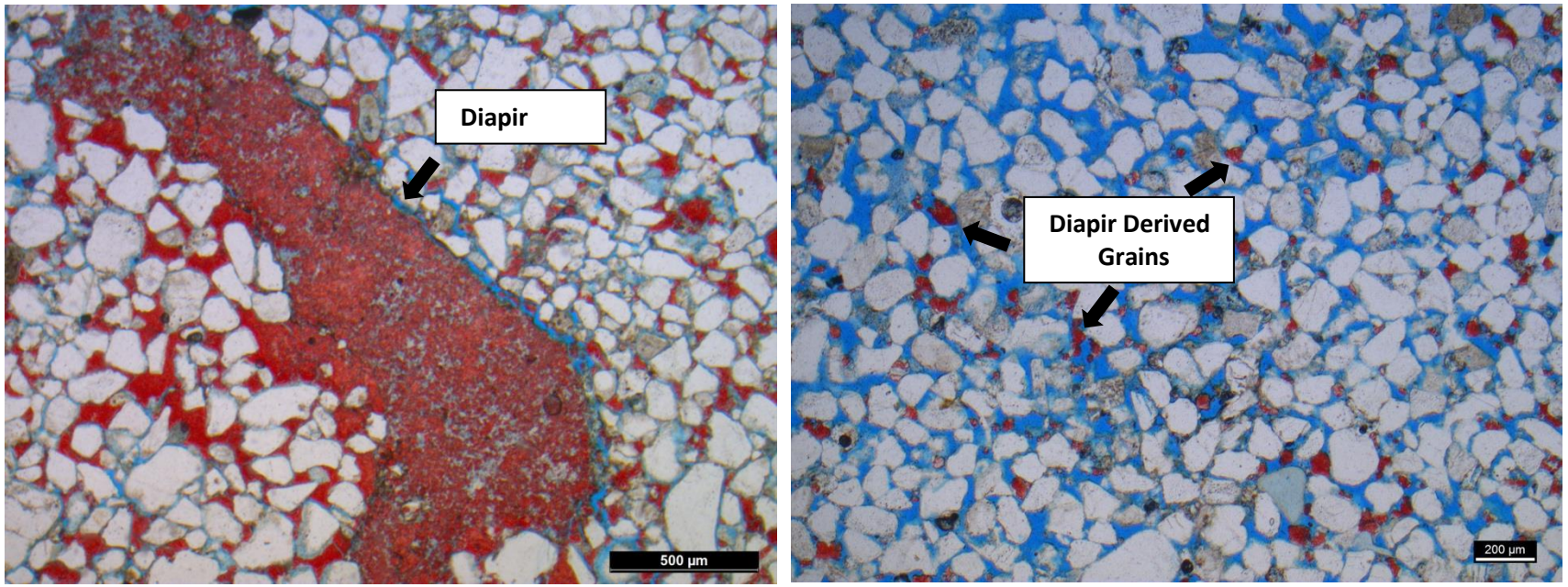

Figure 4.19: A) Thin section photo taken from GV-29 (left). The large red stained clast identified in this figure from PFA5 could be interpreted as having originated from the diapir. Similar clasts are observed in PFA2. B) Thin section photo of sample GV-26 (right) shows very-fine sized detrital carbonate grains that are also likely derived from the diapir and are present in PFA2, PFA3, PFA4, PFA5, and PFA6

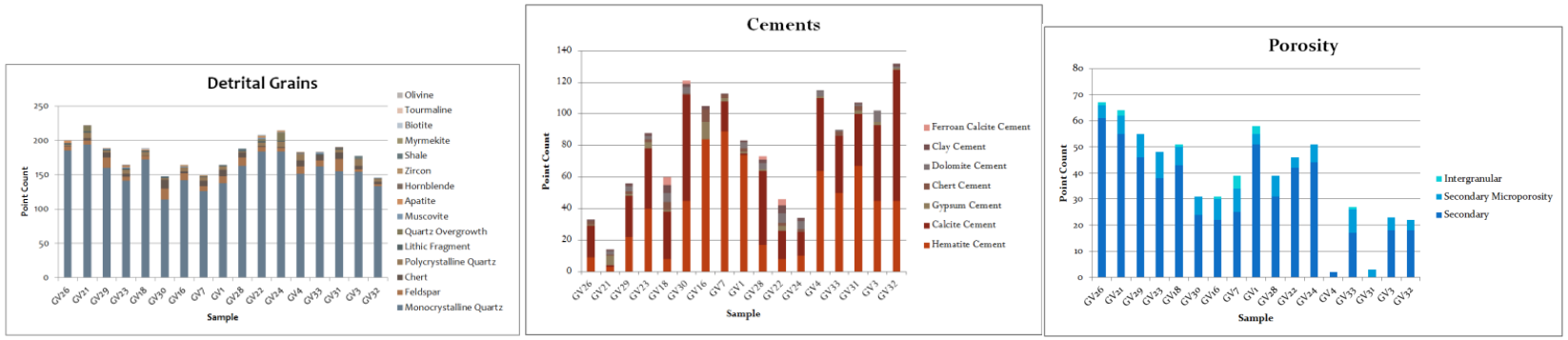

Figure 4.20A: The stack charts above represent the petrographic analysis of samples that are on the salt shoulder. Detrital grain type is displayed on the left chart, cement type in the middle and porosity type on the right.

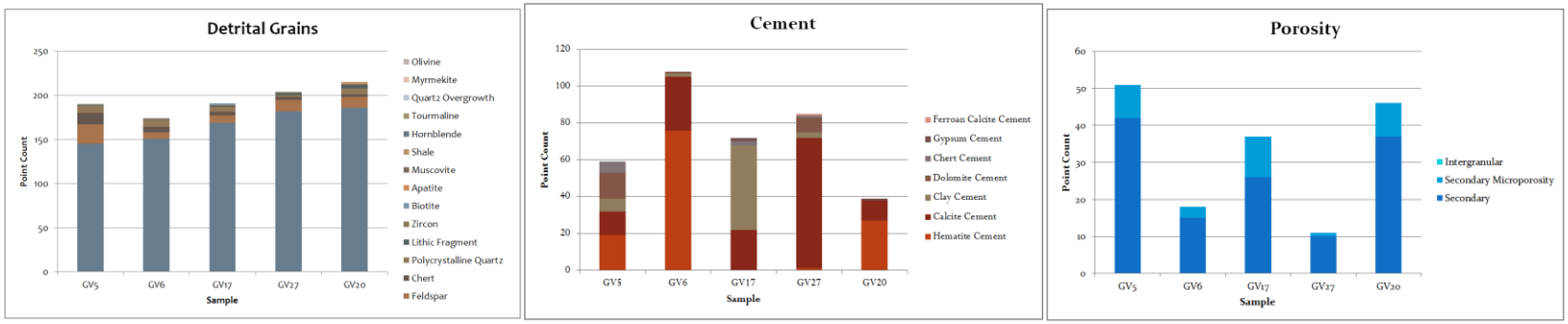

Figure 4.20B: The stack charts above represent the petrographic analysis of samples that are on the salt shoulder and have been altered by the fluid flow through fractures in these units. Detrital grain type is displayed on the left chart, cement type in the middle and porosity type on the right.

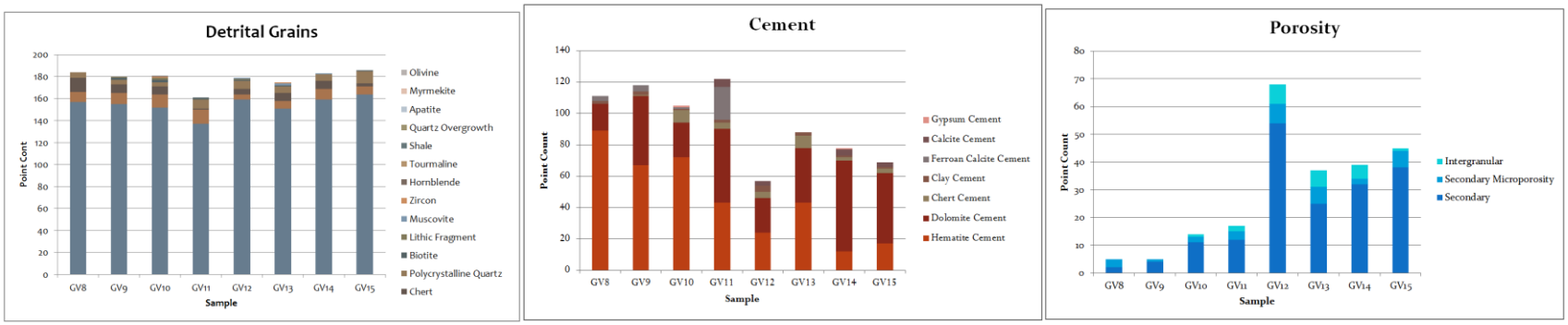

Figure 4.20C: The stack charts above represent the petrographic analysis for samples from Slick Rock Canyon. Detrital grain type is displayed on the left chart, cement type in the middle and porosity type on the right.

Chapter 5: Discussion

5.1 Thickness Variations

Although no halokinetic sequences form within the Entrada/Carmel formations in the study area at the GVSW in Little Gypsum Valley (Fig. 1.1), substantial evidence from the facies and petrographic analysis of this study indicate that the salt diapir has affected them in a variety of ways. Previous studies have suggested that the Entrada experiences gradual thickness changes over tens of kilomers (Carter 1953; Otto and Picard 1975).

On the salt shoulder, sections ranged from 10-30 meters thinner than the measured section 13 kilometers to the southwest at Slick Rock Canyon (Fig. 3.3 and Fig. 1.1). On the shoulder of the main study area sections themselves vary by 10-20 meters over less than 2 kilometers (Fig. 3.3 and Fig. 5.1). The thicker section in the Slick Rock Canyon section can partially be ascribed to its being on the flank of the Disappointment Valley salt-withdrawl minibasin (Fig. 1.1 and 3.3). In contrast, Entrada units in the study area on the shoulder crest in Gypsum Valley are likely thinned due to the lesser subsidence of the diapir during deposition (Fig. 3.7).

The sections measured on the crest of the diapir shoulder are thinner than other sections in the study area and may continue to thin along the crest as the units move towards the south (Delfin, 2018 in preparation) (Fig. 3.3 and Fig. 5.1). This suggests that accommodation space must have decreased to the south reflecting more active continued diapirism, in contrast to the study area and the rest of Little Gypsum Valley, where no further diapirism occurred after the deposition of the Carmel/Entrada.

When observing the thickness of the measured sections some many of them appear to be of comparable thickness; however, it is important to note that thinning in some units may be

accompanied by thickening in others. All correlative units exhibit noticeable variations in thickness at some point and in most cases several times. This supports the interpretation that these changes are affected more by highly localized accommodation space fluctuations from salt diapirism.

Thickness changes to the Carmel (6-9m) are not quite as evident as those observed within the Entrada sandstone (20-40m) (Fig. 3.3). The lesser amount of diapir related thinning that does occur in the Carmel can be observed at the crest of the salt shoulder, which is also consistent where the Entrada units are thinnest (Fig. 5.1). The overall thickness variations in measured sections reveal a significant syncline whose axis is about 300m SW of the salt shoulder where sections are thickest (Sections 3 and 7) is along strike with the thinnest units on the shoulder (Cater 1970) (Fig. 5.1). The thinner units represent areas of lesser subsidence of the diapir and the syncline reflects the greatest amount of subsidence in the study area. Units that account for the greatest discrepancies in thickness are E5-E7. As these thickest units continue to dip to the SW they experience drastic thinning revealing another localized area where the dipir did not experience the same amount of subsidence.

5.2 Facies Distributions

Facies distributions are also laterally affected when there are changes to accommodation space (Blakey and Gubitosa, 1984; Lucas et al. 1997; Matthews 2007). As a result of localized accommodation changes on the Entrada salt shoulder, the occurrence of facies changes differs. One such facies affected by this type of setting is wet interdunes. Wet interdunes in the Entrada have been encountered at other locations in earlier studies (Kocurek 1981; Eckdale and Picard 1981). However, the topographic lows of this study that allowed for formation of ephemeral ponds or lacustrine environments creating these wet interdune facies are most likely attributed to

salt tectonic processes considering that no wet interdune facies are observed in the Slick Rock Canyon section (Fig. 2.10). This study favors previous work that interprets similar processes as being eolian dunes formations influenced by a sabkha environment (Kockurek 1981; Crabaugh and Krocurek 1993; Peterson 1994). Wet interdunes are persistent throughout all sections in the main study area regardless of whether the intervals thicken, or thin. Grain size in the wet interdune facies associations is slightly finer, and is consistent with a marine transgression when these interdunes would have become flooded. An upward increasing size of asymmetrical wave ripples indicates a shallowing of water as these ponds dried out before transitioning back to eolian dune facies (Evans 1942). Wave ripple sets are also thicker at the southern end of the section (upwards to 2 meters) implying an increasing proximity to the paleocoastline.

One facies association not typically seen within the Entrada and only present in Section 4 (Fig. 3.3) is paleosol. Because of the arid climate associated with sabkhas, paleosols that do form are usually not well-developed profiles because of a lack of rainfall and therefore vegetation to disrupt the existing siliciclastics (Malisce and Mazzullo 2012). This appears to be the case with this facies observed in Little Gypsum Valley. The soil horizon is discontinuous, persisting less than 100 meters laterally and is absent of root traces. Nevertheless, additional features still support its classification as a paleosol. Primary disruption of sedimentary features in this case is likely similar to the precipitation and collapse of puffy ground structures and haloturbation processes described by Mlisce and Mazzullo (2012) and common of a sabkha setting. The color also grades downward from a dark red to a light pink reflecting dehydration of discrete parts of the profile containing different amounts of translocated iron (Brown and Kraus 1987).

Even typical Entrada dune sets formed by wind driven processes are affected by changes in accommodation space related to the salt diapirism. Some dunes have classic well-defined

cross-strata, wind ripples, grainflows and other facies typical of an eolian dune environment. The width of the cross-strata at Little Gypsum Valley salt shoulder; however, is much smaller (a few meters) compared those of the central erg that can reach up to 80 meters. Kocurek (1981) attributes these smaller sets to areas of the Entrada that are proximal to the paleocoastline as they are subject to more variable winds and periodic flooding. Unit E7 of the Entrada, which happens to corresponds with FA-SC (Fig. 3.3 and Fig. 2.10) also looks very different from what is described in other studies and what was observed at Slick Rock Canyon. What is normally a very thick set of large well defined eolian cross-beds, avalanche flows and coarse-grained wind ripples become a notably thinner unit with indistinguishable sedimentary structures and wavy irregular bedding (Fig. 2.6 and Fig. 2.8). This type of bedding corresponds with changes in wind speed, topography, and fluctuation in surface wetness (Grotzinger et al. 2005). All of these processes can be explained as direct effects of salt tectonics.

The Carmel Formation facies distribution in the study area does not appear to be nearly as affected by the salt diapirism and resembles the description of other studies, which interpret it as a tidal flat environment (Harshbarger et al. 1957; Phoenix 1958; Blakey, et al. 1983). The only visible evidence that could be diapir related is coarse clasts of evaporite material near the base of the Carmel indicating dry episodes typical of a sabkha enviroments and possibly tied to topographic changes connected with salt tectonics (Kocurek 1981).

5.3 Intertonguing Relationships

Intertonguing relationships are an atypical feature observed at the thickest sections (3 and 7) when units begin to dip perpendicular to the salt wall into the valley (Fig. 3.1 and 3.3). These stratigraphic repetitions result from flooding events interpreted to be the result of localized diapir related subsidence (Mader 1985). Gradational contacts are also observed at boundaries of units in

contact with wet interdune deposits (FA-WI) (Fig. 2.10). The first assemblage of intertonguing is observed across measured Sections 3 and 4 between units C7 and E1 (Fig. 3.3). Intertonguing of the eolian Entrada with tidal Carmel indicates that the dunes began to advancing while tide sedimentation was still taking place. The second is at Section 7 towards the south between units E4 and E5 (Fig. 3.3). This means that eolian dune advance was contemporaneous with sedimentation of damp interdunes (Mountney and Jagger 2004). The topographic lows required for flooding of the dunes that create intertonguing assemblages in this case comes back to the concept of salt diapirism creating the necessary accommodation space (Kocurek 1981).

5.4 Petrographic Interpretations

Detrital grain composition in the Entrada and Carmel samples, both on the salt shoulder and at Slick Rock Canyon, suggest a distant source of recycled sedimentary and granitic rocks (Otto & Picard 1976) with hardly any direct influence from the diapir. Primary sediment sources have been interpreted with relation to tectonic activity associated with the Uncompahgre Uplift and the Colorado Front Range of the Ancestral Rocky Mountain Highlands (ARM) (Otto & Picard 1976; Peterson 1989; Trudgill & Paz 2009). Lower amounts of feldspar in these samples compared to others farther north suggest this part of the Entrada/Carmel isn't as proximal to the source of feldspar. Small, but relatively consistent amounts of chert throughout the samples indicates the presence of preexisting sedimentary rock in the source areas (Otto & Picard 1976).

The most common authigenic cements in the Entrada and Carmel Formations are hematite, calcite, and dolomite. Hematite cement is the most abundant and comprises 1-30% of the thin sections and is present in all thin sections. Textural characteristics suggest that precipitation has occurred in at least two stages.

In general, samples that are on the salt shoulder and at Slick Rock Canyon tend to have higher porosities in the Entrada Formation (7-20%) than the Carmel. Porosity is present in most samples and is almost entirely secondary as a result of dissolution of cements and partial to complete dissolution of detrital grains.

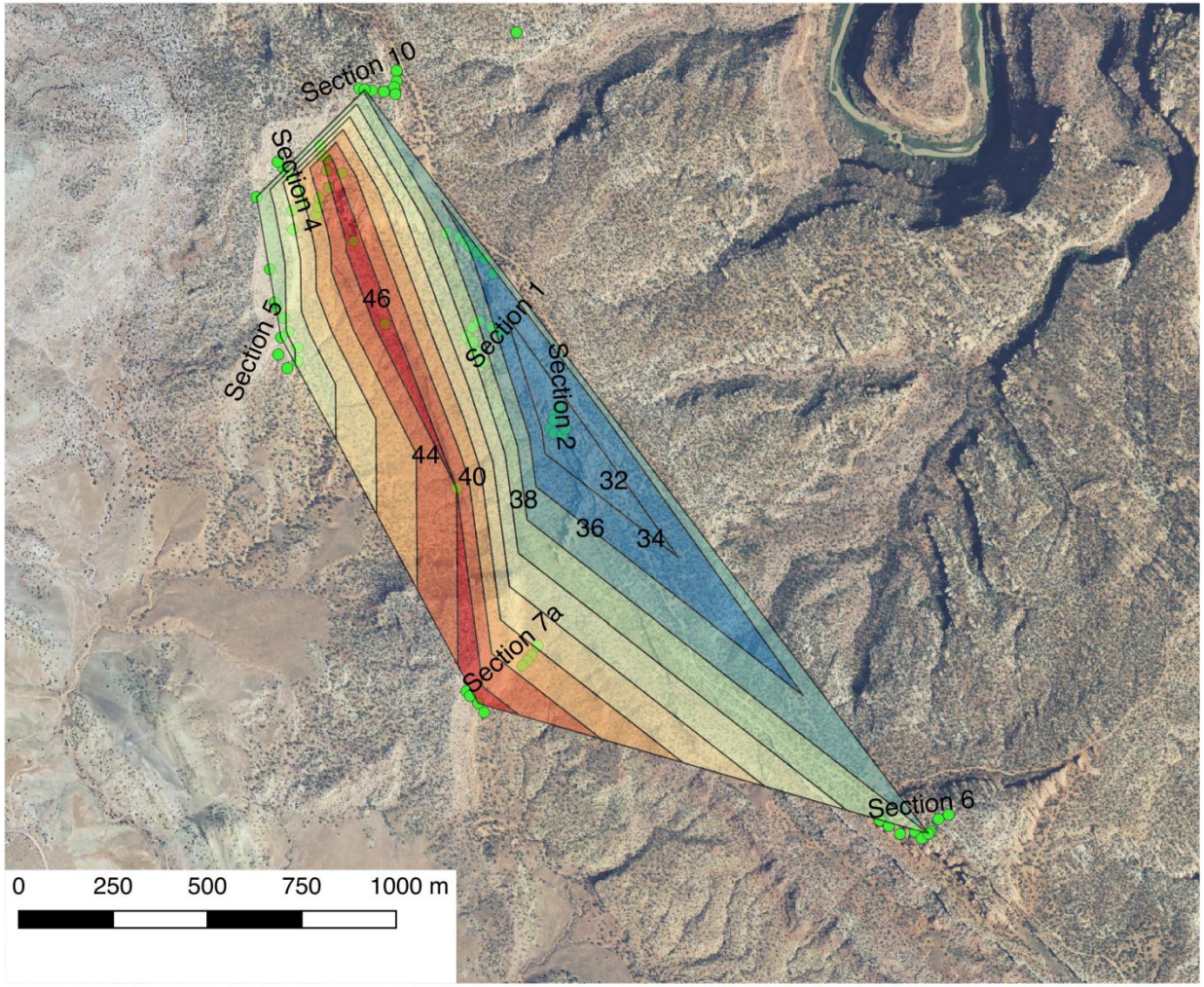

Figure 5.1: Isopach map displaying the total thickness across the study area based on data from measured sections. Sections are thinnest on top the shoulder crest and thickest where a syncline forms about 300 meters to the SW of the crest.

Chapter 6: Conclusion

1. One of the most significant macroscopic changes observed in the stratigraphy of the sections on the salt shoulder compared to previous studies and the section at Slick Rock Canyon are local variations in thickness over the study area. Thickness variations between 10-20 meters happen across a very short distance of less than 2 km. These changes are therefore attributed to diapir related changes in accommodation space from differential loading, localized subsidence and dissolution. Thickness of the salt shoulder sections overall were also notably thinner than the Slick Rock Canyon section by 10-30 meters. Entrada units experience greater thickness variations than those of the Carmel that thin only slightly towards the south.
2. Eight Facies associations and eleven lithofacies were classified within the Entrada Sandstone and Carmel Formation. Facies associations include tidal flat deposits (FA-TF), wet interdune deposits (FA-WI), small eolian dune deposits (FA-SE), paleosols (FA-PS), large eolian dune deposits (FA-LE), dry interdune deposits (FA-DI), eolian deposits with coarse shallowly scoured bedding (FA-SC), and mottled eolian deposits (FA-ME). Many of these reflect salt tectonic related influences when observed laterally across the study area. The only evidence of diapir related influence in the Carmel is coarse evaporate-derived carbonate clasts near the bottom of Unit C1 where lag deposits are present indicating erosion of the diapir. The Entrada exhibits substantial changes in facies distributions. Wet interdune deposits occur within topographic lows where the accommodation space that is created is attributed to salt diapirism. Wavy irregular bedding encountered within Unit E7, and that corresponds

with FA-SC is caused by changes in wind speed, topography and fluctuation in surface wetness.

3. Eleven petrofacies were classified based on the composition of grain type, cement, and porosity in 30 samples analyzed. Petrofacies 1-8 correspond with Little Gypsum Valley samples taken from the sections on the salt shoulder. Petrofacies 9-11 correspond with samples taken at Slick Rock Canyon approximately 13 kilometers away. Porosity is almost exclusively secondary resulting from dissolution. Facies on the salt shoulder show higher porosity values within Entrada samples (7-20%). Conversely, Carmel samples from Slick Rock Canyon are the ones that show higher porosity values (8-18%). Samples display varying levels of compaction and cements. There is little diversity in composition as quartz makes up 77-94% of the grain composition. Samples fall into the categories subarkose, quartzarenite, and sublitharenite.
4. Paragenetic sequences of samples from the salt shoulder and the minibasin in Slick Rock Canyon are complex. Calcite cements are predominant on the salt shoulder, whereas dolomite cements are found in Slick Rock Canyon. The complexity of samples on the salt shoulder is likely related to fluid migration through fractures related to salt tectonics. The paragenetic sequence for samples on the salt shoulder is as follows: 1) Early iron cementation 2) Calcite cementation 3) Compaction event 4) Late void filling calcite cementation 5) Partial dissolution of calcite cement 6) Late iron cementation 7) Localized dolomitization of calcite. The paragenetic sequence for Slick Rock Canyon samples is as follows: 1) Early iron cementation 2) Calcite cementation 3) Compaction event 4) Late void filling calcite cementation 5) Near

complete dolomitization of calcite 6) Partial dissolution of dolomite and calcite cements 7) Late iron cementation.

References

Ahlbrandt, T.S., and Fryberger, S.G., 1981. Sedimentary features and significance of interdune deposits, in Ethridge, F.G., and Flores, R.M., eds., Recent and ancient nonmarine depositional environments: Society of Economic Paleontologists and Mineralogists Special Publication 31, p. 293-314

Allen, P.A. and Allen, J.R., 2013. Basin analysis: Principles and application to petroleum play assessment. Third Edition. John Wiley & Sons

Baars, D. L., and Stevenson, G. M., 1981. Tectonic evolution of the Paradox basin, Utah and Colorado; in, Geology of the Paradox Basin, D. L. Wiegand, ed.: Rocky Mountain Association of Geologists, 1981 Field Conference, p. 23-31

Bailey, C.H. 2016. Anomalous Slat Wash Member of the Jurassic Morrison Formation in 'The Hat' Syncline at Gypsum Valley Salt Wall, Paradox Basin, Southeastern Colorado. GSA Annual meeting; 28 Sep 2016; Denver, Colorado

Barbeau, D.L., 2003. A flexural model for the Paradox Basin: implications for the tectonics of the Ancestral Rocky Mountains. Basin Research 15, 97–115

Blakey, R.C., Knepp, R., 1989. Pennsylvanian and Permian geology of Arizona. In: Jenney, J.P., Reynolds, S.J. (Eds.), Geologic Evolution of Arizona. Ariz. Geol. Soc. Dig., vol. 17, pp. 313 – 347

Blakey, R.C., and Gubitosa, R., 1984. Sandstone body geometry and architecture of the Triassic Chinle Formation, Colorado Plateau: Sedimentary Geology, v. 38, p. 51-86

Blakey, R. C., and Gubitosa, R., 1983. Late Triassic pa- leogeography and depositional history of the Chinle Formation, southern Utah and northern Arizona, in Reynolds, M. W., and Dolly, E. D., eds., Mesozoic Paleogeography of the west-central United States: Rocky Mountain Paleogeography Symposium 2, p. 57-76

Blatt, H., Christie, J. M. 1963, Undulatory extinction in quartz of igneous and metamorphic rocks and its significance in provenance studies of sedimentary rocks. I. sedim. Petrol. 33 (3) : 559-79

Brown D.L., Johnson J.B., Kraus A.P., Duke R.A., Barrett M.R., 1987. Computed tomography with intraperitoneal contrast medium for localization of peritoneal dialysis leaks. J Comput Assist Tomogr 11(2): 276-278

Cadigan, R. A., 1967. Petrology of the Morrison Formation in. the Colorado Plateau region: U.S. Geol. Survey Prof. Paper 556, 113 p.

Cater Jr, F.W., 1955. Geology of the Gypsum Gap quadrangle, Colorado: US Geol. Survey Geol. Quadrangle Map GQ-59

Cater, F.W., 1970. Geology of the Salt Anticline Region in southwestern Colorado. U.S. Geol. Surv., Prof. Pap., 637: 80 pp.

Cattaneo, A., Steel, R.J., 2003. Transgressive deposits: a review of their variability. Earth-Science Reviews 62 (3 – 4), 187 – 228

Chan, M.A., Parry, W.T., and Bowman, J.R., 2000. Diagenetic hematite and manganese oxides and fault- related fluid flow in Jurassic sandstones southeastern Utah: American Association of Petroleum Geology Bulletin , v. 84p. 1281-1310

Condon, S. M., 1997. Geology of the Pennsylvanian and Permian Cutler Group and Permian Kaibab Limestone in the Paradox Basin, Southeastern Utah and southwestern Colorado. U. S. Geological Survey, Professional Paper, 2000-P

Crabaugh, M. and Kocurek, G., 1993. Entrada Sandstone: an example of a wet aeolian system. *Geological Society, London, Special Publications, 72*(1), pp.103-126

Clarke, L.H., 2010. *Facing age: Women growing older in anti-aging culture* (Vol. 1). Rowman & Littlefield Publishers

Demko, T.M., Currie, B.S. and Nicoll, K.A., 2004. Regional paleoclimatic and stratigraphic implications of paleosols and fluvial/overbank architecture in the Morrison Formation (Upper Jurassic), Western Interior, USA. *Sedimentary Geology*, *167*(3-4), pp.115-135

Doelger, N.M., 1987. The stratigraphy of the Nugget Sandstone.Doelling 1987. pp. 163-178

Doelling, H.H., Oviatt, C.G. and Huntoon, P.W., 1988. *Salt deformation in the Paradox region* (Vol. 122). Utah Geological Survey

Doelling, H.H., Ross, M.L., Willis, G.C. and Douglas, L.J., 1998. *Geologic map of the Big Bend quadrangle, Grand County, Utah*. Utah Geological Survey.Driese, et al. 1981

Elston, D.P., Shoemaker, E.M. and Landis, E.R., 1962. Uncompahgre front and salt anticline region of Paradox Basin, Colorado and Utah. *AAPG Bulletin*, *46*(10), pp.1857-1878

Evans, O.F., 1942. The relation between the size of wave-formed ripple marks, depth of water, and the size of the generating waves. *Journal of Sedimentary Research*, *12*(1), pp.31-35

Folk, R.L., 1980. *Petrology of sedimentary rocks*. Hemphill Publishing Company

Ford, R.L., Gillman, S.L., Wilkins, D.E., Clement, W.P. and Nicoll, K., 2010. Geology and Geomorphology of Coral Pink Sand Dunes State Park, Utah. *Geology of Utah's Parks and Monuments, Utah Geological Association*, pp.379-406

Foxford, K. A., I. R. Garden, S. C. Guscott, S. D. Burley, J. J. M. Lewis, J. J. Walsh, and J. Watterson, 1996, The field geology of the Moab fault, in A. C. Huffman, Jr., W. R. Lund, and L. H. Godwin, eds., Geology and resources of the Paradox basin: Utah Geological Association Guidebook 25, p. 265–283.

Fryberger, S.G. and Dean, G., 1979. Dune forms and wind regime. In *A study of global sand seas* (Vol. 1052, pp. 137-169). Washington DC: US Geological Survey Professional Paper

Ge, H., Jackson, M.P. and Vendeville, B.C., 1997. Kinematics and dynamics of salt tectonics driven by progradation. *AAPG bulletin*, *81*(3), pp.398-423

Giles, K.A. and Lawton, T.F., 2002. Halokinetic sequence stratigraphy adjacent to the El Papalote diapir, northeastern Mexico. *AAPG bulletin*, *86*(5), pp.823-840

Grotzinger, J.P., Arvidson, R.E., Bell Iii, J.F., Calvin, W., Clark, B.C., Fike, D.A., Golombek, M., Greeley, R., Haldemann, A., Herkenhoff, K.E. and Jolliff, B.L., 2005. Stratigraphy and sedimentology of a dry to wet eolian depositional system, Burns formation, Meridiani Planum, Mars. *Earth and Planetary Science Letters*, *240*(1), pp.11-72

Verbeek, E.R. and Grout, M.A., 1997. Joint networks in reservoir rocks: case studies of prediction at depth

Handschy, J.W. and Dyer, R., 1987. Polyphase deformation in Sierra del Cuervo, Chihuahua, Mexico: evidence for ancestral Rocky Mountain tectonics in the Ouachita foreland of northern Mexico. *Geological Society of America Bulletin*, *99*(5), pp.618-632

Harshbarger, J.W., Repenning, C.A. and Irwin, J.H., 1957. *Stratigraphy of the uppermost Triassic and the Jurassic rocks of the Navajo country* (No. 291)

Hunter, R.E., 1977. Basic types of stratification in small eolian dunes. *Sedimentology*, *24*(3), pp.361-387

Jacobson, M.E., 1994. Chemical and biological mobilization of Fe (III) in marsh sediments. Biogeochemistry, 25(1), pp.41-60.

Kinsman, D.J., 1969. Interpretation of Sr (super+ 2) concentrations in carbonate minerals and rocks. *Journal of Sedimentary Research*, *39*(2), pp.486-508

Kluth, C.F. and Coney, P.J., 1981. Plate tectonics of the ancestral Rocky Mountains. *Geology*, *9*(1), pp.10-15

Kocurek, G., 1981. Erg reconstruction: the Entrada sandstone (Jurassic) of northern Utah and Colorado. *Palaeogeography, Palaeoclimatology, Palaeoecology*, *36*(1-2), pp.125-153.

Kraus, M.J., 1999. Paleosols in clastic sedimentary rocks: their geologic applications. *Earth-Science Reviews*, *47*(1-2), pp.41-70.Krynine, P.D., 1940. *Petrology and genesis of the Third Bradford Sand* (No. 29). School of Mineral Industries, Pennsylvania State College

Lancaster, N., 1988. Controls of eolian dune size and spacing. *Geology*, *16*(11), pp.972-975

Langford, R. and Chan, M.A., 1988. Flood surfaces and deflation surfaces within the Cutler Formation and Cedar Mesa Sandstone (Permian), southeastern Utah. *Geological Society of America Bulletin*, *100*(10), pp.1541-1549

Langford, R.P., Gill, T.E. and Jones, S.B., 2016. Transport and mixing of eolian sand from local sources resulting in variations in grain size in a gypsum dune field, White Sands, New Mexico, USA. *Sedimentary Geology*, *333*, pp.184-197

Leckie, D.A. and Walker, R.G., 1982. Storm-and tide-dominated shorelines in Cretaceous Moosebar-Lower Gates interval--outcrop equivalents of Deep Basin gas trap in western Canada. *AAPG Bulletin*, *66*(2), pp.138-157

Lucas, S.G., Krainer, K. and Bergolf, W.R., 2014. Folding in the Middle Jurassic Todilto Formation, New Mexico-Colorado, USA. *Volumina Jurassica*, *12*(2), pp.39-54

Woodward, L.A., Anderson, O.J. and Lucas, S.G., 1997. Tectonics of the Four Corners region of the Colorado Plateau. *Mesozoic geology and paleontology of the Four Corners area: New Mexico Geological Society, Guidebook*, *48*, pp.57-64

Mack, G.H. and Rasmussen, K.A., 1984. Alluvial-fan sedimentation of the Cutler Formation (Permo-Pennsylvanian) near Gateway, Colorado. *Geological Society of America Bulletin*, *95*(1), pp.109-116.

Mader, D., 1985. Depositional mechanisms and facies models of intertonguing aeolian environment and fluvial milieu in the Middle Buntsandstein of the Mid-European Triassic Basin. In *Aspects of Fluvial Sedimentation in the Lower Triassic Buntsandstein of Europe* (pp. 127-164). Springer, Berlin, Heidelberg

Matthews, W.J., Hampson, G.J., Trudgill, B.D. and Underhill, J.R., 2007. Controls on fluviolacustrine reservoir distribution and architecture in passive salt-diapir provinces: Insights from outcrop analogs. *AAPG bulletin*, *91*(10), pp.1367-1403

McFarland, J.C., 2016. *Structural and stratigraphic development of a salt-diapir shoulder, Gypsum Valley, Colorado*. The University of Texas at El Paso.

McKee, E.D. and Bigarella, J.J., 1979. Sedimentary structures in dunes. *McKee (Ed.), A Study of Global Sand Seas. US Geological Survey Professional Paper, 1052*, pp.83-134.

Mountney, N.P. and Jagger, A., 2004. Stratigraphic evolution of an aeolian erg margin system: the Permian Cedar Mesa Sandstone, SE Utah, USA. *Sedimentology*, *51*(4), pp.713-743

Nio, S.D. and Yang, C.S., 1991. Sea-level fluctuations and the geometric variability of tide-dominated sandbodies. *Sedimentary Geology*, *70*(2-4), pp.161-193

Nio, S.-D., and C.-S. Yang, 1991. Diagnostic attributes of clastic tidal deposits: A review, in Clastic Tidal Sedimentology, edited by D. G. Smith et al., Mem. Can. Soc. Pet. Geol., 16, 3-27

Nuccio, V. F. & Condon, S. M., 1996. Burial and thermal history of the Paradox Basin, Utah and Colorado, and petroleum potential of the middle Pennsylvanian Paradox Formation. US Geol. Surv. Bull. 76, O1–O41

O'Sullivan, R.B., 1981. Stratigraphic sections of Middle Jurassic Entrada sandstone and related rocks from Salt Valley to Dewey Bridge in East-Central Utah

O'Sullivan, R.B., 1980, Stratigraphic sections of Middle Jurassic San Rafael Group from Wilson Arch to Bluff in southeastern Utah: U.S. Geological Survey Oil and Gas Investigations Chart OC-102

Otto, E.P. and Picard, M.D., 1976. Petrology of Entrada Sandstone (Jurassic) northeastern Utah. In: Symposium on the Geology of the Cordilleran Hingeline, Rocky Mountain Association of Geologists, 1976 Symposium, pp. 231- 245

Owen, G., 1996. Experimental soft-sediment deformation: structures formed by the liquefaction of unconsolidated sands and some ancient examples. *Sedimentology*, *43*(2), pp.279-293

Peterson, J.A., 1989. *Geology and petroleum resources, Paradox basin Province*. US Geological Survey.

Peterson, J.A. and Hite, R.J., 1969. Pennsylvanian evaporite-carbonate cycles and their relation to petroleum occurrence, southern Rocky Mountains. *AAPG bulletin*, *53*(4), pp.884-908.

Phoenix, D.A., 1958. Sandstone cylinders as possible guides to paleomovement of ground water. In *New Mexico Geological Society, Guidebook of 9th Field Trip Conference* (pp. 194-196).

Pipiringos, G.N. and O'Sullivan, R.B., 1978. *Principal unconformities in Triassic and Jurassic rocks, western interior United States; a preliminary survey* (No. 1035-A). United States Government Printing Office

Pollastro, R.M., 2003. *Total petroleum systems of the Paleozoic and Jurassic, Greater Ghawar Uplift and adjoining provinces of central Saudi Arabia and northern Arabian-Persian Gulf* (pp. 2202-H). US Department of the Interior, US Geological Survey

Rasmussen, D., (2015) Subsurface and surface stratigraphic evidence for surface extrusions of Pennsylvanian Paradox salt beginning in the Early Permian and still happening, Paradox Basin, SE Utah and SW Colorado. RMS-SEPM Lecture Abstract, 2015

Reineck, H.E., and Sing, I.B., 1980, Depositional Sedimentary Environments, 2rid edition: New York, Springer-Verlag

Reineck, H.E. and Wunderlich, F., 1968. Classification and origin of flaser and lenticular bedding. *Sedimentology*, *11*(1-2), pp.99-104

Retallack, G., 1986. Reappraisal of a 2200 Ma-old paleosol near Waterval Onder, South Africa. *Precambrian Research*, *32*(2-3), pp.195-232

Shaw, J., Munro-Stasiuk, M., Sawyer, B., Beaney, C., Lesemann, J.E., Musacchio, A., Rains, B. and Young, R.R., 1999. The channeled scabland: back to Bretz?. *Geology*, *27*(7), pp.605-608.

Shawe, D.R., Simmons, G.C. and Archbold, N.L., 1968. *Stratigraphy of Slick Rock District and vicinity, San Miguel and Dolores Counties, Colorado* (No. 576-A). US Government Printing Office

Shoemaker, E.M., Case, J.E., and Elston, D.P. (1958) Salt Anticlines of the Paradox Basin, Intermountain Assocation of Petroleum Geologists, U.S. Geological Survey, p. 39-58

Shawe, D.R., Simmons, G.C. and Archbold, N.L., (1968) Stratigraphy of Slick Rock District and vicinity San Miguel and Dolores Counties, CO: U.S. Geol. Survey Prof. Paper 576-A.

Stewart, W.D. and Walker, R.G., 1980. Eolian coastal dune deposits and surrounding marine sandstones, Rocky Mountain Supergroup (Lower Pennsylvanian), southeastern British Columbia. *Canadian Journal of Earth Sciences*, *17*(9), pp.1125-1140

Stokes, W.L. and Phoenix, D.A., 1948. *Geology of the Egnar-Gypsum Valley Area, San Miguel and Montrose Counties, Colorado* (No. 93)

Terwindt, J.H.J., 1988. Palaeo-tidal reconstructions of inshore tidal depositional environments. *Tide-influenced sedimentary environments and facies*, pp.233-263

Trudgill, B. D., N. Banbury, and J. R. Underhill, 2004. Salt evolution as a control on structural and stratigraphic systems: Northern Paradox foreland basin, SE Utah, U.S.A., in P. J. Post, D. L. Olson, K. T. Lyons, S. L. Palmes, P. F.Harrison, and N.C.Rosen, eds., Salt sediment interactions and hydrocarbon prospectivity: Proceedings of 24th Annual Gulf Coast Section SEPM Foundation Bob F. Perkins Research Conference, p. 669–700. 92

Trudgill, B. D., 2011. Evolution of salt structures in the northern Paradox Basin: Controls on evaporite deposition, salt wall growth and supra-salt stratigraphic architecture: Basin Research, v. 23, p. 208–238

Trudgill, B.D., 2010, Evolution of salt structures in the Paradox Basin: Controls on evaporite deposition, salt wall growth and supra-salt stratigraphic architecture: Basin Research, v. 23, p. 208-238

Trudgill, B.D., and Paz, M., 2009. Restoration of Mountain Front and Salt Structures in the Northern Paradox Basin, SE Utah, in W.S. Houston, L.L. Wray, and P.G. Moreland, eds., The Paradox Basin Revisited – New Developments in Petroleum Systems and Basin Analysis: RMAG 2009 Special Publication – The Paradox Basin, p. 132-177

Tsoar, H. and Blumberg, D.G. 2002. Formation of parabolic dunes from barchans and transverse dunes along Israel's Mediterranean coast. Earth Surface Processes and Landforms 27: 1147-1161.

Veiga, G.D., Spalletti, L.A. and Flint, S., 2002. Aeolian/fluvial interactions and high-resolution sequence stratigraphy of a non-marine lowstand wedge: the Avilé Member of the Agrio Formation (Lower Cretaceous), central Neuquén Basin, Argentina. *Sedimentology*, *49*(5), pp.1001-1019

Werner, B.T., 1995. Eolian dunes: computer simulations and attractor interpretation. *Geology*, *23*(12), pp.1107-1110

White, M. A., and M. I. Jacobson, 1983, Structures associated with the southwest margin of the Ancestral Uncompahgre uplift, in W. R. Averett, ed., Northern Paradox basin-Uncompahgre uplift: Grand Junction Geological Society Guidebook, p. 33–39

Wright, J.C., Shawe, D.R. and Lohman, S.W., 1962. Definition of members of Jurassic Entrada Sandstone in east-central Utah and west-central Colorado. *AAPG Bulletin*, *46*(11), pp.2057-2070

Zerfass, H., Lavina, E.L., Schultz, C.L., Garcia, A.J.V., Faccini, U.F. and Chemale Jr, F., 2003. Sequence stratigraphy of continental Triassic strata of Southernmost Brazil: a contribution to Southwestern Gondwana palaeogeography and palaeoclimate. *Sedimentary Geology*, *161*(1-2), pp.85-105

Appendix 1

Section 1

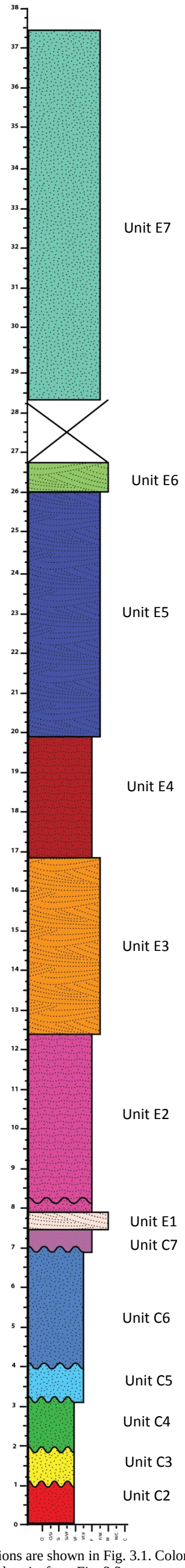

Section locations are shown in Fig. 3.1. Colors shown are consistent with units from Fig. 3.3.

Section 2

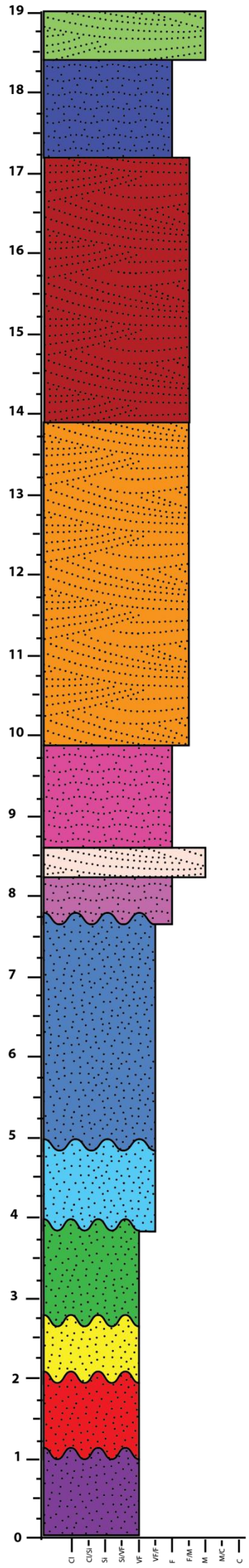
19
18
17
16
15
14
13
12
11
10
9
8
7
6
5
4
3
2
1
0
Cl
Cl/Sl
Sl
Sl/Vf
Vf
Vf/F
F
F/M
M
M/C
C

Section 3

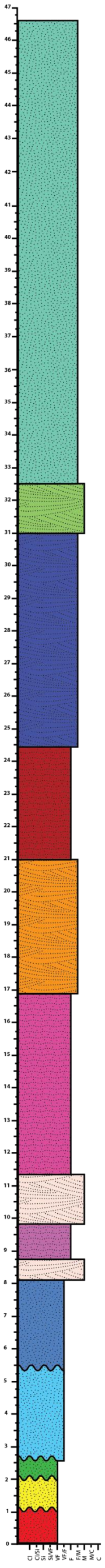
47
46
45
44
43
42
41
40
39
38
37
36
35
34
33
32
31
30
29
28
27
26
25
24
23
22
21
20
19
18
17
16
15
14
13
12
11
10
9
8
7
6
5
4
3
2
1
0
Cl
Cl/Si
Si/Vf
Vf/F
F
F/M
M
M/C
C

Section 4

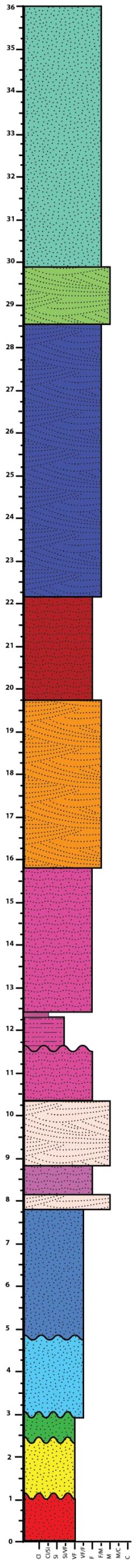
36
35
34
33
32
31
30
29
28
27
26
25
24
23
22
21
20
19
18
17
16
15
14
13
12
11
10
9
8
7
6
5
4
3
2
1
0
Cl
Cl/Si
Si
Si/VF
VF
VF/F
F
F/M
M
M/C
C

Section 5

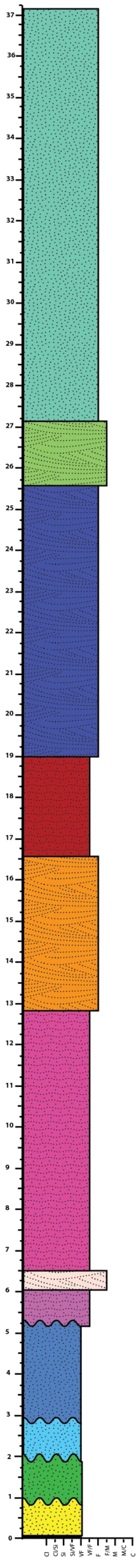
37
36
35
34
33
32
31
30
29
28
27
26
25
24
23
22
21
20
19
18
17
16
15
14
13
12
11
10
9
8
7
6
5
4
3
2
1
0
Cl
Cl/Si
Si
Si/VF
VF
VF/F
F
F/M
M
M/C
C

Section 6

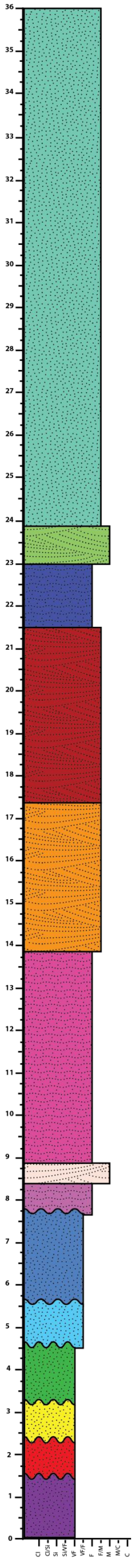
36
35
34
33
32
31
30
29
28
27
26
25
24
23
22
21
20
19
18
17
16
15
14
13
12
11
10
9
8
7
6
5
4
3
2
1
0
Cl
Cl/Si
Si
Si/VF
VF
VF/F
F
F/M
M
M/C
C

Section 7

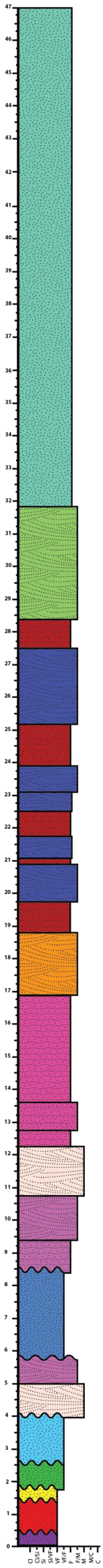
47
46
45
44
43
42
41
40
39
38
37
36
35
34
33
32
31
30
29
28
27
26
25
24
23
22
21
20
19
18
17
16
15
14
13
12
11
10
9
8
7
6
5
4
3
2
1
0
Cl
Cl/Si
Si
Si/VF
VF
VF/F
F
F/M
M
M/C
C

Section 8

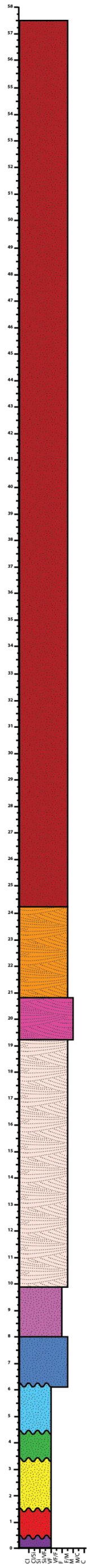
58
57
56
55
54
53
52
51
50
49
48
47
46
45
44
43
42
41
40
39
38
37
36
35
34
33
32
31
30
29
28
27
26
25
24
23
22
21
20
19
18
17
16
15
14
13
12
11
10
9
8
7
6
5
4
3
2
1
0
Cl
Si
SiVF
VF
F
M
MC
C

Section 9

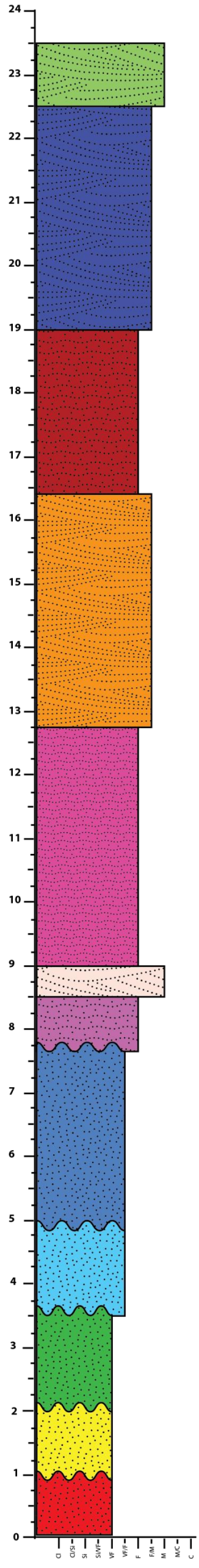
24
23
22
21
20
19
18
17
16
15
14
13
12
11
10
9
8
7
6
5
4
3
2
1
0
Cl
Cl/Si
Si
Si/VF
VF
VF/F
F
F/M
M
M/C
C

Section 10

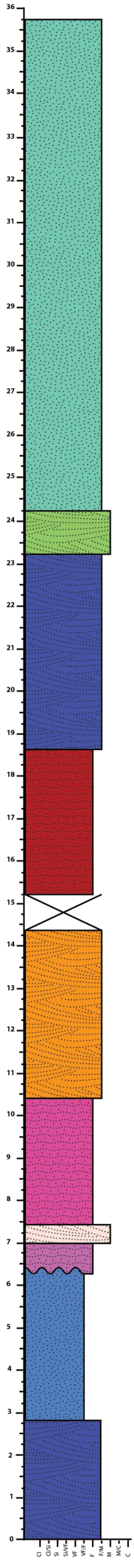
36
35
34
33
32
31
30
29
28
27
26
25
24
23
22
21
20
19
18
17
16
15
14
13
12
11
10
9
8
7
6
5
4
3
2
1
0
Cl
Cl/Si
Si
SiVF
VF
VFF
F
F/M
M
MC
C

Appendix 2

Sample #	GV26	GV21	GV29	GV23	GV18	GV30	GV16	GV7	GV1	GV28	GV22	GV24	GV4	GV33	GV31	GV3	GV32	GV8	GV9	GV10	GV11	GV12	GV13	GV14	GV15	GV5	GV6	GV17	GV27	GV20
Quartz	62.3%	67.3%	54.3%	49.0%	59.0%	38.7%	49.3%	43.7%	47.7%	55.0%	63.0%	64.0%	53.3%	54.0%	53.3%	54.3%	45.7%	54.0%	53.0%	52.0%	48.3%	55.3%	52.3%	55.0%	58.3%	50.7%	52.7%	58.3%	61.3%	64.3%
Feldspar	2.0%	2.0%	5.0%	2.0%	1.7%	5.3%	3.3%	2.3%	3.3%	4.0%	2.0%	1.7%	3.7%	3.0%	6.0%	1.3%	1.0%	3.0%	3.3%	4.0%	4.3%	1.7%	2.3%	3.3%	2.3%	7.3%	2.3%	2.7%	4.3%	4.0%
Chert	0.3%	1.0%	2.3%	1.3%	0.3%	4.3%	1.0%	2.7%	3.0%	2.3%	0.7%	0.3%	3.0%	2.7%	3.0%	1.7%	1.3%	4.3%	2.7%	2.3%	0.3%	1.7%	2.3%	2.3%	1.0%	4.3%	2.0%	1.3%	1.0%	1.0%
Lithics	2.0%	3.7%	1.3%	2.3%	3.7%	1.7%	1.0%	1.0%	0.7%	2.0%	5.0%	5.7%	1.0%	1.3%	1.0%	1.7%	0.7%	1.0%	2.3%	2.3%	7.7%	1.0%	1.3%	0.3%	0.3%	1.0%	1.0%	1.3%	1.7%	2.3%
Hematite Cement	3.0%	1.0%	7.3%	13.3%	2.7%	15.0%	28.0%	29.7%	24.7%	5.7%	2.7%	3.3%	21.3%	16.7%	22.3%	15.0%	15.0%	29.7%	22.3%	24.0%	14.3%	8.0%	14.3%	4.0%	5.7%	6.3%	25.3%	0.0%	0.3%	9.0%
Clay Cement	0.3%	0.3%	0.7%	0.7%	1.7%	0.7%	0.7%	0.3%	0.3%	0.7%	1.7%	0.7%	0.0%	0.0%	0.3%	0.0%	0.7%	0.7%	0.7%	0.3%	0.7%	1.3%	0.7%	0.3%	0.3%	2.3%	0.7%	15.3%	1.0%	0.0%
Dolomite Cement		0.7%	1.0%	0.7%	2.0%	1.3%	0.0%	0.0%	1.3%	1.3%	2.0%	1.7%	1.3%	0.3%	0.3%	2.3%	0.3%	5.7%	14.7%	7.3%	15.7%	7.3%	11.7%	19.3%	15.0%	4.7%	0.3%	0.0%	2.7%	0.0%
Chert Cement	0.7%	0.3%	0.7%	0.7%	1.7%	0.3%	2.7%	0.7%	0.7%	0.0%	0.7%	0.7%	0.0%	1.0%	1.0%	0.0%	0.0%	0.0%	0.3%	2.7%	1.3%	1.3%	2.7%	0.7%	1.0%	2.0%	0.0%	0.7%	0.3%	0.0%
Calcite Cement	6.7%	0.3%	8.7%	12.7%	10.0%	22.3%	0.0%	6.3%	0.3%	15.7%	6.0%	5.0%	15.3%	12.0%	11.0%	16.0%	27.7%	0.0%	0.0%	0.0%	1.7%	1.0%	0.0%	1.3%	1.0%	4.3%	9.7%	7.3%	23.7%	3.7%
Gypsum Cement	0.3%	2.0%	0.3%	1.3%	0.3%	0.0%	3.7%	0.7%	0.3%	0.3%	1.0%	0.0%	0.3%	0.0%	0.7%	0.7%	0.3%	0.0%	0.0%	0.3%	0.0%	0.0%	0.0%	0.3%	0.0%	0.0%	0.0%	0.7%	0.0%	0.3%
Intergranular	0.3%	0.7%	0.0%	0.0%	0.3%	0.0%	0.3%	1.7%	1.0%	0.0%	0.0%	0.0%	0.0%	0.3%	0.0%	0.0%	0.0%	0.0%	0.0%	0.3%	0.7%	2.3%	2.0%	1.7%	0.3%	0.3%	0.0%	0.0%	0.0%	0.0%
Secondary	20.3%	18.3%	15.3%	12.7%	14.3%	8.0%	7.3%	8.3%	17.0%	10.3%	14.0%	14.7%	0.7%	5.7%	0.0%	6.0%	6.0%	0.7%	1.3%	3.7%	4.0%	18.0%	8.3%	10.7%	12.7%	14.0%	5.0%	8.7%	3.3%	12.3%
Secondary Microporosity	1.7%	2.3%	3.0%	3.3%	2.3%	2.3%	2.7%	3.0%	1.3%	2.7%	1.3%	2.3%	0.0%	3.0%	1.0%	1.7%	1.3%	1.0%	0.3%	0.7%	1.0%	2.3%	2.0%	0.7%	2.0%	3.0%	1.0%	3.7%	0.3%	3.0%

Curriculum Vita

Ryan Burtron Ronson was born in Provo, Utah on November 22, 1989. The oldest of three children by Shawn Julie Ronson, he was always scientifically and musically inclined. He graduated from American Fork High School in 2008. He went on to pursue a Bachelor's of Geology at Brigham Young University-Idaho. During this time, he regularly participated in geology related clubs and also competed in the 2015 Imperial Barrel Award competition. Upon graduation he worked as a petroleum intern for the LDS Church. Shortly after completing his internship, Mr. Ronson was accepted at The University of Texas at El Paso to pursue a Master of Science degree in geological sciences. For the duration of his graduate education, he had the opportunity to work as a teaching assistant instructing undergraduate geology labs. He is a current member of UTEP's AAPG chapter, and the Sigma Gamma Epsilon-Alpha Lambda chapter. Throughout his time at UTEP he also volunteered regularly at department run events. For demonstrating excellence in sedimentary geology, he received a number of scholarships from the West Texas Geological Society, AAPG Southwest Section, and the UTEP Geological Sciences Department.

Contact Information: ryan.ronson@gmail.com

This thesis was typed by Ryan Ronson